The PHILOSOPHICAL MAGAZINE

FIRST PUBLISHED IN 1798

L. 46 SEVENTH SERIES No. 378 July 1955

A Journal of Theoretical Experimental and Applied Physics

PRICE 15s. 0d.
Annual Subscription £8 0s. 0d. payable in advance

D AND PUBLISHED BY TAYLOR & FRANCIS LTD., RED LION COURT, FLEET ST., LONDON, E.C.4.

LXXIX. *The Internal Conversion Electron Spectrum of* ^{241}Am

By J. F. Turner
Atomic Energy Research Establishment, Harwell, Berks.*

[Received February 15, 1955]

Abstract.

Observations of the internal conversion electron spectrum of ^{241}Am and of e^-–e^- coincidences, using a pair of magnetic lens spectrometers, afford evidence in support of the level scheme in ^{237}Np derived from Asaro's α-particle observations, except that no indication of transitions to the ground state is found. Information on the half lives and multipole orders of certain of the γ-transitions in ^{237}Np is obtained.

Introduction

From the work of Asaro, Reynolds and Perlman (1952) on the complex α-spectrum of ^{241}Am, a level scheme in ^{237}Np as shown in Fig. 7 may be deduced. Beling, Newton and Rose (1952 a, b) have observed γ-rays of energies 59 kev and 26 kev, presumably from the 71 kev level of this scheme, and from limits imposed on their internal conversion through α- and γ-ray intensity considerations, have shown them to be of electric dipole nature. Delayed α–γ coincidence measurements by the same authors gave a value for the half life of the 71 kev level of 6×10^{-8} sec.

Conversion electrons of the 59 kev γ-ray have been observed by O'Kelley (1951) in spectrometer measurements, and by Prohaska (1951) in α–e^- coincidence absorption measurements. Freedman, Wagner and Engelkemeir (1952) have also seen these lines, and in addition one interpreted as due to a 41·4 kev γ-ray, another transition which might be predicted from the scheme. Dunlavey and Seaborg (1952), in photographic emulsion observations, have found evidence for a complex electron spectrum.

The work reported below is a reinvestigation of the electron spectrum, reinforced by e^-–e^- coincidence measurements, in an attempt to establish more fully the level scheme of ^{237}Np, and to obtain further evidence on the nature of the transitions involved. A brief and not altogether accurate summary of these observations has appeared elsewhere (1953).

§2. The Electron Spectrum

Observations of the electron spectrum from ^{241}Am were made using a thin lens β-spectrometer with 3% and also with 1% resolution. The detector was an anthracene scintillator, covered with 10 μg/cm^2 nylon

* Communicated by the Author.

film to reduce evaporation loss, used with an E.M.I. photomultiplier type 5045 and conventional amplifier and discriminator circuits.

The observations were made over a range of focused electron energy 17 kev to 200 kev, the lower limit being set by the multiplier noise. Figure 1 shows the spectrum obtained with 3% resolution, the inset showing a section remeasured with 1% resolution. The lines observed and the interpretations placed on them are listed in table 1.

Table 1. Lines Observed in ^{241}Am Electron Spectrum

Electron Energy (kev)	γ-ray Energy (kev)
20·3	42·7 (L_I) } + ~ 26·5 (M)
21·4	43·0 (L_{II}) }
25·2	42·8 (L_{III}) + ~ 26·5 (N)
26·8	32·5 (M_I)
31·2	32·7 (N_I)
37·0	59·0 (L_{I+II}) + 42·7 (M_I)
41·6	59·2 (L_{III}) + 43·1 N_I
53·6	59·3 (M_I)
~58	~59 (N)

No lines were observed at energies above that of the 59 kev group, with an upper limit of intensity of 2% of the 37 kev line.

The results of almost simultaneous spectrometer observations made by J. L. Wolfson of Chalk River, using a thin-windowed gas counter as detector, have come to hand (private communication). There is substantial agreement with the above table, but lines of a 99 kev γ-ray with a total intensity of about $1\frac{1}{2}$% of the 37 kev line are also observed. The use of the gas counter has extended the range of observation down to ~ 4 kev.

As may be seen, a number of the lines observed were mixed in origin, so that coincidence measurements were necessary before positive identification of lines, and hence estimations of conversion coefficients, could be made.

§ 3. Experimental Arrangement for e^-–e^- Coincidences

In view of the complexity of the electron spectrum, a reasonably high resolution in energy was necessary in each of the coincidence channels. The experimental arrangement used, then, consisted of two thin lens spectrometers mounted coaxially. The spectrometers were made magnetically independent by the use of two sets of coils wound on the vacuum chambers, each fed in series with the appropriate focusing coil. In a similar manner the fields in the counter spaces were neutralized. This method of field compensation over the whole of the trajectory space made

the use of ring focusing possible, so that each spectrometer could be used with a resolution of about 3% and 0·4% transmission.

The source, of thickness about 45 μg/cm^2, was mounted on a nylon-collodion sandwich film, source charging being eliminated by a thin layer of graphite on the back of the mounting. The total backing thickness was about 30 μg/cm^2.

Fig. 1

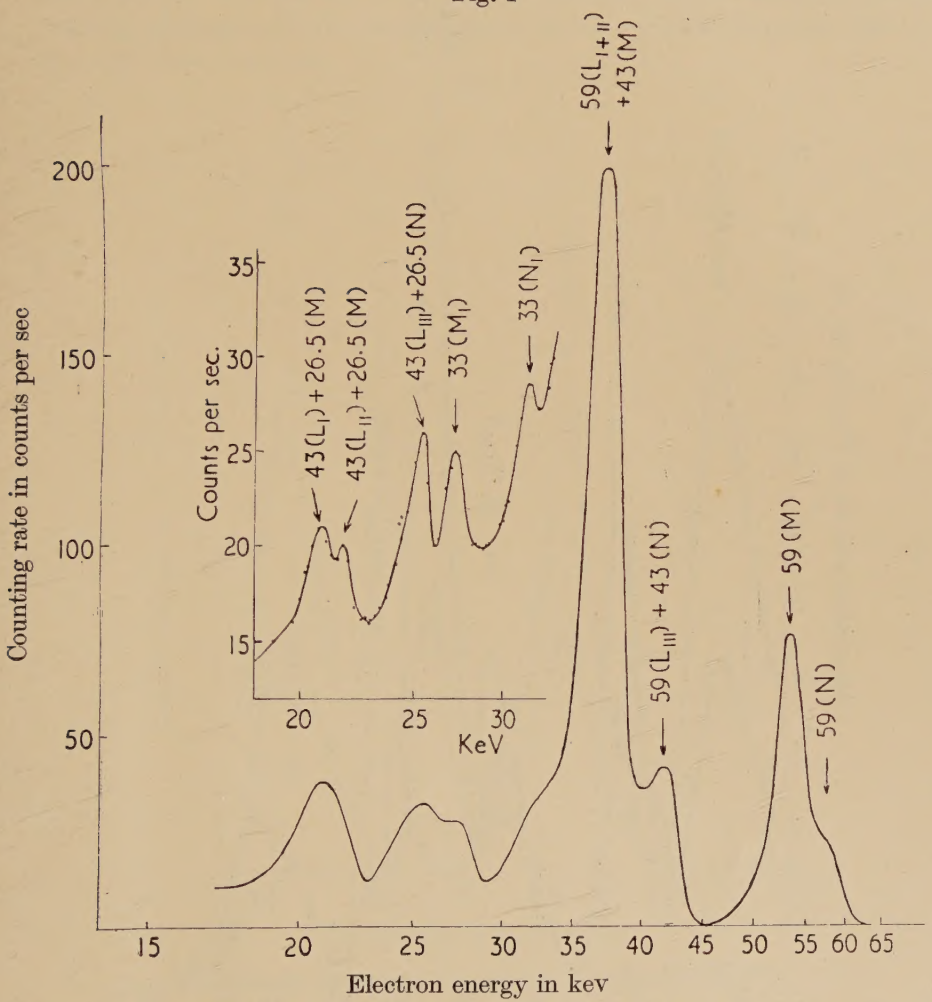

Internal conversion electron spectrum of ^{241}Am.
Lower curve 3% resolution. Inset curve 1% resolution.

The detectors were again anthracene scintillators, used with E.M.I. 14-stage photomultipliers. The outputs from these were fed into a coincidence unit type 1153 A. This unit was of a now conventional design, in which the output of a slow coincidence circuit with input pulse height discrimination is gated by that of a fast coincidence circuit in

which only time resolution is obtained, to give a final coincidence output in which both pulse height discrimination and short resolving time are achieved. In the unit used the slow coincidence resolving time was 10^{-7} sec and the fast resolving time variable between 10^{-8} and 4×10^{-8} sec.

Fig. 2

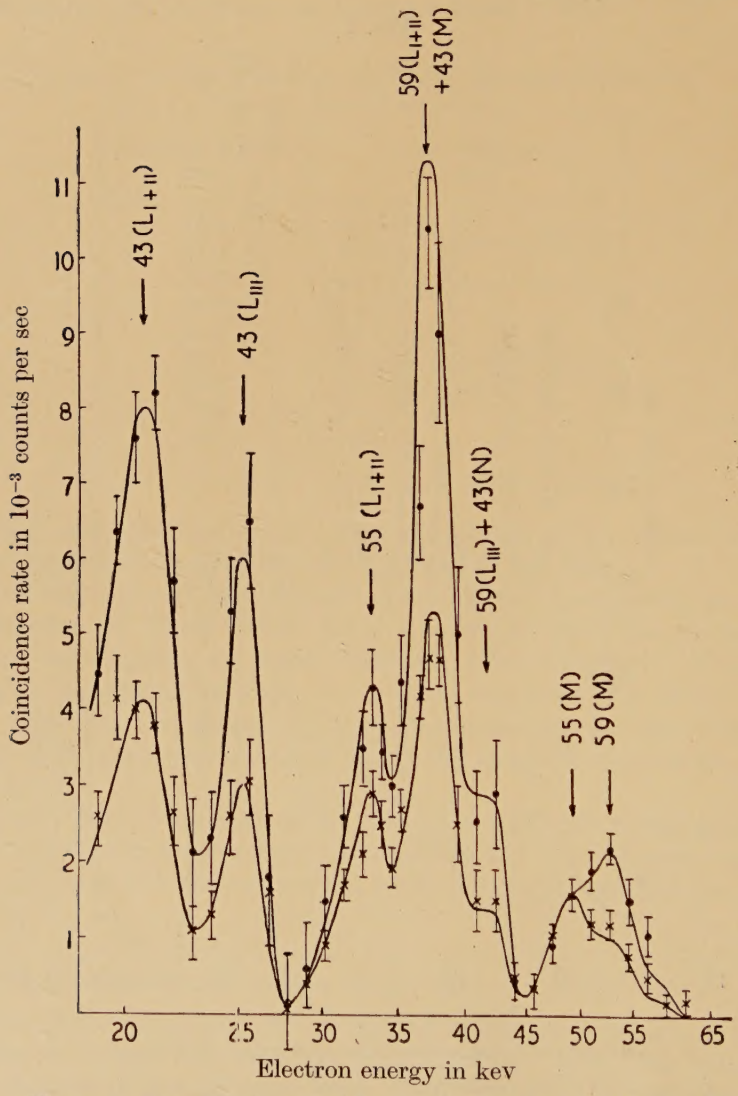

Electron spectrum in coincidence with 59 (L_{I+II})+43 (M) line.
● Resolving time 10^{-7} sec. × Resolving time 2×10^{-8} sec.

§ 4. Coincidence Measurements

Observations were made of the electron spectra in coincidence with certain of the major electron lines, each line being selected in turn in one spectrometer, while the other was swept through the complete electron

spectrum a number of times, in 2% momentum steps. This observation of complete coincidence spectra, in contrast to the more customary measurement of coincidences between selected lines, has resulted, as will be seen below, in the detection of lines not resolved in the single spectrum.

The maximum coincidence rate reached in these runs was about 10^{-2} counts per sec, so that the time taken to obtain the spectrum in fig. 2, for example, was about 900 operating hours. The overall time taken was cut down by the use of an automatic control, which recorded scaler readings photographically, and stepped on the variable focusing current, at preset time intervals.

Fig. 3

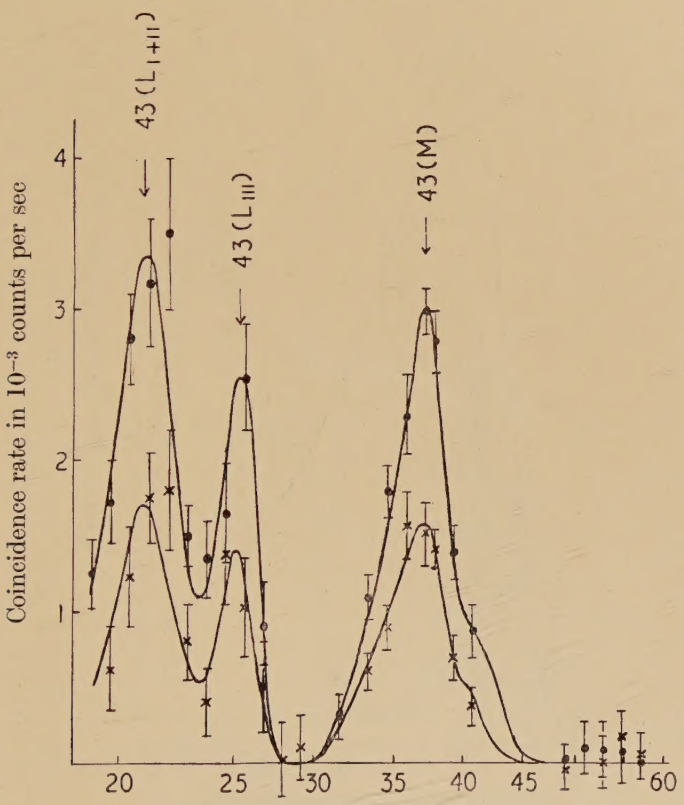

Electron spectrum in coincidence with 59 (M) line.

● Resolving time 10^{-7} sec. × Resolving time 2×10^{-8} sec.

Where necessary these measurements were supplemented by observations of delayed coincidences between selected lines.

The data obtained may be grouped as below :—

(*a*) *Evidence for a* 55 kev–43 kev–59 kev *cascade of γ-transitions*

The spectra of electrons in coincidence with the 59 (L_{I+II})+43 (M) line (fig. 2) and with the 59 (M) line (fig. 3) show line structures which

would arise from a 43 kev and a 59 kev γ-transition in cascade. The simultaneous recording of coincidence rates from the slow and fast coincidence channels (fast resolving time 2×10^{-8} sec) shows that this cascade involves a level of half life about 6×10^{-8} sec. Confirmation of this half life as $6\pm2\times10^{-8}$ sec and evidence showing that the 43 kev transition precedes the level concerned are obtained from an observation of delayed coincidences between the 59 (L_{I+II}) and 43 (L_{I+II}) lines (fig. 4).

Fig. 4

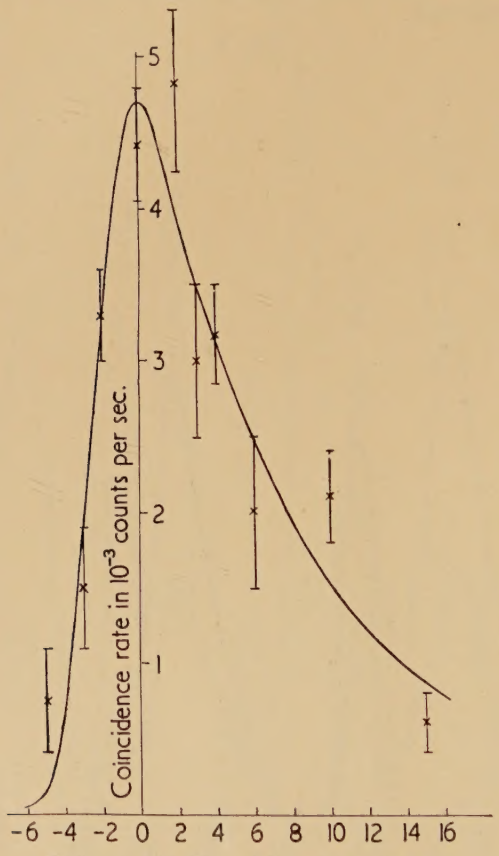

Delayed coincidences between 59 (L_{I+II}) and 43 (L_{I+II}) lines.
Resolving time 2×10^{-8} sec.
Fitted curve for a 6×10^{-8} sec half life following the 43 kev transition.

In addition to the lines mentioned above, the spectrum in coincidence with the 59 (L_{I+II})+43 (M) line shows L_{I+II} and M conversion lines of a 55·4 kev γ-transition, not observed in the single spectrum.* They are

* A recent letter by Milsted, Rosenblum and Valadares (1954) describes the direct observation of the lines in a high resolution β-spectrometer.

associated with a half life of $<1{\cdot}6\times10^{-8}$ sec, as seen from the dependence of coincidence rate on resolving time. These lines are not observed in coincidence with the 59 (M) line. This 55 kev transition, then, is in casade with the 43 kev transition and must, like the latter, precede the 6×10^{-8} sec level, since this longer half life is not observed.

Fig. 5

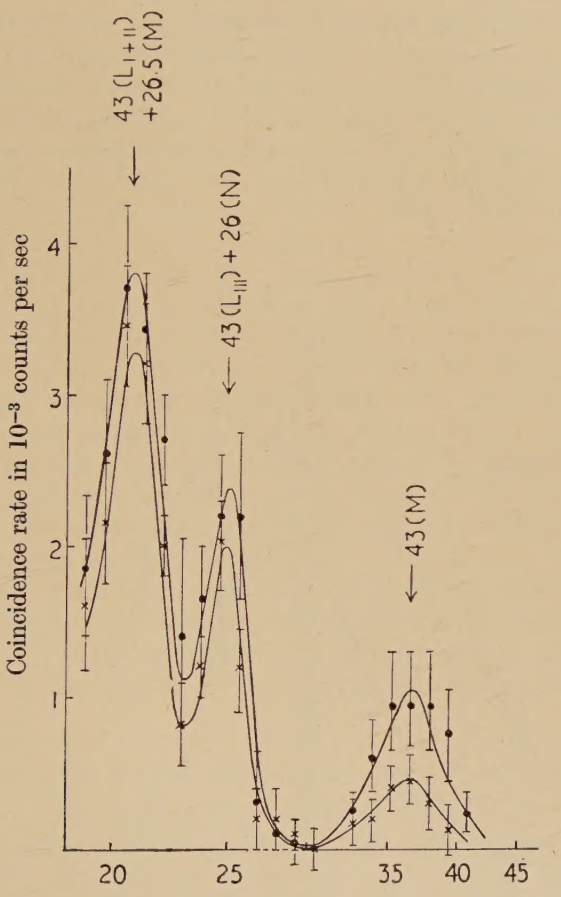

Electron energy in kev

Electron spectrum in coincidence with 33 (M) line.

● Resolving time 10^{-7} sec. × Resolving time 2×10^{-8} sec.

(*b*) *Evidence for a* 43 kev–26 kev–33 kev *cascade*

Figure 5 shows the electron spectrum observed in coincidence with the 33 (M) line. Lines are observed corresponding to 43 (L_{I+II})+26 (M), 43 (L_{III})+26 (N) and 43 (M) conversion electrons, the first two groups being associated with somewhat shorter effective half lives than the last.

Delayed coincidence measurements on the 43 (L_{I+II})+26 (M) line, with resolving times 10^{-8} sec and 2×10^{-8} sec, resulted in the experimental

data plotted in fig. 6. A simple analysis of this data would indicate the presence of a half life of about 10^{-8} sec, a value which, in view of the low energies of electrons recorded in each channel, and hence the small number of photons produced in the scintillators, might have arisen solely from the detector time constants.

Observations in the same experimental conditions, of β–e^- coincidences from ^{166}Ho, involving the $1{\cdot}7\times10^{-9}$ sec, 80 kev level of ^{166}Er (McGowan 1952) showed that a half life $5\pm1\times10^{-9}$ sec was in fact introduced by each detector, plus associated circuits, when recording 22 kev electrons. This compares with a value of about $1{\cdot}5\times10^{-9}$ sec, observed for incident electrons of about 300 kev energy, in which case the delay is presumably mainly due to amplifier characteristics and is certainly compatible with the band width of about 100 Mc/s used.

Fig. 6

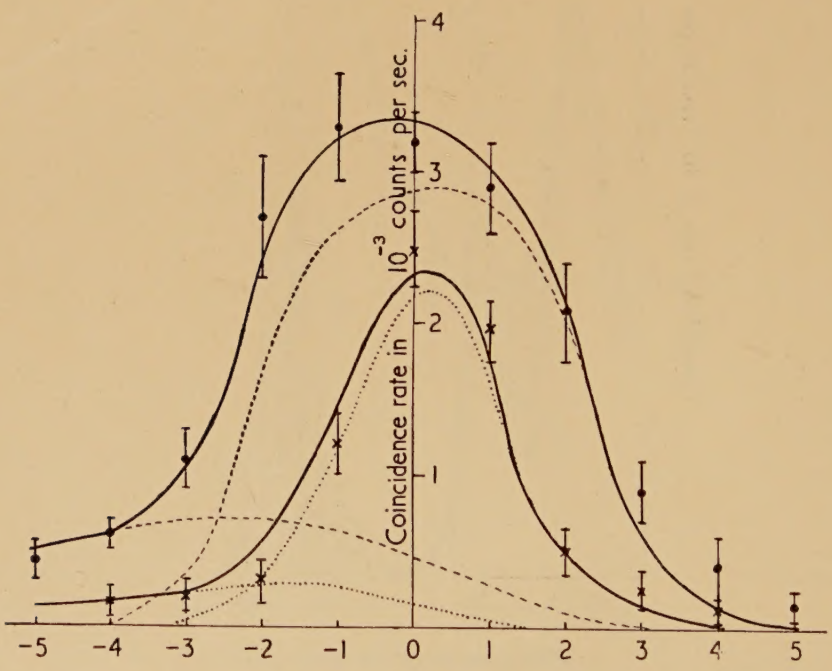

Delay in 33 (M) line in 10^{-8} sec

Delayed coincidences between 43 (L_{I+II})+26 (M) and 33 (M) lines.

● – – – Resolving time $2{\cdot}3\times10^{-8}$ sec. × . . . Resolving time 10^{-8} sec. Curves fitted as described in text.

This information was used, with the assumption that the detector half life varied inversely as the electron energy over the narrow energy range involved, to reconstruct delay curves fitting the data of fig. 6. A good fit to the data can be obtained only if the presence of two coincidence

processes is assumed, one associated with a half life less than 6×10^{-9} sec, the other with a half life greater than 3×10^{-8} sec. In the latter process the 33 kev transition follows the level concerned.

Similar observations, made with resolving time 2×10^{-8} sec on the 43 (L_{III})+26 (N) line, gave results compatible with the short half life above, but the data were not sufficiently detailed to resolve a long period component. Delayed coincidence measurements on the 43 (M) line gave evidence only for a long half life, the dependence of coincidence rate on resolving time confirming this as $\sim 6\times10^{-8}$ sec.

On the simplest view, namely that the long period components are due to the same long lived level, the evidence obtained here suggests that the 33 kev transition follows a 43 kev transition through a $\sim 6\times10^{-8}$ sec level, and is in coincidence with a 26 kev transition through a level of shorter half life. The 26 kev transition, then, must also follow the $\sim 6\times10^{-8}$ sec level.

The 43 kev transition involved here precedes a $\sim 6\times10^{-8}$ sec level, and so may reasonably be identified with that mentioned in § 4 (*a*). Corroborative evidence for this is supplied by the absence of a 33 (M) line in the electron spectrum coincident with the 59 (N) line (fig. 3). The upper limit set on its intensity, taken with the known intensities of the 59 (M) and 33 (M) lines and the known source strength, shows that the 59 kev and 33 kev transitions cannot be directly in cascade. In the above arrangement they are in parallel. The intensity of the 43 (M) line in the spectrum in coincidence with the 33 (M) line (fig. 5) is also in agreement with this arrangement.

If the delayed coincidence data of fig. 6 are re-examined on this basis, and an intensity of the long period component is assumed from the known 43 (L_{I+II})/43 (M) ratio (from § 4 (*a*)), a value of the shorter half life of $<4\times10^{-9}$ sec results. The curves pertaining to this result are shown in fig. 6.

§ 5. Quantitative Comparison with the α-Particle Scheme

It is plain that the evidence of § 4, while not defining a unique level scheme in ^{237}Np, is strongly in favour of that deduced from Asaro's work. If this scheme is taken as the correct one, and the data obtained above, together with that from coincidence measurements made between the 43 (L_{I+II})+26 (M) and 43(L_{III})+26 (N) lines in various combinations, are analysed on that basis, a separated line intensity scheme as in table 2 is obtained. If the data of Beling *et al.* on γ-ray intensities are also taken into account, a quantitative decay scheme as in fig. 7 results, quite compatible with Asaro's α-particle intensity meaurements.

However, no evidence for a 43 kev γ-transition to the supposed ground state of ^{237}Np (designated 43_{II} in table 2) arises from the analysis ; no evidence for a 71 kev transition to this level has been observed either here or at Chalk River ; no evidence for an 11 kev transition has been observed in the latter measurements (private communication). The

Table 2. Analysis of ^{241}Am Electron Spectrum

γ-transition energy in kev	Electron line intensities as percentage of total α-emission				L Conversion coefficients						Probable multipole order
					Measured			Calculated			
	L_{I+II}	L_{III}	M	N	$\alpha(L_{I+II})$	$\alpha(L_{III})$	$\frac{\alpha(L_{I+II})}{\alpha L_{III}}$	$\alpha(L_{I+II})$	$\alpha(L_{III})$	$\frac{\alpha L_{I+II}}{\alpha L_{III}}$	
26·5	—	—	1·6±0·5	0·7±0·3	L (Total) 6·7±3·0			L (Total)		4·2 E1	E1
32·6	—	—	3·2±0·3	1·6±0·3	L (Total) >240			L (Total)		2·1 E1 ~134 M1 ~2600 E2	E2 (or M1)
42·8	5·0±0·6	3·1±0·6	4·5±0·6	0·88±0·4	>12·0	>7·25	1·6±0·2	320 E2 55 M1 0·55 E1	250 E2 0·07 M1 0·33 E1	1·3 E2 800 M1 1·7 E1	E2 (+M1?)
43_{II}	−0·2±0·9	0·3±1·0	—	—	—	—	—	—	—	—	—
55·4	0·42±0·15	—	0·28±0·15		>0·3						
59·2	22·5±2·5	3·5±0·5	10±0·5	(M+N)	0·56±0·01	0·088±0·01	6·4±0·8	0·28 E1	0·14 E1	2·0 E1	E1 (+M2?)

implication here is that the high energy α-particle group observed by Asaro and Perlman does not belong to the decay of ^{241}Am, and that the true ground state is that previously labelled 11 kev. At the time of writing a letter has appeared (Asaro and Perlman 1954) confirming that the high energy α-group is instrumental. The energy levels in fig. 7 are derived on this basis.

Fig. 7.

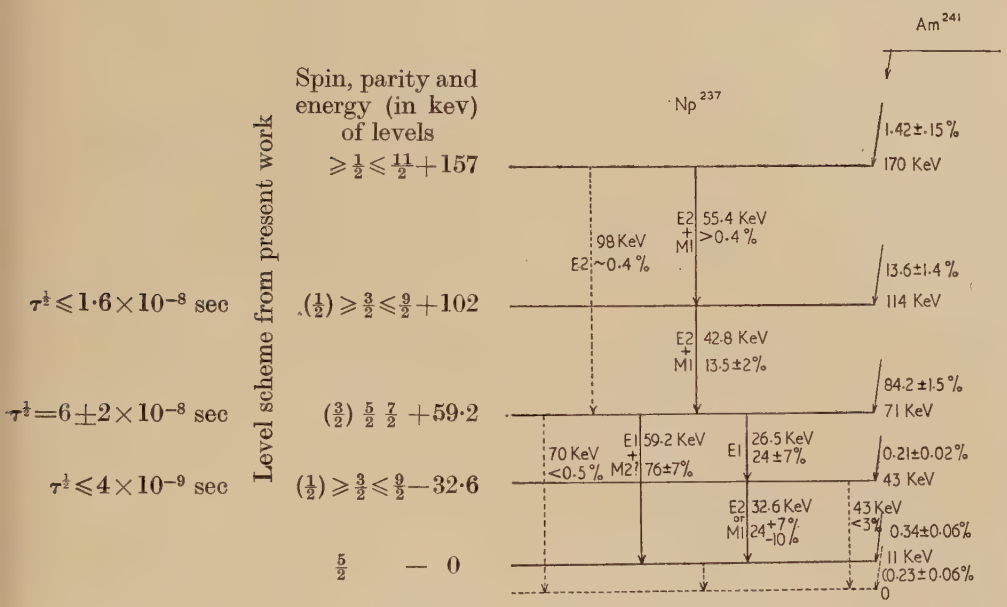

Disintegration scheme of ^{241}Am.

§ 6. Conversion Coefficients and Multipole Order Assignment

L conversion coefficients, separated into L_{I+II} and L_{III} components, where these are known, are shown in table 2. These are obtained from the present measurements taken together with the γ-ray intensity values of Beling *et al.* and of Newton and Rose (1953). The values for the 43, 55 and 59 kev transitions are from direct observation of the L lines; those for the 26 and 33 kev transitions from measurement of M and N conversion intensities and transition branching ratios.

As may be seen, the coefficients for the 43 kev transition from the 102 kev level in ^{237}Np are in closest agreement with the theoretical values of Gellman, Griffith and Stanley (1952) for an E2 transition, but the $\alpha L_{I+II}/\alpha L_{III}$ is rather high, suggesting an M1 admixture of order 10% per transition. Those for the 59 kev transition agree with the theoretical values for an E1 transition (in agreement with Beling *et al.*) although in this case the ratio $\alpha(L_{I+II})/\alpha(L_{III})$ is high by a factor 3 compared with theory.

The less accurate value of total L conversion coefficient for the 26 kev transition is in agreement with the value for an E1 transition obtained by extrapolation from Gellman's data. The limit imposed on the total L conversion coefficient for the 33 kev transition rules out an E1 assignment, and appears high for an M1 transition, but here too the theoretical values have been obtained by extrapolation and are of somewhat doubtful accuracy. The half life of this transition, $<4\times10^{-9}$ sec, is consistent with an M1 nature, or with E2 if specially favoured, as it would be, for example, in a rotational model of the nucleus.

No certain assignment can be made for the 55 kev transition, since the L_{III} line is obscured, even in the coincident spectrum. However, if the 99 kev transition observed by Wolfson is assumed to be that between the 157 and 59 kev levels, as recent precision measurements of electron line energies (Milsted, Rosenblum and Valadares 1954) appear to confirm, then an E1 nature of this transition is ruled out by the relative intensities of the electron lines and α-excitation of the 157 kev level. The L conversion ratios (Wolfson) suggest a largely E2 nature. In these conditions the 55 kev transition can only be M1 and/or E2 on parity and branching ratio grounds, with a best fit intensity data given by a largely E2 character. A very recent letter by Milsted, Rosenblum and Valadares (1954) agrees with these assignments of multipole order.

§ 7. Assignment of Parity and Spin to the Levels of ^{237}Np

The ground state of ^{237}Np has measured spin 5/2 (Tomkins 1948), the shell model then suggesting it to be an f 5/2 state, i.e. of odd parity. On this basis the parity of the other levels follows unambiguously from the present measurements.

Unfortunately the presence of the two largely E1 transitions with transition probabilities $\sim 3\times10^{-5}$ of the single particle predictions makes spin assignment to the levels very far from precise, in that similarly suppressed E1 crossover transitions from the 102 kev and 157 kev levels cannot be ruled out within the observed intensity limits. With E1, M2 and higher order transitions permitted no further selection of spin can be obtained from the crossover data. Such limits as can be placed on spin, and parity assignments, are shown in fig. 7.

However, a further limiting of spin assignment may be made from the experimental data of Wagner, Freedman, Engelkemeir and Huizenga (1953) on the decay of ^{237}U. From spin relations derived from the measured *ft* value of the 245 kev β-transition, from the non-observed β-transitions to the 59 kev level and ground states of ^{237}Np (here estimates of intensity were made from a Kurie plot in the above paper), and from an assumed M1+E2 character for the 207 kev γ-transition, a reasonable assumption on the published conversion data, it appears unlikely that the 59 kev level can have spin 3/2. This would eliminate spin 1/2 for the 33 kev level. These eliminations are shown by brackets in fig. 7.

§ 8. Discussion

(*a*) The investigation of the electron spectrum of ^{241}Am supports the level scheme in ^{237}Np derived from Asaro's earlier α-particle measurements, except that no positive evidence is obtained for any transition to the ground state. The implication here is that the highest energy α-particle group observed by Asaro does not belong to ^{241}Am, and that the true ground state is that at present labelled 11 kev. At the time of writing a letter has been published (Asaro and Perlman 1954) to the effect that this α-particle group is instrumental.

(*b*) A value of $6\pm2\times10^{-8}$ sec is obtained for the half life of the 59 kev level in ^{237}Np, in agreement with the value obtained by Beling *et al.* The measured L_{I+II}/L_{III} ratio for the 59 kev transition from this level differs from Gellman's calculations by a factor 3, if an E1 nature is assigned. In view of the low probability of an E1 transition, as indicated by the long life associated with this transition, the discrepancy may be an indication of an appreciable M2 admixture, rather than an error in conversion coefficient calculations. Insufficient M2 conversion coefficient data are available for comparison.

The present measurements result in an L conversion electron abundance for the 59 kev transition of $0{\cdot}26\pm0{\cdot}03$ per α-particle, in good agreement with the value obtained by O'Kelley. The value for the total intensity of conversion electrons of the 59 kev transition is $0{\cdot}36\pm0{\cdot}04$ per α-particle, compared with Prohaska's value of $\sim 0{\cdot}49$.

(*c*) As has been pointed out by Asaro and Perlman (1954) and Rasmussen (1954), the 102 and 157 kev levels in ^{237}Np may be considered as rotational excited states of the 59 kev level, in that the energy spacing leads to a rotational quantum comparable with that of nearby even–even nuclei. A spin of 5/2 of the 59 kev level arises from this treatment. Rasmussen has also suggested that the 33 kev level is the first rotational excited state of the ground state, a view which is supported by the equal retardation of the 26 kev and 59 kev transitions relative to the Weisskopf predictions. Rasmussen suggests an explanation of the large retardation factors of these γ-transitions which depends on collective motion of the nucleons.

The results of the present work are in agreement with this view. The spin of the 59 kev level is experimentally 5/2 or 7/2. The 43 kev transition between 102 and 59 kev levels, although largely E2 in character, has a transition probability at least 4 times the upper limit predicted for the single particle model, and similarly the 33 kev transition to the ground state, for which a partial E2 character is probable, has a transition probability at least 15 times higher than the single particle prediction for an E2 transition (Blatt and Weisskopf 1952). Such enhanced E2 (+M1) transitions would be expected on the rotational model.

The lack of evidence for higher levels of the ground state rotational band is not unexpected, as α-transitions from ^{241}Am to the ground state and 33 kev level in ^{237}Np are suppressed by factors of order 1000, and α-excitation of other members of the rotational band would be similarly

suppressed, i.e. would take place only to order 0·1% per ^{241}Am disintegration. E1 γ-transitions between the two rotational groups would presumably be suppressed by factors similar to that of the E1 transitions from the 59 kev level, so that excitation of the ground state band by this means would again not lead to measurable intensities.

Acknowledgments

I wish to thank Dr. P. E. Cavanagh for advice given during the preparation of this paper. The coincidence unit used in this investigation was designed by Mr. F. H. Wells of this Establishment. Thanks are also due to Dr. Milsted and Mr. Beadle, also of this establishment, who supplied and purified the source material and prepared the source.

References

Asaro, F., Reynolds, F. L., and Perlman, I., 1952, *Phys. Rev.*, **87,** 277.
Asaro, F., and Perlman, I., 1954, *Phys. Rev.*, **93,** 1423.
Beling, J. K., Newton, J. O., and Rose, B., 1952 a, *Phys. Rev.*, **86,** 797 ; 1952 b, *Ibid.*, **87,** 670.
Blatt, J. M., and Weisskopf, V. F., 1952, *Theoretical Nuclear Physics* (New York : John Wiley), p. 627.
Dunlavey, D. C., and Seaborg, G. T., 1952, *U.C.R.L.*, 1783.
Freedman, M. S., Wagner, F., and Englekemeir, D. W., 1952, *Phys. Rev.*, **88,** 1155.
Gellman, H., Griffith, B. A., and Stanley, J. P., 1952, *Phys. Rev.*, **85,** 944.
McGowan, F. K., 1950, *Phys. Rev.*, **80,** 923.
Milsted, J., Rosenblum, S., and Valadares, M., 1954, *Compt. Rend.*, **239,** 259, 700.
Newton, J. O., and Rose, B., 1953, *Phys. Rev.*, **89,** 1157.
O'Kelley, G. D., 1951, *U.C.R.L.*, 1243.
Prohaska, C. A., 1951, *U.C.R.L.*, 1395.
Rasmussen, J. O., 1954, *Arkiv. f. Fys.*, **7,** 185.
Tomkins, F. S., 1948, *Phys. Rev.*, **73,** 1214.
Turner, J. F., 1953, *Reports on the Birmingham Conference on Nuclear Physics*, p. 29.
Wagner, F., Freedman, M. S., Engelkemeir, D. W., and Huizenga, J. R., 1953, *Phys. Rev.*, **89,** 502.

LXXX. *A Note on the Interatomic and Lattice Potentials in Solid Helium*

By D. J. Hooton
Max Planck Inst. für Physik, Göttingen*

[Received January 24, 1955]

Summary

The interatomic potential $\phi(r)$ has been recently re-determined from gaseous data by Yntema and Schneider (1950) and by Mason and Rice (1954). In this determination the main significance comes from smaller values of r than are encountered in lattice dynamics; the same may be said for the simpler Lennard-Jones approximations, which have also been put forward at various times. It is suggested here that, for the purposes of lattice theory, a better approximation would be to choose a Lennard-Jones potential by directly fitting it, within the crystal range of r, to the most accurate gaseous estimate of $\phi(r)$ available. In illustration, a comparison of some quantities relevant to lattice dynamics is given for Yntema and Schneider's curve, and for a 6–12 Lennard-Jones potential fitted to it in this way.

The characteristics of several recent or well-known estimates of $\phi(r)$ are tabulated, and the lattice potential Φ is calculated from the more important of them. The equivalence of the cubic and hexagonal close-packed structures is demonstrated, and its physical significance for helium is discussed.

§ 1. Introduction

In this note two subjects will be considered: firstly, the interatomic potential $\phi(r)$ (where r is the distance between any two helium atoms), treated from the point of view of lattice theory; secondly, the lattice potential $\Phi(a)$ (where a is the next-neighbour distance in the helium lattice), calculated on the basis of the most recent estimates of ϕ and in terms of various possible lattice structures.

Solid helium melts at a molar volume of 21·5 cm^3 at 0°K and has been studied under increased pressure up to a density $\sim$0·38 gm/cm^3, or molar volume 10·5 cm^3 (Dugdale and Simon 1953). In the lattice dynamics of helium $\phi(r)$ is therefore needed essentially over a range of r extending from about 2·9 to 3·7 Å, which are roughly the next-neighbour distances at the above volumes ($V=Na^3/\sqrt{2}$). On the other hand, the determination of ϕ is based on integrals which describe the gaseous state and in which r runs from $0-\infty$. Yntema and Schneider (1950), and later Mason and Rice (1954), give the most exact formulae

* Communicated by Sir Francis Simon, F.R.S.

found in this way; besides the dipole–dipole van der Waals attractive term proportional to r^{-6} (and in the first case the further dipole–quadrupole term proportional to r^{-8}), the formulae contain an exponential repulsion factor. In both papers it is shown that the simpler Lennard-Jones potential, with repulsion factor proportional to r^{-12}, cannot be made to fit the experimental measurements over the whole temperature range in which records are available, even when quantum effects are allowed for; nevertheless, a reasonable fit can be obtained by choosing different parameters r_m, ϕ_m (which define the minimum) for different parts of the range. Now at the lower temperatures ($\sim \leqslant 0°$C) the range of r of interest in lattice dynamics gives a significant contribution to the integrals of the gaseous theory, whereas at higher temperatures only smaller values of r (much less than r_m) are important. Thus the different Lennard-Jones approximations refer really to different ranges of the variable r, and it might be expected that a similar 6–12 potential would give a good approximation when restricted to the *larger* values of r alone, that is, when fitted to the needs of lattice theory.

It is of considerable convenience, in making lattice calculations, to use a Lennard-Jones potential for $\phi(r)$, since all its properties, as well as those of the lattice potential Φ, depend in a simple fashion on the two minimum parameters r_m, ϕ_m. The calculation of infinite lattice sums involving exponentials is also avoided, although in practice the presence of an exponential is not a serious disadvantage, since in such terms it is usually sufficient to consider first (or first and second) neighbour interactions only. A Lennard-Jones approximation was in fact used in a recent vibrational study of solid helium (Hooton 1955 a, b), where it was also necessary to calculate the first six derivatives of $\phi(r)$. It is the purpose of § 2 to illustrate the nature of this approximation, especially in reference to the critical parameters which may be taken to characterize the lattice theory. At the same time this section will serve to give the numerical basis of the vibrational study quoted above.

In connection with the potential $\phi(r)$, Yntema and Schneider remark that "it would be highly desirable to have accurate crystal data in order to establish the position of the minimum" r_m, ϕ_m. While for a determined lattice structure and chosen potential ϕ it is easy to work out the relation between r_m and the next-neighbour distance for static equilibrium of the lattice as a whole, it should be remembered that for helium the observed lattice spacing a may be very different from the equilibrium value, even at 0°K, because of the large expansion caused by the zero-point vibrations. Moreover, the lattice energy cannot be separated simply from this vibrational energy, so that a relation between r_m and a would have to be deduced from the full equation of state $\partial F/\partial V = -P$ (F the free energy, P the pressure, $\sim$1000 atm.). Since the simple harmonic formulae of lattice dynamics do not apply to helium (Hooton 1955 a), the resulting calculation of r_m would be so complicated as to be of little use.

In § 3 the lattice potential Φ will be calculated (additive central forces being used throughout).* Helium is found from x-ray analysis near absolute zero to have the hexagonal close-packed structure, in contrast to the other inert gas solids, which have the close-packed cubic. However, complete lattice calculations (Prins 1952, Kihara and Koba 1952) show that when $\phi(r)$ is of the Lennard-Jones or exponential-6 form as discussed here, the difference in lattice potential Φ between the two structures is completely negligible. Kihara and Koba (1952) give the relative displacement as of the order 10^{-4} (the hexagonal potential the deeper of the two), which for helium means at the most a difference of four units in the second decimal place ($\Phi \sim 100$ cal/mole). One may therefore use either structure in calculating Φ, but the assumption of cubic symmetry may be of advantage in other connections.

There are also physical reasons to support the use of a cubic lattice which it is of interest to note here. Dugdale and Simon (1953) interpret a phase transition which they have found in solid helium at about 15°K (molar volume ~ 12 cm^3) as a change from the hexagonal (lower temperatures) to the cubic form; and the thermodynamical differences at the transition point are very slight. The two structures have, of course, the same number of next-neighbours and (for given next-neighbour distance) the same molar volume. The first and second neighbour distances—all that is required in the exponential factor that appears in Φ—are also identical. For the lattice dynamics of solid helium as so far developed (Hooton 1955 a) the difference in symmetry is unimportant, since the calculation of a lattice spectrum in any case cannot be made in the usual way (the customary harmonic lattice frequencies may become imaginary). An effective lattice spectrum *can* be defined, but no actual lattice calculation has so far been made, recourse being had to a Debye approximation instead. Since cubic and isotropic symmetry give the same averaged elastic velocity in a continuum, an isotropic Debye approximation may be used; hexagonal symmetry would not give a very different result.

An earlier calculation of the helium potential, based on the diamond lattice, was made by London (1936); apart from the x-ray evidence, it is clear from the figure, in which his potential is plotted according to molar volume, that this can no longer be regarded as a possibility. It should here be mentioned that the other curves shown are in reasonable agreement with estimates made from the experimental thermodynamical properties (Dugdale and Simon 1953, Hooton 1955 a).

§ 2. An Approximation to $\phi(r)$

At the time when the vibrational study of helium (Hooton 1955 a) was made, the potential of Yntema and Schneider (1950) was the most accurate available. Since the shape and position of the potential curve

* The usual lattice symbol Φ is used here, whereas in the paper referred to it was more convenient to write U for the lattice potential.

essentially in the region between the minimum and inflexion point are all that are of importance in lattice theory, it was decided to choose a Lennard-Jones approximation to ϕ which fitted Yntema and Schneider's curve as closely as possible in this region; this was preferred to the Lennard-Jones potential approximated by Yntema and Schneider themselves at the lower gaseous temperatures, since the latter still derives its largest significance from smaller values of r, outside the crystal range. Of course, the same must be said of the potential (1), or of any other potential fitted to the gaseous data (see, for example, Yntema and Schneider 1950, fig. 3); however, a curve containing an exponential factor does allow the closest fit with the virial experiments, and so long as this fit is also good at low temperatures, the exponential-type curve may be taken to provide the best estimate of ϕ for crystal purposes as well. In this respect the potential given by Mason and Rice (1954) should be a better one, since they have taken proper account of quantum effects on the second virial coefficient, and it is just at the relatively low temperatures, at which these effects are of importance, that the crystal range of r (say $>2{\cdot}9$ Å) contributes significantly to the determination of ϕ. Nevertheless, for the purpose of illustrating the nature of the approximation the more recent corrections of Mason and Rice need not be taken into account. Further, these corrections would have only a small effect in the application to the vibrational theory quoted above; the numerical results of the latter are derived from the Lennard-Jones approximation about to be described, and table 1 represents a part of the more extensive calculations underlying the previous work.

Yntema and Schneider give for $\phi(r)$

$$\phi(r)=\xi \exp(-\lambda r)-\eta r^{-6}-\zeta r^{-8}, \quad . \quad . \quad . \quad . \quad . \quad . \quad (1)$$

where $\xi=1{\cdot}20\times10^{-9}$ erg, $\eta=1{\cdot}24\times10^{-12}$ erg Å^6, $\zeta=1{\cdot}89\times10^{-12}$ erg Å^8, $\lambda=4{\cdot}717$ (r in Å); the minimum is at $r_m=2{\cdot}99$ Å, $\phi_m=-1{\cdot}13\times10^{-15}$ erg. As an approximation to (1) for use in the lattice theory the following Lennard-Jones potential of the 6–12 form was chosen:

$$\phi(r)=\phi_m\left\{2\left(\frac{r_m}{r}\right)^6-\left(\frac{r_m}{r}\right)^{12}\right\}, \quad . \quad . \quad . \quad . \quad . \quad . \quad (2)$$

in which the parameters are $r_m=3$ Å, $\phi_m=-1{\cdot}15$ erg. The exact choice of these parameters is of course arbitrary; the above values have been used to combine a reasonably close fit (over the first six derivatives) with some convenience in calculation.

It has been found (Hooton 1955 a) that, in the dynamical theory, second and fourth derivatives of ϕ (with respect to r) play an equal rôle. Table 1 shows some values of these derivatives, ϕ^{II}, ϕ^{IV}, together with ϕ and ϕ^{I}, according to (1) (top entries) and (2) (lower entries); the average discrepancy is about 8%. A more important comparison is that of the turning points of Φ, since these points characterize the vibrational properties of the lattice; the minimum would be the true point of static equilibrium, if it existed, while the inflexion point is that at which the

ordinary harmonic theory (expressed in terms of the Debye approximation) breaks down (Domb 1952). Φ will be calculated from (1) and (2) for the close-packed (cubic or hexagonal) structure in § 3 ; the comparison of its turning points is given in table 2. The absolute values of Φ differ by about $7\frac{1}{2}\%$, but this is not of great importance in solid helium, where the zero point energy is on the average some 50% greater than Φ ; on the other hand, the critical volumes (or next-neighbour distances) are practically identical.

Table 1. Comparison of ϕ-derivatives (top entries (1), lower entries (2))

r (Å)	$\phi\times10^{15}$ (ergs)	$\phi^{\mathrm{I}}\times10^{15}$ (ergs/Å)	$\phi^{\mathrm{II}}\times10^{15}$ (ergs/Å^2)	$\phi^{\mathrm{IV}}\times10^{13}$ (ergs/Å^4)
2·8	−0·87	−3·46	30·7	9·00
	−0·85	−3·82	33·7	12·3
3·0	−1·13	1·26	8·83	3·33
	−1·15	0	9·20	3·79
3·2	−0·99	1·02	1·51	1·20
	−1·03	0·94	1·67	1·21
3·4	−0·78	1·05	− 0·68	0·40
	−0·83	1·01	− 0·49	0·38
3·6	−0·59	0·86	− 1·09	0·12
	−0·64	0·85	− 0·94	0·11
3·8	−0·44	0·65	− 0·98	0·02
	−0·49	0·67	− 0·89	0·03

Table 2. Comparison of the Stationary Points of Φ (top entries (1), lower entries (2))

	Minimum	Inflexion point
a (Å)	2·914	3·229
	2·914	3·230
V (cm^3)	12·414	13·756
	12·414	13·760
$-\Phi$ (cals/mole)	132·85	103·14
	142·59	112·21

Mason and Rice (1954) give the potential

$$\phi(r)=\xi\exp(-\lambda r)-\eta r^{-6}, \quad \ldots\ldots \quad (3)$$

where now $\xi = 2{\cdot}88 \times 10^{-10}$ erg, $\eta = 2{\cdot}32 \times 10^{-12}$ erg Å^6, $\lambda = 3{\cdot}955$ (r in Å). The minimum occurs at $r_m = 3{\cdot}14$ Å, $\phi_m = -1{\cdot}26 \times 10^{-15}$ erg, and is deeper than (1) or (2). In table 3 the minimum parameters and inflexion point are shown for each potential $\phi(r)$ mentioned in the present note. The Lennard-Jones approximation (2) lies between (1) and (3), and may therefore be a slight improvement on (1) for crystal work. The 6–12 Lennard-Jones potential of de Boer and Michels (1938),

$$r_m = 2{\cdot}87 \text{ Å}, \qquad \phi_m = -1{\cdot}41 \times 10^{-15} \text{ erg}, \qquad . \ . \ . \quad (4)$$

is quoted by Mason and Rice as fitting the virial coefficient equally as well as (3) at low temperatures. De Boer's curve must therefore also derive considerable significance from the crystal range of r, and it is of interest to compare it with the approximation (2), chosen for quite different reasons within the same range. The difference between the two is evident in table 3. Part of this difference must correspond to the quantum effects omitted in Yntema and Schneider's potential, to which

Table 3. Stationary Points of $\phi(r)$

Potential	Minimum		Point of inflexion	
	r (Å)	$-\phi \times 10^{15}$ (ergs)	r (Å)	$-\phi \times 10^{15}$ (ergs)
(1) Yntema–Schneider exp-6, 8	2·987	1·132	3·304	0·882
(2) 6–12	3·000	1·150	3·325	0·910
(3) Mason–Rice exp-6	3·135	1·264	3·533	0·934
(4) de Boer–Michels 6–12	2·869	1·409	3·181	1·109
(5) Slater–Kirkwood exp-6	2·931	1·297	3·260	1·011
Yntema–Schneider low temp. 6–12	2·950	0·836	3·270	0·658
Yntema–Schneider average 6–12	2·975	0·686	3·298	0·540

(2) is fitted, and this would be removed by fitting (2) to Mason and Rice's potential instead. The rest—indicated already by the difference between de Boer's curve and (3)—is concerned with effects at the smaller values of r, outside the crystal range, irrelevant for the purpose of lattice dynamics.

It is also evident that de Boer's curve is very different from the 6–12 potential given by Yntema and Schneider; this is presumably again an expression of quantum effects, since the wider range of r is now in both cases relevant. If a Lennard-Jones potential is to be used, on grounds of convenience in lattice calculations, it is best chosen by an empirical fitting in the relevant range of r; in view of the later work, the curve (2) cannot be considered the most suitable but it will serve to show the effects of such a procedure.

The Slater–Kirkwood potential, as used earlier by London (1936), has also been included in table 3:

$$\left.\begin{aligned} \phi(r)=\xi \exp(-\lambda r)-\eta r^{-6}, \qquad & \xi=7{\cdot}70\times10^{-10}\ \text{erg}, \\ \eta=1{\cdot}49\times10^{-12}\ \text{erg Å}^6, \qquad & \lambda=4{\cdot}609\ (r\ \text{in Å}). \end{aligned}\right\} \quad . \quad (5)$$

§ 3. The Lattice Potential

The calculation of $\Phi(a)$ for the cubic and hexagonal close-packed structures has been carried out by Kihara and Koba (1952) for arbitrary Lennard-Jones potentials, and partially completed for an arbitrary exp-6 potential of the type given by Mason and Rice; the extension to Yntema and Schneider's exp-6, 8 potential is immediate. Kihara and Koba have worked out the relevant lattice sums,* which have the form

$$S_n=\frac{1}{a^n}\sum_i n_i\left(\frac{a}{r_i}\right)^n, \qquad \sum_i n_i \exp(-\lambda r_i),$$

where $i=1, 2, \ldots$ denotes the ith shell of neighbours, and a is the next-neighbour distance. For the potentials $\phi(r)$ considered here S_6, S_8, S_{12} are required: they are given in table 4.

Table 4. Lattice Sums S_n

n	S_n (cubic)	S_n (hexagonal)
6	14·45392	14·45489
8	12·80194	12·80282
12	12·13188	12·13229

* These authors do not mention the thorough-going work of Born and Misra on such lattice sums, in which the general notation of lattice dynamics is used. Two exact methods of calculation are developed for cubic lattices by Misra (1940) and Born and Misra (1940). The sums $(1/2^n)S_n$ (a is the lattice constant in their work) are tabulated for $n=4$ to 13, in exact agreement with $(1/2^n)S_n$ as derived from Kihara and Koba's table; the quantities n_i, r_i are also given up to $i=16$. Born (1944) has tabulated n_i, r_i up to $i=5$ for various hexagonal lattices, and his quite general method of enumeration is clearer than that of Prins *et al.* (1952) used by Kihara and Koba.

In the summation over exponentials it is sufficient for all the potentials (1), (3) and (5) to keep first and second neighbours only ($i=1$, 2), and to this extent the cubic and hexagonal lattices are identical. The percentage contributions to the exponential sum in Φ from successive shells are in fact of the order 100% ($i=1$), 0·1% ($i=2$), 0·01% ($i=3$, hexagonal), 0·01% ($i=3$, cubic; $i=4$, hexagonal), ...

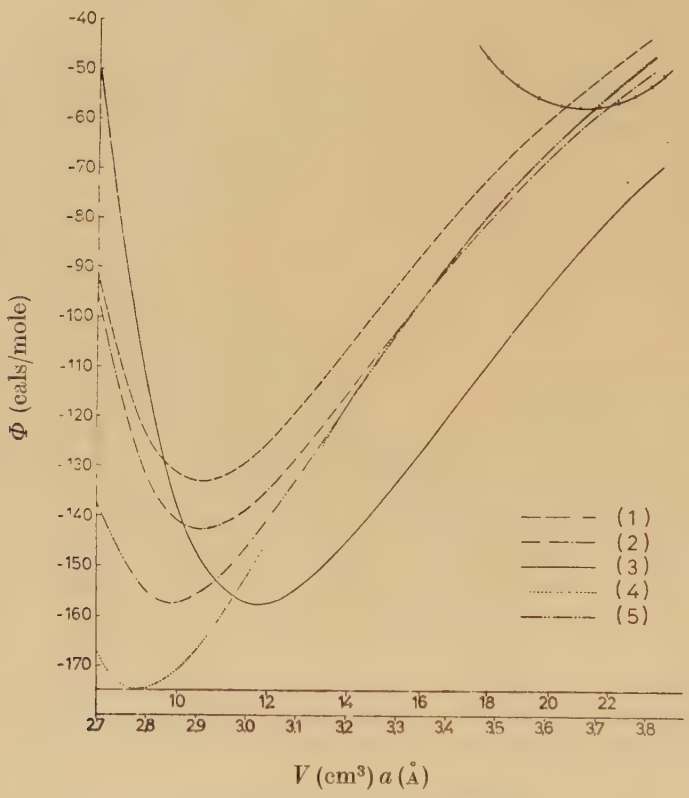

The helium lattice potential.

In the figure, $\Phi(a)$ is drawn corresponding to (1), (3) and (5), to the Lennard-Jones approximation (2), and to de Boer's Lennard-Jones potential (4) (regarded as the best Lennard-Jones curve for the *gas* theory). In all cases the cubic and hexagonal curves are indistinguishable. The formulae used are summarized in (6), the various coefficients* being given in table 5:

$$\Phi(a)=A\,[\exp(-\lambda a)+\tfrac{1}{2}\exp(-\lambda a\sqrt{2})]+Ba^{-12}-Ca^{-6}-Da^{-8}. \quad (6)$$

* Although, for example, the curve (3) has here been written in a different form to that given by Mason and Rice, for this as for the other potentials the published values of the numerical constants have been used directly in calculating Φ. The coefficients shown for the Slater–Kirkwood close-packed cubic case nevertheless differ a little from those given by London.

Table 5. Coefficients in $\Phi(a)$

Potential $\phi(r)$	(1)	(2)	(3)	(4)	(5)
$A\times10^{-7}$ (cals/mole)	10·37	—	2·486	—	6·653
$B\times10^{-7}$ (cals Å^{12}/mole)	—	5·338	—	3·828	—
$C\times10^{-5}$ (cals Å^{6}/mole)	1·290	1·745	2·420	1·635	1·551
$D\times10^{-5}$ (cals Å^{8}/mole)	1·742	—	—	—	—
λ (Å^{-1})	4·717	—	3·955	—	4·608

The influence of the two structures on the coefficients of the power terms may give rise to a difference of two units in the fifth significant figure, which implies never more than a change of four units in the second decimal place of $\Phi(a)$. The coefficients are therefore rounded to four significant figures, and values of Φ corrected to one decimal place are given in table 6.

Table 6. The Lattice Potential Φ (a the next-neighbour distance, V the molar volume, for the close-packed structures)

a (Å)	V (cm^3)	$-\Phi$ (cals/mole)				
		(1)	(2)	(3)	(4)	(5)
2·8	9·35	123·5	132·2	113·0	174·6	155·2
3·0	11·50	129·3	138·9	157·7	152·3	146·4
3·2	13·96	107·0	116·2	145·9	119·1	118·3
3·4	16·74	82·1	90·6	120·7	89·8	90·0
3·6	19·88	61·1	68·9	94·9	67·1	67·1
3·8	23·37	45·2	52·1	72·9	50·1	49·8

Finally, the curve on the right of the figure is London's (1936) $\Phi(V)$ according to the diamond lattice (for which $V=8Na^3/\sqrt{27}$). This has already been commented upon, and clearly his use of the Slater–Kirkwood potential for ϕ has nothing to do with the discrepancy.

Acknowledgment

I should like to acknowledge the generosity of the Carnegie Trust for Scotland for grants received during the course of this work.

References

Boer, J. de, and Michels, A., 1938, *Physica*, **5**, 945.
Born, M., 1942, *Proc. Camb. Phil. Soc.*, **38**, 82; 1944, *Ibid.*, **40**, 262.
Born, M., and Misra, R. D., 1940, *Proc. Camb. Phil. Soc.*, **36**, 466.
Domb, C., 1952, *C. R. 2e Réunion Chimie Physique Paris.*
Dugdale, J. S., and Simon, F. E., 1953, *Proc. Roy. Soc.* A, **218**, 291.

Hooton, D. J., 1955 a, *Phil. Mag.* (7), **46,** 485; 1955 b, *Z. f. Naturforschung*, "Anharmonische Gitterschwingungen und die lineare Kette" (in preparation).
Kihara, T., and Koba, S., 1952, *Journ. Phys. Soc. Japan*, **7,** 348.
London, F., 1936, *Proc. Roy. Soc.* A, **153,** 576.
Mason, E. A., and Rice, W. E., 1954, *Journ. Chem. Phys.*, **22,** 522.
Misra, R. D., 1940, *Proc. Camb. Phil. Soc.*, **36,** 173.
Prins, J. A., *et al.*, 1952, *Physica*, **18,** 307.
Yntema, J. L., and Schneider, W. G., 1950, *Journ. Chem. Phys.*, **18,** 646.

LXXXI. *Annealing of Point Defects in Metals and Alloys*

By W. M. Lomer
Atomic Energy Research Establishment, Harwell

and A. H. Cottrell
Department of Physical Metallurgy, University of Birmingham*

[Received January 1, 1955]

Abstract

An analysis is made of published data on the recovery of resistivity during the annealing of metals at low temperatures, after damage by irradiation, quenching, or cold work. Interpreted in terms of the migration and annihilation of point defects, the experimental observations show two annealing stages, in the second of which the number of migratory jumps made by a defect before annihilation appears anomalously small. It is suggested that during the first stage some of the defects become trapped (e.g. on impurity atoms), and that the second stage is concerned with the evaporation of these defects from their traps ; this leads to a reasonable number of jumps for the second stage. The theory is applied to some results of quenching experiments by Roswell and Nowick. Finally, it is pointed out that the unexpectedly large number of jumps observed in stage 1 annealing, after irradiation or cold work, can be accounted for if the interstitial mechanism provides a random walk in only one dimension, as in the case of ' crowdions '.

§ 1. Introduction

Some experiments made in recent years purport to show the annealing out, at temperatures well below those of normal self-diffusion, of excess point defects introduced into metals by quenching, cold working, or irradiation with atomic particles. In most of these experiments, which have been reviewed by Broom (1954), electrical resistivity was used as the indicator of recovery, although in one case (Roswell and Nowick 1953) internal friction was used.

The reasons for believing that the low-temperature resistivity changes (e.g. at temperatures below 300°K for copper, silver and gold) are in fact due to the migration and annihilation of point defects are as follows :—

1. In the quenching experiments no types of disorder other than vacancies can be expected to be trapped in the crystals.

* Communicated by the Authors.

2. In the irradiation experiments it is not obvious that any types of disorder other than vacancies and interstitialcies (possibly clustered) can persist. Thermal spikes, local melting, and even small dislocation loops, must be very short-lived at all temperatures.

3. Although dislocations are created in the cold working experiments in addition to point defects, the recovery from cold work damage at low temperatures is similar in many respects to recovery from irradiation damage. Furthermore, these low-temperature resistivity changes in cold worked metals sometimes occur without appreciable change in mechanical properties.

4. The magnitudes of the resistivity changes are broadly consistent with the values deduced from the atomic concentrations of point defects expected to be present (of order 10^{-4}; Overhauser 1953, Roswell and Nowick 1953) and from their expected contributions to the resistivity ($1{\cdot}3\times10^{-6}$ ohms cm^{-1} for 1 at. % vacancies in copper; Jongenburger 1953).

§ 2. Rates of Recovery

Table 1, based on the resistivity results gathered together by Broom in his fig. 18, summarizes observations on various metals. The first column of figures in the table gives the reported activation energy Q, in electron volts, for various observed stages of recovery, while the second column gives the mean annealing temperatures for these stages.

In copper, on which most of the observations have been made, some recovery occurs with a variable activation energy that is roughly proportional to the annealing temperature (Overhauser 1953). In addition, there are two fairly well-defined stages of recovery, one at about -150°c with an activation energy of about 0·2 ev, and one at about -30°c with an energy of about 0·7 ev. These two energies agree roughly with the theoretically estimated activation energies for the migration of interstitialcies (0·25 ev, Huntington 1953) and vacancies (1 ev, Huntington 1942) in copper, respectively, and this has led to the suggestion (Huntington 1953) that the two stages may be due to the annealing out separately of these two defects. This would imply, of course, that these defects disappear by a mechanism other than recombination, since in the irradiation experiments vacancies are created no more abundantly than interstitialcies.

In this note we shall examine the average number n of migratory jumps made by a mobile point defect before it is annihilated or otherwise rendered ineffective. If ν ($\simeq10^{13}$ per second) is the vibration frequency of a defect, and J is its activation energy for jumping, defects of this type anneal out at a temperature T in a time

$$t=n\nu^{-1}\exp(J/kT). \qquad (1)$$

On the simplest theoretical model we expect that recovery of the irradiated specimens occurs by recombination, since the concentration of annihilation sites provided for (mobile) interstitialcies by (immobile)

Table 1. Recovery of Resistivity in Metals

Metal	Q, ev	Mean T°c	n, from eqn. (1)	Observer and Method
Copper	0·15, 0·2	−150	10^6 to 10^8	Marx *et al.* (1952), irradiation
,,	0·2	−110	10^6 to 10^8	Manintfeld (1952), light work
,,	0·25	−110	10^6 to 10^8	Manintfeld (1953), heavy work
,,	0·2	−180	10^6 to 10^8	Overhauser (1953), irradiation
,,	0·4 to 0·6	−110 to −40	10^0 to 10^2	Overhauser (1953), irradiation
,,	0·44	−120	10^0 to 10^2	Eggleston (1952), heavy work
,,	0·67	− 40	10^0 to 10^2	Eggleston (1952), heavy work
,,	0·68	− 30	10^0 to 10^2	Overhauser (1953), irradiation
,,	0·72	− 30	10^0 to 10^2	Eggleston (1953), irradiation
,,	0·82	− 20	10^0 to 10^2	Manintfeld (1953), heavy work
,,	0·88	+ 20	10^0 to 10^2	Manintfeld (1952), light work
,,	~1·0	+ 30	10^0 to 10^2	Marx *et al.* (1952), irradiation
,,	~1·1	+140	10^0 to 10^2	Smart *et al.* (1941), heavy work
,,	1·25	+180	10^0 to 10^2	Bowen *et al.* (1952) heavy work
Gold	0·15 to 0·2	−150	10^6 to 10^8	Marx *et al.* (1952), irradiation
,,	0·29	−100	10^6 to 10^8	Manintfeld (1952), light work
,,	0·68	+ 30	10^6 to 10^7	Kauffman and Koehler (1955), quenching
,,	0·69	+ 20	10^3 to 10^5	Manintfeld (1952), light work
,,	~1·0	+ 20	10^0 to 10^2	Marx *et al.* (1952), irradiation
Silver	0·15, 0·2	−150	10^6 to 10^8	Marx *et al.* (1952), irradiation
,,	0·18	−150	10^6 to 10^8	Manintfeld (1952), light work
,,	0·69	− 40	10^0 to 10^2	Manintfeld (1952), light work
,,	~1·0	+ 40	10^0 to 10^2	Marx *et al.* (1952), irradiation
Nickel and Tantalum	0·2	−180	10^3 to 10^5	Marx *et al.* (1952), irradiation
	0·3	− 70	10^5 to 10^8	Marx *et al.* (1952), irradiation
,,	~1·0	+ 40	10^0 to 10^2	Marx *et al.* (1952), irradiation
Platinum	1·2	+ 80	10^1 to 10^2	Dugdale (1952), cold work and irradiation

vacancies is much greater (e.g. 10^{-4}) than that provided by dislocations and grain boundaries (e.g. 10^{-7} for random annihilation on dislocations of the usual density of about 10^8 cm^{-2}). Each migrating interstitialcy meets αz new sites of the crystal, where z is the coordination number and $\alpha \simeq \frac{1}{2}$, each time it enters a new site. Thus if it moves in a three-dimensional random walk it makes on average 10^3 jumps to 10^4 before annihilation when the distribution of defects in the crystal is random, and less than this number when the vacancies and interstitialcies are clustered. Similar values of n are expected in the cold worked specimens, although in this case dislocations exist in much greater abundance (e.g. 10^{11} to 10^{12} cm^{-2}) and may compete seriously with vacancies as centres for the annihilation of interstitialcies. In quenched specimens interstitialcies are not created and in this case n represents the number of jumps made by a vacancy before it finds an annihilation centre on a dislocation, a grain boundary, or a void. The observation by Roswell and Nowick (1953) that small amounts of cold work speed up the annealing process in quenched specimens supports the view that the vacancies annihilate themselves predominantly on dislocations in this case; we thus expect a value $n \simeq 10^7$ for quenched and unworked specimens.

Experimental values of n can be deduced from the data summarized by Broom (1954). Taking t in eqn. (1) as the experimental annealing time (taking actual time where given; assuming 10^3 sec where unspecified) and identifying J with the reported activation energy Q, we deduce the values of n given in table 1. Apart from one possible exception (gold, after quenching) there is no agreement with the above predictions. In most cases the annealing takes place in two or more distinct stages. Stage 1, which occurs at low temperatures, appears to involve a much larger value of n, usually about 10^7, than expected for irradiated and cold worked specimens, and stage 2 likewise appears to involve a much smaller value of n, usually about 10^1.

On the theory so far described the results for stage 2 might be interpreted in terms of the recombination of closely spaced vacancies and interstitialcies (Brinkman, Dixon and Meechan 1954), although such pairs could hardly be expected to survive the long-range migrations of stage 1.

§ 3. Trapping of Point Defects

One way of overcoming the difficulty of the stage 2 processes is to suppose that, in addition to annihilation centres, *trapping centres* such as impurity atoms also exist in the crystal. This leads naturally to two or more annealing stages even when only a single species of point defect is active. During the first stage of annealing these defects migrate, some to annihilation sites and the remainder to trapping sites, according to the relative abundance of the two types. Those defects caught by immobile traps are themselves immobilized until the temperature is

raised sufficiently to release them from their traps, or to render their traps mobile. Stage 2 then begins.

In a metal such as copper a small impurity ion in substitutional solution provides a powerful trap for an interstitialcy, since the misfit energy of an interstitial copper atom is very large (about 5 ev, according to Huntington 1953) and a substantial reduction of this energy is possible when a small solute atom replaces the copper atom in the interstitialcy; a binding energy of 0·5 ev would seem a modest expectation in such cases. The strong effects of phosphorus and arsenic in retarding the release of stored energy in cold worked copper (Clarebrough *et al.* 1952) are consistent with this conclusion. An interstitialcy trapped on an impurity atom can move only by breaking away from its trap, or by the impurity atom itself migrating through the interstices of the copper lattice, and the latter process is likely to require a much larger activation energy (Huntington, private communication 1954) than the normal interstitialcy mechanism (Seitz 1950).

A vacancy may attach itself to an impurity atom through both elastic and electrical interactions. An elastic attraction should exist whether the stress field of the solute atom is positive or negative, since in either case these stresses must be relaxed near the vacancy. In general, these interactions will be smaller than in the case of interstitialcies, since the energy of formation of a vacancy is much smaller; in § 4 we shall discuss a particular case where the binding energy between a vacancy and a solute atom is considered to be 0·3 ev. The extent to which a vacancy–solute pair are immobile depends on the solute atom (Johnson 1939). If this changes place with its vacancy at least as rapidly as does a solvent atom next to the vacancy, then the vacancy–solute pair moves with a mobility of about one-tenth that of a free vacancy. During the annealing out of vacancies in quenched specimens, therefore, such solute atoms will be carried along with vacancies as part of the stage 1 process. On the other hand, if the activation energy for vacancy–solute interchanges is only slightly (e.g. 0·1 ev) larger than that for vacancy–solvent interchanges, the mobility of vacancy–solute pairs becomes so much reduced, compared with that of free vacancies, that the latter may provide the faster annealing process even though they have first to be freed by thermal decomposition of vacancy–solute pairs.

This theory of the trapping of point defects on impurity atoms leads to the result that, in stage 2, the observed activation energy Q can no longer be identified purely with the energy for jumping J; it must also contain the binding energy B of the defects in the traps. As a consequence eqn. (1), although still valid for stage 1, gives spurious values for n when applied to stage 2.

We shall now modify eqn. (1) for the case, appropriate to stage 2, where the concentration c_t of trapping sites is greater than the concentration of point defects. The proportion of time that a defect in the crystal is free from traps is $c_t^{-1} \exp(-B/kT)$. During free periods it

jumps at the rate $\nu \exp(-J/kT)$ per second. Hence, on the average, the time taken for a defect to make n jumps is given by

$$t = c_t n \nu^{-1} \exp[(B+J)/kT], \qquad (2)$$

which replaces eqn. (1) for stage 2 processes.

According to this theory, then, the second stage of annealing out of a species of point defects differs from the first stage in two respects :—

1. The activation energy Q for the process is larger ($B+J$ instead of J).

2. For a given Q, the time of annealing is reduced, in proportion to the concentration of trapping sites. If the latter lies in the range 10^{-4} to 10^{-5}, which is reasonable for most specimens of high purity, then the value of n for stage 2 is raised to the same order of magnitude (10^6 to 10^7) as in stage 1, and the difficulty of the short paths no longer arises.

A further consequence of the theory is that, when more than one type of trapping site is present, each with its own values of B and c_t, stage 2 will itself occur in a series of stages as successively deeper traps release their imprisoned defects. Thus specimens containing several types of impurities in comparable abundances should anneal in stage 2 with a variable activation energy largely proportional to the annealing temperature.

§ 4. Experiments of Roswell and Nowick

It is interesting to apply the theory to the observations of Roswell and Nowick (1953). Using an alloy of 33·5 atomic per cent of zinc in silver, they introduced vacancies by means of quenching and detected the migrations of these defects at temperatures in the range 50 to 80°C by an internal friction method. The annealing out of the defects occurred in two stages, each of which followed an exponential decay law of the type $\exp(-t/\theta)$, where the decay time t depended on temperature as

$$\theta = \theta_0 \exp(Q/kT). \qquad (3)$$

The values deduced by Roswell and Nowick for stage 1 are $Q = 0{\cdot}8$ ev and $\theta_0 = 10^{-8}$ seconds. Assuming a frequency factor of 10^{13} per second, we deduce from this that the average number of jumps of a defect in stage 1, before it is rendered ineffective, is 10^5.

Roswell and Nowick give $Q = 1{\cdot}1$ ev for stage 2. From this value, and from the measured rates of decay, we deduce that $\theta_0 \simeq 10^{-11}$ seconds in stage 2, which gives an average number of jumps of 10^2. Thus, this appears to correspond to the stage 2 processes in the resistivity experiments. If the theory of § 3 is applicable to these results, we have $Q = J = 0{\cdot}8$ for stage 1 and $Q = B+J = 1{\cdot}1$ for stage 2, so that the binding energy, B, of a vacancy in a trap is 0·3 ev.

An independent estimate of B can be made from a knowledge of the concentrations at which the reaction changes from stage 1 to stage 2.

The change should occur when the concentration of free vacancies in the lattice is given by

$$c \simeq \exp(-B/kT), \qquad (4)$$

since for concentrations much greater than this practically all traps are full and a stage 1 process must occur, and for concentrations much smaller than this many traps will be empty and the process will be of stage 2 type. From fig. 5 of the paper by Roswell and Nowick, and from the reported as-quenched concentration of vacancies ($2{\cdot}5\times10^{-4}$) we deduce the concentration of the latter at the change point in the reaction to be as follows :—

Temperature of annealing (°c)	80	69	60	51
Concentration ($\times10^{-5}$)	3	2·6	2·5	1·3

The value at 80°c, when substituted in eqn. (4), gives $B=0{\cdot}31$ ev in good agreement with our previous estimate. A further experimental check is possible ; taking $B=0{\cdot}31$ ev, we can calculate the expected change-point concentrations at the other annealing temperatures. The values thus deduced from eqn. (4) are 2·1, 1·6 and 1·2, at 69, 60 and 51°c, respectively, in fair agreement with the observed ones.

§ 5. Migration of Interstitialcies

We turn now to the other problem raised in § 2. If, after irradiation, the concentration of vacancies in the metal is c, then an interstitialcy wandering randomly in three dimensions ought to recombine with a vacancy after $(\alpha zc)^{-1}$ jumps on average, if the point defects are randomly distributed. This is typically about 10^3 to 10^4 jumps, whereas the experimental evidence yields values in the range 10^6 to 10^8.

It would thus appear necessary to postulate a repulsive force between the defects, to decrease the probability of recombination by a factor of about 10^3 to 10^4. But there is no obvious reason for such a force. An alternative view, which escapes this difficulty, is to suppose that the interstitialcy does not move freely in three dimensions but, at low temperatures at least, is constrained to move as a ' crowdion ' (Paneth 1950) along a line.

We shall consider briefly the possibility that the interstitialcy may be most conveniently accommodated in the lattice in the form of a crowdion in which $m+1$ atoms occupy m sites along a close-packed [110] row. Some preliminary calculations have been made of the probable length of such an array, using only the closed-shell interaction

$$V(r) \propto \exp[-14(a-r)/a]$$

between the copper ions, ignoring electrostatic and other terms which are important in determining the absolute energy of the arrangement but not, it is hoped, its length (cf. Huntington 1953). The result is that, without allowing any atomic displacements except in the close-packed row considered, the length is about six atoms ; the effect of relaxation

of neighbouring atoms is to increase this length and so it seems at first sight that a rather well-extended crowdion could exist in copper. The reason for this extent can easily be seen physically. The highest potential an ion experiences as a result of the lattice interaction occurs as it passes through a (110) plane, at a distance $(\sqrt{3}/2)a$ (a=atomic spacing) from four neighbours. The maximum force it experiences from the lattice corresponds to a distance of about $0{\cdot}9a$ from four ions. In view of the rapid rise of the exponential repulsion, this implies that the spacing in the row of ions cannot be less than about $0{\cdot}8a$, so we need at least about five atom spacings to accommodate the interstitial*. It is hoped to undertake more detailed calculations to investigate the relative energies of such crowdions and the configurations considered by Huntington. There is of course no tendency for a vacancy to spread out in this way, since in this case the forces imposed by the lattice would always exceed those in a close-packed row stretched beyond the usual lattice spacing.

The number of new sites visited by a defect while making n jumps diffusing through a lattice depends on whether the defect is free to move in three dimensions or in only one. In either case the probability distribution is approximately a Gaussian of half width $n^{1/2}$; in one dimension this contains only about $n^{1/2}$ sites, while in three dimensions it contains about $n^{3/2}$, so that in three dimensions, for large n, most visited sites are visited only once, whereas in one dimension the central sites are visited many times. Since the formation of a crowdion rather than a spherically symmetrical interstitialcy would confine the motion to a single row of atoms, we must now evaluate the mean lifetime of a crowdion in a given density of traps randomly distributed.

The crowdion starts at the origin, and performs a random walk with equal probability of moving left or right. The first traps along the line in each direction are assumed to be at x_1 and $-x_2$ respectively. The evaluation of the mean number of unit jumps before reaching one of the traps is precisely the ' problem of the gambler's ruin ' where the mean duration of a game between players with starting capital x_1 and x_2 is required. This is treated by Feller (1950) and the result is

$$\bar{n}(x_1x_2)=x_1x_2. \qquad (5)$$

The probability that the first traps lie at x_1 and x_2, in terms of the probability p that any site is a trap, is

$$p(x_1x_2)=p^2(1-p)^{x_1+x_2-1}.$$

The final mean number of jumps to reach a trap is thus

$$\bar{n}=\sum_{x_1=1}^{\infty}\sum_{x_2=1}^{\infty}x_1x_2\frac{p^2}{(1-p)}(1-p)^{x_1+x_2}$$
$$=\frac{p^2}{(1-p)}\left[\sum_{x=1}^{\infty}x(1-p)^x\right]^2$$

*Note added in proof: A detailed calculation by E. Fuess and H. Stumf, *Z. Naturforsch.*, 1955, **10a,** 136, confirms these figures.

since x_1 and x_2 are independent of each other. Thus, performing the summation,

$$\bar{n}=(1-p)/p^2, \qquad \ldots\ldots\ldots \quad (6)$$

which is effectively p^{-2} since p $(=\alpha zc)$ is very small.

Thus, if the density of interstitials and vacancies corresponds to $c=10^{-4}$ the mean number of jumps of the crowdion to destruction is of order 10^7, in agreement with observation. If this crowdion model is accepted, a second possibility arises for explaining those stage 2 processes which have well-defined activation energies. A crowdion may be trapped by a vacancy which lies a few atomic rows off its track, and subsequent movement of the vacancy to combine with it would require only a small number of jumps. To differentiate between this suggested mechanism for the stage 2 processes, and that described in § 3, experiments on materials containing controlled impurity additions would be helpful.

Acknowledgments

During the course of this work the authors were helped greatly by discussions with several members of the Metallurgy Division, Atomic Energy Research Establishment, Harwell, especially Mr. A. D. Le Claire, Dr. J. H. O. Varley, and Dr. M. J. Makin, and by correspondence with Dr. H. B. Huntington.

References

Brinkman, J. A., Dixon, C. E., and Meechan, C. J., 1954, *Acta Met.*, **2,** 88.
Broom, T., 1954, *Advances in Physics*, **3,** 26.
Clarebrough, L. M., Hargreaves, M. E., Michell, D., and West, G. W., 1952, *Proc. Roy. Soc.* A, **215,** 507.
Feller, W., 1950, *Probability Theory and its Applications*, Vol. I (New York : Wiley).
Huntington, H. B., 1942, *Phys. Rev.*, **61,** 325 ; 1953, *Ibid.*, **91,** 1092.
Johnson, R. P., 1939, *Phys. Rev.*, **56,** 814.
Jongenburger, P., 1953, *Phys. Rev.*, **90,** 710.
Kaufmann, J. W., and Koehler, J. S., 1955, *Phys. Rev.*, **97,** 555.
Overhauser, A. W., 1953, *Phys. Rev.*, **90,** 393.
Paneth, H., 1950, *Phys. Rev.*, **80,** 708.
Roswell, A. E., and Nowick, A. S., 1953, *Journal of Metals*, Sept., 1259.
Seitz, F., 1950, *Acta Cryst.*, **3,** 355 ; 1953, *Acta Met.*, **1,** 355.

LXXXII. *On the Thermal Expansion of Solids at Low Temperatures*

By T. H. K. Barron
Clarendon Laboratory, University of Oxford*

[Received February 5, 1955]

Abstract

Following recent experiments in which Grüneisen's γ was observed to decrease at temperatures below $0{\cdot}3\,\Theta$, an investigation is made of the variation of γ with temperature according to the lattice dynamics of Born and von Kármán. γ is defined as a function of T, and a general analysis applicable to all lattices is used to derive the low and high temperature limits γ_0 and γ_∞. By expressing γ as a quotient of power series in T^{-1} it is shown that the main variation between these limits occurs at temperatures of the order of $0{\cdot}2\,\Theta$. Calculations are carried out for a cubic close packed lattice with central forces between nearest neighbours; it is found that $\gamma_\infty-\gamma_0=0{\cdot}3$, and that the behaviour of γ is qualitatively similar to that found experimentally in monatomic metals. The amount of variation in γ is decreased when interaction between more distant neighbours is taken into account, and a model representing the heavier inert gas solids gives $\gamma\sim 3$ and $\gamma_\infty-\gamma_0\sim 0{\cdot}15$.

§ 1. Introduction

(a) *Account of previous work*

Gruneisen's rule states that at low temperatures the coefficient of thermal expansion α should be proportional to the specific C_v. This is known experimentally to be true for many crystalline solids over ranges of temperature below the Debye equivalent Θ, and has therefore been used in default of direct measurement to estimate the coefficients of expansion below 90°K. Recently, however, experiments by Bijl and Pullan (1954, 1955) on the thermal expansion of copper, aluminium and iron covered the range 20° to 90°K, and gave evidence of a breakdown in Grüneisen's rule at temperatures below $0{\cdot}3\,\Theta$. According to the later and more accurate experiments the expansion is less than that predicted by the theory. Since the breakdown occurred at temperatures too high for the conduction electrons to play much part, it was concluded that the explanation was to be found in the properties of the vibrational spectrum of the crystal.

In these experiments the thermal expansion changed the capacity in the tank circuit of a radio frequency oscillator, and so could be measured

* Communicated by Sir Francis Simon, F.R.S.

by finding the variation of the frequency with temperature. At higher temperatures this technique gave excellent agreement with earlier work, but there was at first no independent confirmation at the temperatures where Grüneisen's rule fails. However, the thermal expansion of copper in the range below 90°K has now been measured by an interferometric method (Rubin, Altman and Johnston 1954), and with this technique also the expansion at low temperatures was observed to be less than that predicted by Grüneisen's rule, though the amount of divergence was smaller than that found by Bijl and Pullan (1955). And so since this effect appears when either of these techniques is used, there can be little doubt that it is genuine.

According to Grüniesen's theory, the equation of state is

$$pV=-VE_0'(V)+\gamma_e E_T, \qquad (1)$$

where E_T and E_0 are the thermal and non-thermal contributions to the internal energy E, and γ_e is a slowly varying function of V characteristic of the solid. It follows thermodynamically that

$$\frac{\alpha}{\chi}=\left(\frac{\partial p}{\partial T}\right)_V=\frac{\gamma C_v}{V}, \qquad (2)$$

where χ is the compressibility and γ—for the moment—is the same as γ_e. Thus α is proportional to C_v at temperatures low enough for the variation in $\gamma\chi/V$ to be neglected; at higher temperatures—above $0{\cdot}2\,\Theta$, say—changes in α/C_v of the first order in $\Delta V/V$ are to be expected (Grüneisen 1926). If however Grüneisen's theory does not hold, γ and γ_e are not identical and functions of V only, but are distinct functions of both V and T defined by (1) and (2). The variation with temperature of either provides a measure of divergence from Grüneisen's rule, but the function γ is to be preferred in that it shows explicitly what is happening at each small increase of temperature. On the other hand, γ_e gives the total dilatation at each temperature, and so is more directly related to experiment. Both functions are considered in the present paper.

Grüneisen's theory can be derived from the assumption that, if ν_j is the frequency of the jth normal mode of vibration, the quantities

$$\gamma_j=-\mathrm{d}\log\nu_j/\mathrm{d}\log V \qquad (3)$$

are all equal (Slater 1939, p. 219). For most substances there is no reason to suppose that this is true. Bijl and Pullan (1954) give as an example a Debye model, in which there are two values γ_l and γ_t corresponding to longitudinal and transverse waves; these will be equal only if Poisson's ratio σ does not vary with the volume. At high temperatures all the modes are excited and Grüneisen's rule is obeyed with $\gamma=(2\gamma_t+\gamma_l)/3$, but at very low temperatures the value of γ is largely determined by the lower frequency transverse waves. It is found that γ increases or decreases with falling temperature according as $\mathrm{d}\sigma/\mathrm{d}V>$ or <0; the temperature range over which the effect takes place is rather high when compared with experiment.

This approximation was devised to illustrate the behaviour of monatomic crystals, and must be distinguished from the earlier approximation of Born (1923, p. 691) for the variation of γ in alkali halides. Born makes no distinction between longitudinal and transverse branches of the vibrational spectrum, but makes one instead between the acoustical and optical branches. His approximation amounts to replacing the contribution of the three acoustical branches by one Debye term, and each optical branch by an Einstein term, with separate γ's for each term. The characteristic frequencies of each term are suitable averages derived from the dynamical matrix of the lattice, and to this extent the model takes account of the true frequency spectrum.

(b) *Account of the present work*

Both of the models described above involve two approximations: the complicated spectrum of a periodic lattice is replaced by two or more simple components, and the γ_j within each of these components are replaced by an average value. In this paper a more general method will be developed which makes neither of these approximations and considers the actual lattice spectrum with the corresponding γ_j. Briefly it may be said that we are trying to do here for γ what Blackman (1934) did for Θ, when he explained deviations from Debye's specific heat law by analysing the frequency spectrum according to Born–von Kármán lattice dynamics. Since then detailed calculations of this type have explained variations in Θ for a number of simple crystals (see, for example, Leighton 1948), and we shall be able to make use of some of the methods and results of this work on specific heats in the course of our present work on expansion.

The general analysis, independent of the type of crystal, is given in § 2, in some detail because of its universal application. In particular, a full account is given of certain weighted averages of the γ_j, which can be derived from the moments of the frequency spectrum. These include as special cases the limiting values of γ at high and low temperatures, γ_∞ and γ_0; and they are also used to derive high temperature series expansions in T^{-1} for γ and γ_e. The form of these expansions shows that the main variation in γ is to be expected at temperatures of the order of $0{\cdot}2\ \Theta$.

In § 3 the general theory is applied to a specific model, a close packed cubic lattice with central forces between nearest neighbours. With such forces the problem becomes peculiarly simple, as the variation in γ is independent of the type of central force, and with data already available from a study of the specific heat of this lattice (Barron and Domb 1955) γ_0, γ_∞ and the high temperature expansions can all be obtained. It is found that γ decreases with falling temperature, with $\gamma_\infty - \gamma_0 = 0{\cdot}3$; the absolute value of γ depends on the force law. The high temperature expansions are used to draw curves showing the variation of γ and γ_e, which agree quite well with the experimental curves

of Bijl and Pullan both in the shape and in the temperature range of the variation. The amount of variation is however less than that found in the metals.

To account in detail for the behaviour of γ, models must be used in which the interatomic forces are as far as possible like those actually present in specific solids. For most substances this is even more difficult than the related problem of finding the variation of Θ, since knowledge is required of how the forces change with volume. However, the model of § 3 is known to reproduce fairly closely many of the properties of the frozen noble gases, and it can be improved if account is taken of interaction between more distant neighbours. This is done in § 4 for a number of different potentials of the Mie–Lennard-Jones type. For a potential of the form

$$-\lambda r^{-6}+\mu r^{-12},$$

it is found that $\gamma_\infty=3$ and $\gamma_\infty-\gamma_0=0{\cdot}15$, so that Grüniesen's rule should be obeyed fairly closely at all temperatures not too near the melting point. The effect of widening the potential well is to reduce the values both of γ and the difference $\gamma_\infty-\gamma_0$. When sufficient experimental data become available for comparison, additional information may thus be gained about the effective interatomic forces in the solid.

§ 2. General Theory

In the theory of Born and von Kármán (1912), a crystal of N atoms is treated formally as an assembly of $3N$ loosely coupled harmonic oscillators, having the frequencies ν_j of the normal modes of vibration (Slater 1939, p. 219). The equation of state is

$$pV=-VE_0'(V)+\sum_{j=1}^{3N}\gamma_j\frac{h\nu_j}{\exp(h\nu_j/kT)-1}, \quad . \quad . \quad . \quad (4)$$

and if the γ_j are all equal Grüneisen's eqn. (1) follows at once. If the γ_j are not all equal, then comparing (1) with (4) we have

$$\gamma_e=\sum_{j-1}^{3N}\gamma_j\frac{h\nu_j/kT}{\exp(h\nu_j/kT)-1}\Bigg/\sum_{j=1}^{3N}\frac{h\nu_j/kT}{\exp(h\nu_j/kT)-1}. \quad . \quad . \quad (5)$$

Similarly, comparing (2) with the thermodynamic equation

$$\frac{\alpha}{\chi}=\left(\frac{\partial S}{\partial V}\right)_T, \quad . \quad . \quad . \quad . \quad . \quad . \quad . \quad . \quad (6)$$

we have

$$\gamma=\sum_{j=1}^{3N}\gamma_j\frac{(h\nu_j/kT)^2\exp(h\nu_j/kT)}{[\exp(h\nu_j/kT)-1]^2}\Bigg/\sum_{j=1}^{3N}\frac{(h\nu_j/kT)^2\exp(h\nu_j/kT)}{[\exp(h\nu_j/kT)-1]^2}. \quad . \quad (7)$$

The ν_j and γ_j are functions of V, and change as the solid expands by amounts of the first order in the dilatation $\Delta V/V$. For most solids the dilatation is very small at temperatures below $0{\cdot}3\,\Theta$, and this effect can then be neglected in (5) and (7) compared with the direct change with temperature of the parameters $h\nu_j/kT$. But it must be born in mind that it becomes increasingly important at higher temperatures.

Another high temperature effect is the breakdown in the approximation of harmonic vibrations as the amplitude of the vibrations increases. A complete theory must consider these effects, but here we shall neglect both of them, and take (5) and (7) with ν_j and γ_j given by the static lattice.

At low enough temperatures Debye's rule is obeyed with an equivalent temperature Θ_0. Under these conditions Grüneisen's rule is also obeyed (Davies 1952) and γ and γ_e are both equal to the same value γ_0 ;

$$\gamma_0 = -\mathrm{d}\log\Theta_0/\mathrm{d}\log V. \qquad (8)$$

If the velocities of long acoustic waves in a given direction are $v_{(i)}$ $(i=1, 2, 3)$, then

$$\gamma_{(i)} = -\mathrm{d}\log(V^{-1/3}v_{(i)})/\mathrm{d}\log V \qquad (9)$$

and

$$\gamma_0 = \int\int\left(\sum_{i=1}^{3}\gamma_{(i)}v_{(i)}^{-3}\right)\mathrm{d}\omega \Big/ \int\int\left(\sum_{i=1}^{3}v_{(i)}^{-3}\right)\mathrm{d}\omega, \qquad (10)$$

where the integration is to be taken over all directions in the crystal. Alternatively, some approximation may be used in (8) for Θ_0, as for example in § 4.

At high temperatures γ and γ_e again tend to a common limit :

$$\gamma_\infty = \frac{1}{3N}\sum_{j=1}^{3N}\gamma_j. \qquad (11)$$

Since Grüneisen's rule (2) is deduced from (6), γ_∞ may be derived by differentiating $\Theta_\infty^{(S)}$, the Debye temperature giving the entropy at high temperatures :

$$\gamma_\infty = -\mathrm{d}\log\Theta_\infty^{(S)}/\mathrm{d}\log V\,; \qquad (12)$$

this is consistent with (11), since

$$k\Theta_\infty^{(S)} = \exp(\tfrac{1}{3})\,h\left(\prod_{j=1}^{3N}\nu_j\right)^{1/3N} \qquad (13)$$

Here $\Theta_\infty^{(S)}$ must be distinguished from Θ_∞, the Debye temperature giving the specific heat (Kelly and Macdonald 1953) ; the error involved in taking Θ_∞ in (12) will become clear later in this section.

To carry the analysis further, we define a set of weighted averages of the γ_j :

$$\gamma(s) = \sum_{j=1}^{3N}\gamma_j\nu_j^s \Big/ \sum_{j=1}^{3N}\nu_j^s = -\frac{1}{s}\frac{\mathrm{d}\log\mu_s}{\mathrm{d}\log V}, \qquad (14)$$

where

$$\mu_s = \frac{1}{3N}\sum_{j=1}^{3N}\nu_j^s. \qquad (15)$$

The μ_s are moments of the frequency distribution, and have often been used in the theory of specific heats. For some models they can easily be obtained in analytic form for small even integral values of s (Montroll 1942, 1943, Liebfried and Brenig 1953).

Comparing (14) with (10) and (11), we have

$$\gamma_0=\gamma(-3), \qquad \gamma_\infty=\gamma(0), \quad . \quad . \quad . \quad . \quad . \quad . \quad . \quad . \quad (16)$$

where $\gamma(-3)$ is taken as the limit of $\gamma(s)$ as $s\to-3$. If $\gamma(2)$, $\gamma(4)$, . . . , etc. are available from the even moments, then γ_∞ can then be estimated by interpolating for the function $\gamma(s)$. An example of this interpolation is shown in fig. 1. Since $k\Theta_\infty=h(5\mu_2/3)^{1/2}$ (Domb and Salter 1952), we have

$$-\mathrm{d}\log\Theta_\infty/\mathrm{d}\log V=\gamma(2), \quad . \quad . \quad . \quad . \quad . \quad . \quad . \quad . \quad (17)$$

Fig. 1

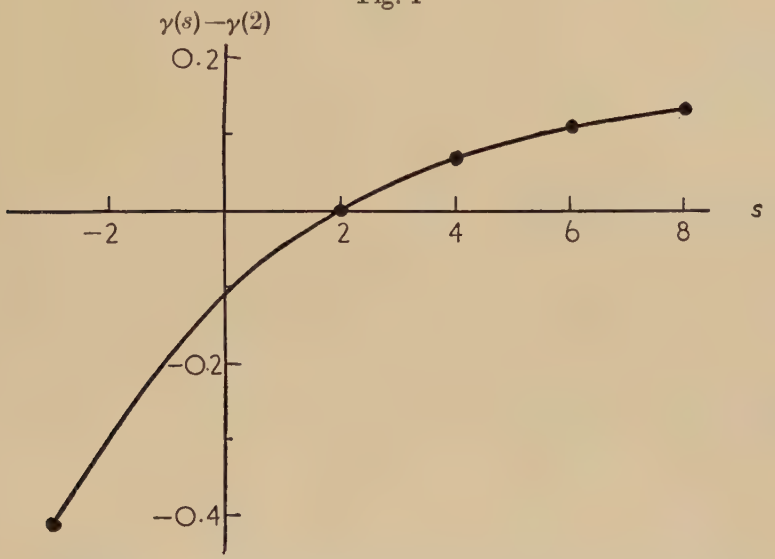

Estimation of γ_∞ by interpolation of $\gamma(s)$, for the model of § 3.

and so the error in taking Θ_∞ in place of $\Theta_\infty^{(S)}$ in (13) depends on the change in $\gamma(s)$ between $s=2$ and $s=0$.

The variation of γ at high temperatures can be obtained by expanding (5) and (7) as quotients of power series in T^{-1}. The series are like those of Thirring (1913) for the specific heat:

$$\gamma_e=\frac{\gamma_\infty-\frac{1}{2}\gamma(1)\mu_1\left(\frac{h}{kT}\right)+\sum_{s=1}^{\infty}(-1)^{s+1}\frac{B_{2s}}{(2s)!}\gamma(2s)\mu_{2s}\left(\frac{h}{kT}\right)^{2s}}{1-\frac{1}{2}\mu_1\left(\frac{h}{kT}\right)+\sum_{s=1}^{\infty}(-1)^{s+1}\frac{B_{2s}}{(2s)!}\mu_{2s}\left(\frac{h}{kT}\right)^{2s}}, \quad . \quad . \quad . \quad (18)$$

$$\gamma=\frac{\gamma_\infty+\sum_{s=1}^{\infty}(-1)^{s}(2s-1)\frac{B_{2s}}{(2s)!}\gamma(2s)\mu_{2s}\left(\frac{h}{kT}\right)^{2s}}{1+\sum_{s=1}^{\infty}(-1)^{s}(2s-1)\frac{B_{2s}}{(2s)!}\mu_{2s}\left(\frac{h}{kT}\right)^{2s}}, \quad . \quad . \quad . \quad . \quad . \quad . \quad . \quad (19)$$

where the B_{2s} are the Bernoulli numbers $B_2=\frac{1}{6}$, $B_4=\frac{1}{30}$, . . . , etc. The quotients can be in turn expressed as simple power series in T^{-1}, which

may be more rapidly convergent than either numerator or denominator considered separately.

It is useful also to express (18) and (19) in terms of the reduced moments

$$I(s)=\mu_s/\nu_m^s, \quad . \quad . \quad . \quad . \quad . \quad . \quad . \quad . \quad . \quad (20)$$

where ν_m is the upper limit of the frequency spectrum. Thus (19) becomes

$$\gamma=\frac{\gamma_\infty+2\sum_{s=1}^{\infty}(-1)^s(2s-1)\,\zeta(2s)I(2s)\gamma(2s)(h\nu_m/2\pi kT)^{2s}}{1+2\sum_{s=1}^{\infty}(-1)^s(2s-1)\,\zeta(2s)I(2s)(h\nu_m/2\pi kT)^{2s}}, \quad . \quad . \quad (21)$$

where the Bernoulli numbers have been expressed in terms of the Riemann Zeta function $\zeta(x)$.

Since $\zeta(2s)$, $I(2s+2)/I(2s)$ and $\gamma(2s+2)/\gamma(2s)$ all tend to unity as $s\to\infty$, the region of convergence of both series is

$$T>h\nu_m/2\pi k\sim 0{\cdot}2\,\Theta. \quad . \quad . \quad . \quad . \quad . \quad . \quad . \quad . \quad (22)$$

Marked variation of γ can therefore only be expected for temperatures of this order of magnitude.

It must be stressed, however, that this is only an order of magnitude; for example, the same argument applies also to the variation of C_v, which is quite marked up to about $0{\cdot}5\,\Theta$. The detailed variation of γ is a property of specific models. The continuum model of Bijl and Pullan gives a gradual variation of γ at temperatures rather high compared with experiment (see figs. 2 and 3). We shall next consider a simple model which takes the periodic structure into account.

§ 3. Application to a Simple Model

The analysis of § 2 is now to be applied to a cubic close packed lattice in which the only interactions are central forces between nearest neighbours. Many frozen gases possess this structure, and so do many metals, including two of the three examined by Bijl and Pullan; but the forces in even the simplest metals are more complicated than those in this model. It has been shown by Fuchs (1936) that central forces between ions in copper are important for the elastic constants, but there is also a large contribution from forces due to the conduction electrons. The present model is not put forward to explain the variation of γ in these particular substances, but as an example of a periodic lattice for which the problem can be solved exactly.

(*a*) *Derivation of γ_j for each mode*

Let the central forces be derived from an interatomic potential $f(r^2)$, where r is the distance between nearest neighbours. The wave number $\boldsymbol{q}$ of any plane wave is given by a point $(1/2\pi)(\alpha_1, \alpha_2, \alpha_3)$ of the reciprocal lattice (Leighton 1948), where

$$\boldsymbol{q}=\frac{1}{2\sqrt{2}\pi r}(\alpha_2+\alpha_3-\alpha_1, \alpha_3+\alpha_1-\alpha_2, \alpha_1+\alpha_2-\alpha_3). \quad . \quad . \quad (23)$$

By substituting a plane wave solution in the equations of motion of the lattice, according to the standard method of Born and von Kármán (see Blackman 1934), the squares of the frequencies of the normal vibrations of the lattice with wave number $\boldsymbol{q}$ are obtained as eigenvalues of the matrix

$$\lambda A+\mu y I, \quad . \quad . \quad . \quad . \quad . \quad . \quad . \quad . \quad . \quad (24)$$

where I is the unit 3×3 matrix, A is a 3×3 matrix with elements given cyclically by

$$\begin{aligned} A_{11}&=4-\{\cos\alpha_2+\cos\alpha_3+\cos(\alpha_1-\alpha_2)+\cos(\alpha_1-\alpha_3)\} \\ A_{23}&=\cos(\alpha_2-\alpha_3)-\cos\alpha_1, \quad . \quad . \quad . \quad . \quad . \quad . \quad . \quad . \quad . \quad (25) \end{aligned}$$

and

$$\begin{aligned} y=6-\{&\cos\alpha_1+\cos\alpha_2+\cos\alpha_3+\cos(\alpha_2-\alpha_3) \\ &+\cos(\alpha_3-\alpha_1)+\cos(\alpha_1-\alpha_2)\}, \quad . \quad . \quad . \quad . \quad . \quad (26) \end{aligned}$$

$$\lambda=r^2f''(r^2)/\pi^2M, \quad \mu=f'(r^2)/\pi^2M. \quad . \quad . \quad . \quad . \quad . \quad (27)$$

The term in μ has usually been neglected in determining the frequency spectrum (e.g. Leighton 1948), since it vanishes for a static lattice in equilibrium, and the frequencies are then all multiples of a single parameter $\lambda^{1/2}$. This is not permissible now that the effect of changing the volume is under consideration, since the derivative $\mu'\neq0$; and indeed for this model the variation of γ with temperature derives entirely from this term. The frequencies given by (24) are

$$\nu_{(i)}^2(\boldsymbol{\alpha})=\{\lambda x_{(i)}(\boldsymbol{\alpha})+\mu y\}, \quad . \quad . \quad . \quad . \quad . \quad (28)$$

where the $x_{(i)}$ are eigenvalues of A. The corresponding values of $\gamma_{(i)}$ are

$$\gamma_{(i)}(\boldsymbol{\alpha})=\tfrac{1}{3}\{-r^2\lambda'/\lambda-y/x_{(i)}\}, \quad . \quad . \quad . \quad . \quad . \quad . \quad . \quad (29)$$

since $\mu=0$ and $r^2\mu'/\lambda=1$; the dashes as usual denote differentiation with respect to r^2.

The first term in (29) is the same for all normal modes, and is dependent on the nature of the interaction between the atoms; it determines the value of γ for each substance. The second term is independent of the nature of the interaction, but is different for each mode and so gives rise to a variation of γ with temperature. It is always negative, and for any $\boldsymbol{\alpha}$ it varies inversely as $\nu_{(i)}^2$, so that it is larger for transverse waves than for the corresponding longitudinal waves. γ may therefore be expected to decrease with falling temperature.

(*b*) *The low temperature limit*

The matrix (24) can be expanded as an even power series in the q_i, and in the limit of long waves only the quadratic term is relevant. The eigenvalues then determine the three velocities of sound, $\nu_{(i)}/q$, in any direction.

Since in this region y/q^2 is independent of direction, $y/x_{(i)}$ varies as $(\nu_{(i)}/q)^{-2}$, and using eqn. (10) we have

$$(-r^2\lambda'/3\lambda)-\gamma_0=\frac{2}{3}\sum_{i=1}^{3}\int\int(x_{(i)}/q)^{-5/2}\,\mathrm{d}\omega \Big/ \sum_{i=1}^{3}\int\int(x_{(i)}/q)^{-3/2}\,\mathrm{d}\omega. \quad . \quad (30)$$

Most of the calculations required to evaluate this expression by numerical integration have already been carried out in a comparison of the specific heats of cubic and hexagonal close packed lattices (Barron and Domb 1955); (30) gives

$$\gamma_0=(-r^2\lambda'/3\lambda)-0{\cdot}907. \quad . \quad . \quad . \quad . \quad . \quad (31)$$

(*c*) *The weighted means* $\gamma(s)$ *and the high temperature limit*

The even moments μ_{2s} are homogeneous polynomials of degree s in λ and μ. Since $\mu=0$, in order to find

$$\gamma(2s)=\frac{1}{3s}r^2\mu'_{2s}/\mu_{2s} \quad . \quad . \quad . \quad . \quad . \quad . \quad . \quad (32)$$

only the coefficients of λ^s and $\lambda^{s-1}\mu$ are needed:

$$\mu_{2s}=a_s\lambda^s+b_s\mu\lambda^{s-1}+\ldots. \quad . \quad . \quad . \quad . \quad . \quad (33)$$

The moments can be calculated from the traces of powers either of the dynamical matrix (24) or of the $3N\times 3N$ secular matrix of the whole lattice. The second of these methods was used to obtain the values of a_s and b_s shown in table 1, which in turn were used to obtain the values of $(-r^2\lambda'/3\lambda)-\gamma(2s)$; the values of a_s agree with those given by Domb and Salter (1952).

Table 1

s	a_s	b_s	$(-r^2\lambda'/3\lambda)-\gamma(2s)$
1	4	6	0·50000
2	20	52	0·43333
3	114	402	0·39181
4	703	3096	0·36700

The high temperature limit γ_∞ is found by interpolating for $\gamma(s)$, using the calculus of finite differences; we find

$$\gamma(0)=(-r^2\lambda'/3\lambda)-0{\cdot}605, \quad . \quad . \quad . \quad . \quad . \quad . \quad . \quad (34)$$

where the error is not more than 2 in the last figure. The total change in γ is then

$$\gamma_\infty-\gamma_0=0{\cdot}302. \quad . \quad . \quad . \quad . \quad . \quad . \quad . \quad . \quad (35)$$

This interpolation is that shown in fig. 1 to illustrate the argument of § 2.

(*d*) *The high temperature series*

For this lattice the maximum frequency is known:

$$\nu_m=2\sqrt{2}\lambda^{1/2}. \quad . \quad . \quad . \quad . \quad . \quad . \quad . \quad . \quad (36)$$

It is therefore convenient to express (18) and (19) in terms of the reduced moments, as in (21). In the expression for γ_c, $\gamma(1)$ and $I(1)$ are found by interpolating according to Newton's forward difference formula:

$$\gamma(1)=(-r^2\lambda'/3\lambda)-0{\cdot}546, \qquad I(1)=0{\cdot}682. \quad . \quad . \quad (37)$$

The series are given in powers of $\sigma=h\nu_m/2\pi kT$:

$$\gamma_e=\gamma_\infty-0{\cdot}125\sigma-0{\cdot}095\sigma^2+0{\cdot}002\sigma^3+0{\cdot}045\sigma^4+0{\cdot}008\sigma^5$$
$$-0{\cdot}025\sigma^6-0{\cdot}008\sigma^7+0{\cdot}016\sigma^8+\ldots \quad (38)$$

$$\gamma=\gamma_\infty-0{\cdot}172\sigma^2+0{\cdot}065\sigma^4-0{\cdot}027\sigma^6+0{\cdot}013\sigma^8-\ldots; \quad (39)$$

Fig. 2

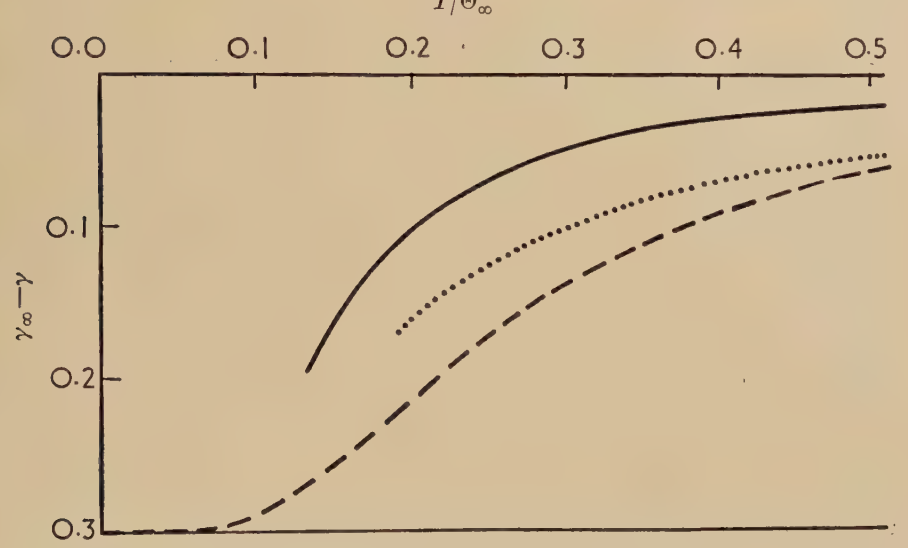

Theoretical deviations from Grüniesen's rule. ———— γ, nearest neighbour model; ..... γ_e, nearest neighbour model; – – – – – γ, continuum model.

Fig. 3

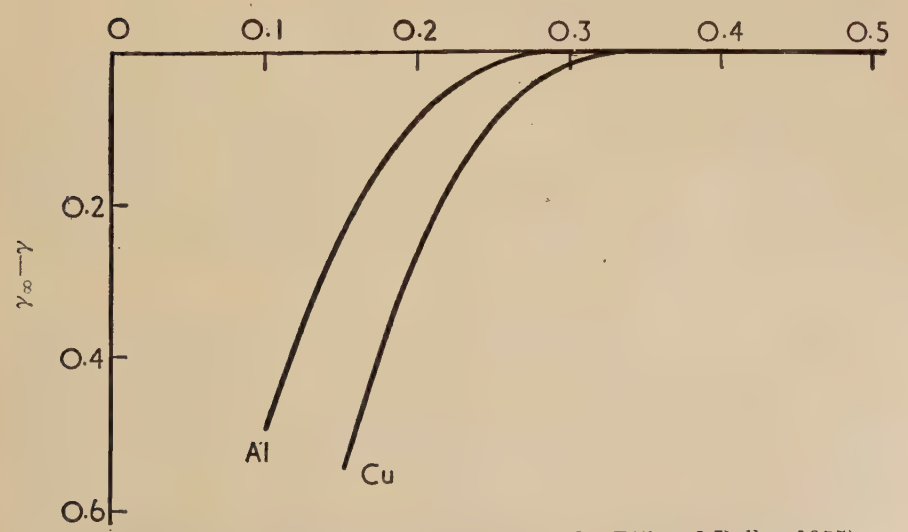

Experimental deviations from Grüniesen's rule (Bijl and Pullan 1955).

the last figure in each coefficient is unreliable, because of the uncertainty in the interpolations for $\gamma(0)$ and $\gamma(1)$. For $\sigma<0{\cdot}9$ and $\sigma<\sqrt{2}$ respectively, the series converge rapidly enough for calculation of γ_e and γ, whose variation in these ranges of temperature is shown in fig. 2. For comparison, the third curve shows the variation of γ in the continuum model for the same value of $\gamma_\infty-\gamma_0$.

(*e*) *Comparison with experiment*

The curves of fig. 3 show the variation of γ observed by Bijl and Pullan in copper and aluminium; both these metals have the same lattice structure as the model. In these curves the high temperature variation due to changes in volume has been eliminated by using the first order correction of Grüneisen, so that if Grüneisen's theory were valid γ would then be constant. This is not quite the same as the theoretical function of eqn. (29), which was obtained by neglecting the change in volume and so strictly refers to a solid under pressure at the volume V_0; but at worst their behaviour should differ only to the first order in $\Delta V/V$.

Rubin and his colleagues (1954) did not express their measurements of the thermal expansion of copper directly in terms of the variation of γ. A comparison of their figures with those of Bijl and Pullan shows that while they also find a decrease in γ at low temperatures, the amount of the decrease is only about one-half that found by Bijl and Pullan. Until both kinds of measurement have been repeated, the precise variation of γ is therefore uncertain.

However, both experiments reveal a behaviour qualitatively similar to that of our model: γ decreases towards low temperatures, the drop becoming sharp below about $0{\cdot}2\,\Theta$. The drop observed by Bijl and Pullan is much greater than that in the model, whose behaviour therefore agrees more closely with that observed by Rubin and his colleagues; although quantitative comparison with such an inadequate model is of little value.

On the other hand, the qualitative agreement is probably significant. We have found that even in a very simple model of a monatomic crystal γ varies at low temperatures, and that the temperature range in which this happens is the same as that in which variations have been observed experimentally. This supports the belief that variation of γ at these temperatures is a normal property of crystal lattices.

(*f*) *Approximations for* γ

The solution obtained for this model can be used to test approximate methods of calculating γ.

Grüneisen (Born 1923, p. 656) obtained γ by differentiating the frequency of vibration of one atom when all the others are kept fixed in their equilibrium positions. The square of this frequency is μ_2, so that the method gives $\gamma(2)$; this should usually be fairly close to γ_∞. It was used by Fröhlich (1937) for the alkali metals, with a Wigner–Seitz

model, but unfortunately the possible error in calculation was estimated to be of the order of $\frac{2}{3}$, probably much larger than $\gamma(2)-\gamma_\infty$.

Some other approximations, including the well-known (e.g. Slater 1939, p. 239)

$$\gamma=-\frac{2}{3}-\frac{1}{2}V\left(\frac{\partial^2 P}{\partial V^2}\right)_T\Big/\left(\frac{\partial P}{\partial V}\right)_T=-\frac{2}{3}+\frac{P_2}{P_1}, \quad . \quad . \quad (40)$$

rely on the assumption that Poisson's ratio is independent of volume, and take

$$\gamma=\tfrac{1}{2}\mathrm{d}\log(\chi/V^{1/3})/\mathrm{d}\log V; \quad . \quad . \quad . \quad . \quad . \quad (41)$$

here χ is the compressibility. This is reliable only to an order of magnitude, and gives for the present model

$$\gamma=(-r^2\lambda'/3\lambda)+\tfrac{1}{6}$$

larger than γ_0 by 1·07. However, the variation of the elastic constants with volume does in principle determine γ_0, and an approximation based on this will be developed in § 4.

§ 4. The Inert Gas Solids

The nearest neighbour model has been used so far only to illustrate the methods of the general analysis, and to give an example of the behaviour of γ in a simple crystal; it bears little resemblance to the metals investigated by Bijl and Pullan. But there is a class of solids—the frozen rare gases—in which central forces are known to be dominant, and to this the model may be reasonably applied. It can be improved, however, by considering the interaction between all pairs of atoms in the crystal, instead of between nearest neighbours only.

For this purpose it is convenient to take the interatomic potential of Mie, which has been shown (see, for example, Lennard-Jones 1924, Corner, 1948) to be a suitable approximation for the inert elements:

$$f(r^2)=(-\epsilon_0)\left\{-2\left(\frac{r_0}{r}\right)^6+\left(\frac{r_0}{r}\right)^{12}\right\}. \quad . \quad . \quad . \quad . \quad (42)$$

Analytic expressions can then be obtained for μ_2 and μ_4 from the $3N\times 3N$ secular matrix (Domb and Salter 1952, Liebfried and Brenig 1953), and these can be used to estimate γ_∞. The calculation of γ_0 is more difficult, since to use equation (8) Θ_0 is required as a function of V. The following method of approximation is indirect, but it is simple to use and is found satisfactory when tested on the nearest neighbour model.

We consider a polycrystalline form of the solid, in which the microcrystals are orientated at random. This is macroscopically isotropic, and its bulk and rigidity moduli determine the longitudinal and transverse velocities of sound. The approximation is to take Θ_0 as given by these velocities according to Debye's equation

$$\Theta_0=\frac{h}{k}\left\{\frac{9}{4\pi}\frac{N}{V}\right\}^{1/3}\left\{\frac{1}{v^3}+\frac{2}{v_t^3}\right\}^{-1/3} \quad . \quad . \quad . \quad . \quad . \quad . \quad (43)$$

But there is a further difficulty, since there is no simple way of finding rigorously the rigidity modulus G. There are however two approximations, due to Voigt and Reuss, for deriving G in terms of the elastic constants of a single crystal, and it has been shown by Hill (1952) that these give upper and lower limits G(V.) and G(R.) respectively. We make the further assumption that the corresponding values derived from (43) and (8) provide limits for Θ_0 and γ_0. This can be verified for the nearest neighbour model, where we find

$$\Theta_0 \Big/ \frac{h}{k}\left(\frac{r^2 f''(r^2)}{M}\right)^{1/2} = \begin{matrix} 0{\cdot}979 \text{ (Voigt)} \\ 0{\cdot}944 \text{ (Exact)} \\ 0{\cdot}928 \text{ (Reuss)} \end{matrix} \qquad \gamma_0 = (-r^2\lambda'/3\lambda) - \begin{matrix} 0{\cdot}78 \\ 0{\cdot}91 \\ 0{\cdot}99 \end{matrix} \qquad (44)$$

For interaction between all neighbours, we require then only the elastic constants of the single crystal, and the lattice sums needed to derive these from a potential of type (42) have already been calculated by Born and Misra (1940).

The results of calculations made for a number of different interatomic potentials are given in table 2. Approximate values for γ_∞ and γ_0 can now be obtained by analogy with the nearest neighbour model, taking

$$\gamma_0 = 0{\cdot}4\gamma_0(\text{V.}) + 0{\cdot}6\gamma_0(\text{R.}), \qquad \gamma_\infty = \gamma(2) - 1{\cdot}6\{\gamma(4) - \gamma(2)\}; \qquad (45)$$

the errors are likely to be of the order of $0{\cdot}2\{\gamma_0(\text{V.}) - \gamma_0(\text{R.})\}$ and $0{\cdot}2\{\gamma(4) - \gamma(2)\}$. These values for γ_0 and γ_∞ are shown in table 3, together with those given by the nearest neighbour model for the same potentials. It is some check on the approximations that $\gamma_\infty - \gamma_0$ should decrease with $\gamma(4) - \gamma(2)$.

Table 2

m	n	$\gamma(4)$	$\gamma(2)$	$\gamma(4)-\gamma(2)$	γ_0(V.)	γ_0(R.)
	6	1·5502	1·5433	0·0069		
4	8	1·9040	1·8939	0·0101		
	10	2·2515	2·2391	0·0124	2·216	2·173
	8	2·3325	2·3076	0·0249	2·215	2·131
6	10	2·6947	2·6649	0·0298		
	12	3·0473	3·0141	0·0333	2·882	2·783

Table 3

		Nearest neighbours		All neighbours		
m	n	γ_0	γ_∞	γ_0	γ_∞	$\gamma_\infty - \gamma_0$
4	10	2·093	2·395	2·19	2·22	0·03
6	8	2·093	2·395	2·16	2·27	0·11
6	12	2·760	3·062	2·82	2·96	0·14

Compared with the nearest neighbour model, γ_∞ is decreased and γ_0 increased, and the amount of variation in γ becomes steadily less as the well in the interatomic potential is widened; this effect depends more critically on m than on n. Another effect of widening the well is to decrease the value of γ, but here m and n are equally important; thus for the nearest neighbour model

$$\gamma_\infty=(m+n)/6+0{\cdot}06. \quad . \quad . \quad . \quad . \quad . \quad . \quad . \quad (46)$$

These two effects should provide a sensitive test of the validity of this model, if accurate measurements can be made of the thermal expansion at temperatures below $0{\cdot}3\,\Theta$, and should give additional information about the effective interatomic potential in the solid state of these elements.

For reasons discussed in § 2, the theory becomes less reliable at high temperatures, and also when there is large zero point energy; it is therefore best applied to the heavier inert elements at low temperatures. To fit properties of both gas and solid Corner (1948) found the best potential (42) to have $m=6$, $n=12$. This would give $\gamma_\infty=3$, with a slight decrease of about 0·15 in the range below $0{\cdot}3\,\Theta$. As yet no experimental results are available for comparison, except for three independent values for the density of solid argon, at 20°, 40°, and 83°K (Simon and von Simson 1924, de Smedt and Keesom 1925, Clusius and Weigand 1940); taking $\Theta=82$°K, within the limits of experimental error these are consistent with $\gamma=3$, but much more accurate data are required to test the theory rigorously.

§ 5. Conclusion

We have seen that variation of γ may be expected in the neighbourhood of $0{\cdot}2\,\Theta$ even in the simplest crystals, and that the type of variation may vary for different solids; indeed, it is quite likely that for some solids γ may increase as the temperature is lowered. Extrapolation, using Grüneisen's rule, is therefore not a reliable substitute for direct measurement of thermal expansion.

At the same time, the breakdown of Grüneisen's rule means that measurement of the thermal expansion provides temperature dependent information about the solid additional to that provided by the specific heat, in a temperature range where for most substances the anharmonicity of the lattice vibrations is small. This information may be useful in the detailed study of specific solids.

Acknowledgments

I wish to express my gratitude to Sir Francis Simon, F.R.S., for his interest; to Professor C. Domb for advice in the preparation of the manuscript; to Dr. D. Bijl and Dr. H. Pullan, both for drawing my attention to the problem and for communicating their results to me before publication; and again to Dr. Bijl for many helpful and illuminating discussions.

References

Barron, T. H. K., and Domb, C., 1955, *Proc. Roy. Soc.* A, **227,** 447.
Bijl, D., and Pullan, H., 1954, *Phil. Mag.*, **45,** 290; 1955, *Physica*, **21,** 285.
Blackman, M., 1934, *Proc. Roy. Soc.* A, **148,** 365.
Born, M., 1923, *Atomtheorie des festen Zustandes* (Leipzig : Teubner).
Born, M., and Misra, R. D., 1940, *Proc. Camb. Phil. Soc.*, **36,** 466.
Born, M., and von Kármán, T., 1912, *Phys. Z.*, **13,** 297.
Clusius, K., and Weigand, K., 1940, *Z. Phys. Chem.* B, **46,** 1.
Corner, J., 1948, *Trans. Faraday Soc.*, **44,** 914.
Davies, R. O., 1952, *Phil. Mag.*, **43,** 472.
de Smedt, J., and Keesom, W. H., 1925, *Commun. physic. Lab. Univ. Leiden.* **178.**
Domb, C., and Salter, L., 1952, *Phil. Mag.*, **43,** 1083.
Fröhlich, H., 1937, *Proc. Roy. Soc.* A, **158,** 97.
Fuchs, K., 1936, *Proc. Roy. Soc.* A, **157,** 444.
Grüneisen, E., 1926, *Handbuch der Physik*, **10,** 1.
Hill, R., 1952, *Proc. Phys. Soc.* A, **65,** 349.
Kelly, F. M., and Macdonald, D. K. C., 1953, *Canad. J. Phys.*, **31,** 147.
Leighton, R. B., 1948, *Rev. Mod. Phys.*, **20,** 165.
Lennard-Jones, J. E., 1924, *Proc. Roy. Soc.* A, **106,** 441, 463, 709.
Liebfried, G., and Brenig, W., 1953, *Z. Phys.*, **134,** 451.
Montroll, E. W., 1942, *J. Chem. Phys.*, **10,** 218; 1943, *Ibid.*, **11,** 481.
Rubin, T., Altman, H. W., and Johnston, H. L., 1954, *J. Amer. Chem. Soc.* **76,** 5289.
Simon, F. E., and von Simson, C., 1924, *Z. Phys.*, **25,** 160.
Slater, J. C., 1939, *Introduction to Chemical Physics* (New York : McGraw-Hill).
Thirring, H., 1913, *Phys. Z.*, **14,** 867.

LXXXIII. *Quench Hardening in Aluminium Single Crystals*

By R. Maddin*
The Johns Hopkins University, Baltimore, Md., U.S.A.
and
A. H. Cottrell
Department of Physical Metallurgy, University of Birmingham †

[Received February 13, 1955]

Summary

A large increase in the critical shear stress of high-purity aluminium single crystals can be achieved by water quenching, instead of furnace cooling, after annealing at a high temperature. This quench-hardening effect is insensitive to purity and is present in crystals of zone-refined aluminium. It increases rapidly with increase in the quenching temperature. The fully hardened state is reached, not instantly upon quenching, but only after ageing at room temperature. Various observations suggest that while quenching strains may be partly responsible for the hardening they cannot account for the whole effect, and that quenched-in vacancies also make an important contribution.

§ 1. Introduction

The purpose of the experiments described below was to alter the state of imperfection in single crystals of aluminium by means of heat treatment, and to examine the effect of this on the plastic properties of the crystals.

There is evidence for such effects in other materials. Blank (1930) showed that rock-salt crystals become hardened as a result of annealing at temperatures above 600°c, an observation recently confirmed by Pratt and Kear (1954). Li, Washburn and Parker (1953) showed that at room temperature the flow stress of zinc crystals rapidly cooled from 400°c exceeds that of slowly cooled ones by about 20%. These authors suggested that this hardening may be caused by quenched-in vacancies which either annihilate themselves on existing dislocations, and thereby cover the latter with jogs and make them more difficult to glide, or condense together to form loops of new, sessile dislocations which provide obstacles to slip.

* Visiting Lecturer in Physical Metallurgy, 1954, University of Birmingham.
† Communicated by the Authors.

Experiments on irradiation damage, in which point defects are created in crystals by bombardment with atomic particles, provide further evidence for this view. In a recent discussion of irradiation hardening in ionic crystals, Pratt (1955) has suggested that the irradiation process strips vacancies off dislocations, so causing the latter to climb out of their slip planes into less mobile orientations. As regards metals, Jamison and Blewitt (1953) observed that neutron irradiation raises the critical shear stress of copper crystals, and in a similar experiment by Kunz and Holden (1954 a, b) the yield stress of single crystals of iron was nearly doubled by neutron irradiation.

In the experiments described below, quenching from a high temperature was used. This has certain advantages as a means of introducing imperfections into a crystal. In the first place, unlike irradiation, the only point defects created in abundance by quenching are vacancies and there is no ' wastage ' of these by mutual annihilation with interstitials. Second, unlike cold-working, there is no large-scale creation of dislocations during quenching.

§ 2. Experimental Method

Four grades of aluminium were used :

(*a*) *Grade C*		
Commercial purity, 99·6% Al	Cylindrical rod	4·5 mm diameter
(*b*) *Grade S*		
High purity, 99·992% Al	Strip	2·2 mm × 11·5 mm
(*c*) *Grade P*		
High purity, 99·997% Al	(*a*) Cylindrical rod	2·5 mm diameter
	(*b*) Square section	3·0 mm square
(*d*) *Grade Z*		
Zone-refined*	Cylindrical rod	2·5 mm diameter

Special care was taken with the zone-refined metal to avoid contamination; degreasing and etching being used at each stage in the preparation of specimens. The square-section crystals of grade P were grown from the melt ; all others by the strain–anneal method. In the case of the zone-refined metal the crystals were supported during growth in boats of sintered high-purity alumina and sealed in evacuated fused silica tubes. The orientations of the crystals, shown in fig. 1, were measured by the back-reflection Laue method. Electropolishing was done in acetic acid and perchloric acid, or in methyl alcohol and nitric acid.

For heat treatment the crystals were suspended in a vertical tube furnace. Quenching was done by opening the lower end of the furnace and cutting the suspension wire, allowing the crystal to fall vertically onto a soft support in a quenching bath. The zone-refined crystals were wrapped tightly in thin foil of zone-refined aluminium during

* The zone refining was done on aluminium initially of 99·994% purity, using ten zone passes, by Mr. S. Marshall, University of Bristol.

annealing and quenching. Plain water and, occasionally, iced brine were used as quenching media. In certain cases, after quenching to room temperature, the crystals were immediately transferred to a bath of liquid air, the total time required to cool from the furnace temperature to liquid air being less than five seconds.

Fig. 1

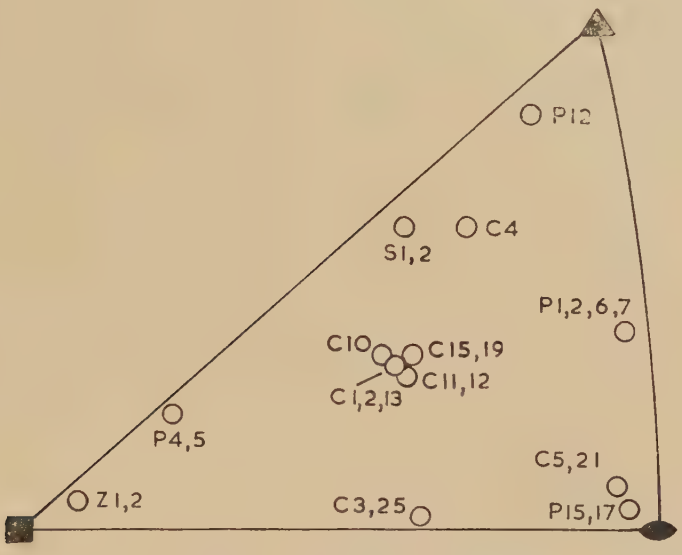

Stereogram of crystals investigated.
C Series 99·6% pure, S Series 99·992% pure, P Series 99·997% pure, Z Series zone-refined.

Except in certain cases mentioned below, each specimen was rested after being heat-treated, for one to four days at room temperature before testing. Most of the room temperature tests were made on specimens 3 to 4 cm long in a beam-type tensile apparatus at a tensile strain rate of 3×10^{-5} to 4×10^{-5} per second. Tests at a low temperature were made by bending, using a simple four-point loading jig immersed in a bath of liquid air, the load being applied by weights and pulleys and the deflection measured optically from mirrors lightly clamped to the ends of the crystal rod. Bending was used in place of tension to avoid the difficulty of mounting and aligning tensile grips on a specimen immersed in liquid air.

§ 3. Results

(*a*) *Effect of Quenching*

Two square-section crystals, numbered P1 and P2, were electropolished and heated at 600°c for one hour. One was then furnace-cooled and the other quenched in iced brine. After electropolishing they were

strained in tension at room temperature to give the stress–strain curves shown in fig. 2. The critical resolved shear stress was remarkably affected by the rate of cooling, being an order of magnitude greater for the quenched sample (518 gm/mm^2) than for the slowly cooled one (57 gm/mm^2). The work-hardening behaviour of the crystals was also affected, being greatly reduced in the quenched specimen ; the stress–strain curve of this specimen was in fact reminiscent of that of a highly alloyed crystal such as alpha brass. Consistent with this is the fact that the slip lines in this specimen, like those in alpha brass, were very long, sharp and straight, and showed prominent cross slip, whereas those in the furnace-cooled crystal were short and overlapped one another, like those usually regarded as typical of aluminium. Photographs of these bands are shown in fig. 3 (Plate 14).

Fig. 2

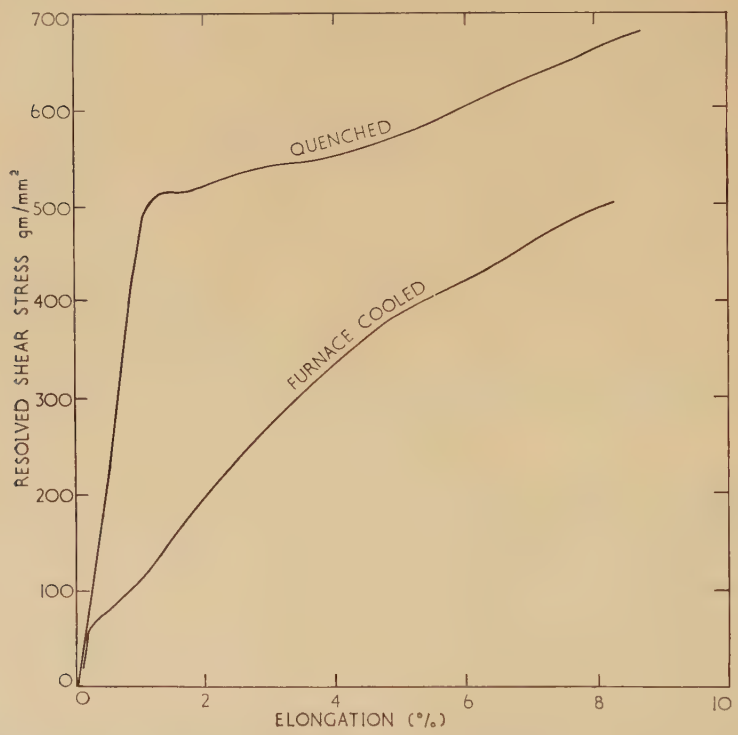

Stress–elongation curves for crystals P1 (furnace-cooled from 600°c) and P2 (quenched from 600° into iced brine).

(*b*) *Effects of Impurities*

The possibility that the quench-hardening effect was due in some way to surface contamination or oxidation during heat treatment was ruled out by the fact that the specimens were electropolished after this treatment. A further check on this point was provided by specimen P12 ;

after cooling in still air from 600°c, but before electropolishing, it was strained to its critical shear stress, which occurred at 325 gm/mm². After unloading and electropolishing it yielded again at the same stress, 325 gm/mm².

General contamination of the specimen during heat treatment was discounted because the hardening was not progressive with prolonged or repeated heating. For example, specimens C1 and C2, which were annealed at 600°c for one, and for twenty-four hours respectively before quenching, yielded at critical resolved shear stresses of 820 gm/mm² and 845 gm/mm², respectively. Another example is provided by specimens C10 and C12, each of which was heat treated (one hour at 600°c) and tested twice, once after furnace cooling and once after quenching. In C10 the furnace cooling was taken before the quenching, and the two critical resolved shear stresses thus obtained were 280 and 850 gm/mm², respectively. In C12, the quenching was taken before the furnace cooling, and the two values in this case were 840 (quenched value) and 280 gm/mm² respectively.

The effect of initial impurities was examined by comparing the quenching effect in the four grades of aluminium. Results are shown in table 1.

Table 1. The Critical Shear Stresses of Aluminium Crystals after Slow and Fast Cooling from 600°c

Grade of aluminium	99·6%	99·992%	99·997%	Zone-refined
Critical shear stress, σ_f, after furnace cooling, gm/mm²	280 (Average of C10, C11, C12, C13)	55 (S2)	55* (Average)	58 (Z1)
Critical shear stress, σ_q, after quenching, gm/mm²	840 (Average of C1, C2, C10, C12)	350 (S1)	605 (Average of P2, P5)	280 (Z2)
$\sigma_q - \sigma_f$	560	295	550	222
σ_q / σ_f	3·00	6·4	11·0	4·85

* Results of Paxton and Cottrell (1953).

Although there is variation from one grade to another, quenching has a strong effect in all and does not vary systematically with purity. This fact, together with general considerations of the smallness of alloy hardening in the purer grades of aluminium, renders an explanation of the quenching effect in terms of impurities unlikely. The low value of σ_q for the zone-refined specimen may be due to a slower rate of

quenching caused by the aluminium foil wrapping. The low value for specimen S1 may be connected with its different cross section, as discussed in § 3 (*c*).

(*c*) *Effects of Various Heat Treatments*

Two other possible causes of the quench-hardening effect—quenching strains, and quenched-in thermal disorder—were next considered. Quenching strains could conceivably harden the material by introducing internal stresses and localized plastic flow. Several possibilities exist for quenched-in thermal disorder. In the first place, a dislocation line held in a crystal at a given temperature should possess, in thermal equilibrium, a certain number of jogs. This number decreases exponentially with decreasing temperature so that, by quenching with sufficient speed from a high temperature, it may be possible to retain quenched-in jogs on dislocations, which would then provide a frictional force resisting the glide motion of the dislocations at room temperature. Another possibility is that suggested by Li, Washburn and Parker (1953), and by Pratt (1955) ; excess vacancies, retained during the quench, migrate at room temperature to dislocations, where they form atmospheres or jogs, or cluster together to form voids or rings of sessile dislocations.

The hypothesis of quenching strains is rather favoured by the fact that the strip crystal (S1) hardened less than those of circular or square cross section. On the other hand, the plastic elongation needed to raise the flow stress of a furnace-cooled crystal to that of a quenched one was, according to fig. 2, about 0·072 ; quenching strains could hardly produce a comparable plastic deformation in view of the fact that the total linear thermal shrinkage of aluminium from 600°c to room temperature is only about 0·013. Furthermore, specimen P12, which was cooled in still air after one hour at 600°c, gave a critical shear stress of 325 gm/mm². This value, although much smaller than those obtained after water quenching (average 605 gm/mm²), is much larger than those obtained after furnace cooling (average 55 gm/mm²) and it is difficult to believe that quenching strains could exert such a large effect in a small air cooled crystal of a highly conducting metal. The fact that air-cooling gave a smaller hardening than water quenching could be explained either in terms of quenching strains or, using quenched-in disorder, in terms of an *effective* quenching temperature, less than 600°c, which became lower as the rate of cooling was reduced.

Three further attempts were made to obtain a clear separation of the contributions of quenching strains and quenched-in disorder to the hardening. In the first, the effect of the quenching temperature upon the intensity of hardening was studied. Crystals of grade C aluminium were heated for one hour at each of a series of temperatures and then water-quenched. The results, which are shown in table 2, failed to give a clear answer. They could be interpreted as showing either, on the quenching strains theory, a linear increase of stress with temperature

above 200°C, or, on the quenched-in disorder theories, an exponential increase of stress with temperature up to about 400°C, above which levelling out begins because the effective quenching temperature lags increasingly behind the actual one.

Table 2. The Effect of Quenching Temperature

Specimen number	C11	C19	C21	C25	C3	C4	C5	C2
Quenching temperature, °C	Furnace-cooled from 600°C	100	200	250	300	400	500	600
Critical shear stress, gm/mm²	280	288	296	400	424	597	649	840

In the second experiment two square-section crystals (P6 and P7) were quenched into agitated brine at +50°C, one down-quenched from +290°C and the other up-quenched from −190°C. No ice was observed to form on the up-quenched crystal. The critical shear stresses measured at +50°C after these treatments were 178 gm/mm² (down-quenched crystal) and 71 gm/mm² (up-quenched crystal). These results clearly favour quenched-in disorder rather than quenching stresses, since up-quenching should have a negligible effect according to the first view, and be nearly as effective as down-quenching according to the second one.

The third experiment was based on the idea that if quenched-in vacancies are the cause of hardening, the fully hardened state is established, not immediately after quenching, but only after a certain time has elapsed, sufficient for the vacancies to migrate to one another or to dislocations. Experiments to study this were made by quenching specimens from 600°C into iced brine and testing them at room temperature within a few minutes of quenching. Specimen C15, treated in this way, gave a critical stress of 595 gm/mm², instead of the 840 gm/mm² obtained by resting a similarly quenched crystal for a few days at room temperature before testing. Similarly, specimen P4, tested within fifteen minutes of quenching, gave a critical stress of 575 gm/mm², whereas its companion, P5, taken from the same crystal but rested a few days before testing, gave a value of 690 gm/mm². Quenching is thus followed by age hardening, in agreement with the vacancy hypothesis.

To examine this effect further some crystals were quenched to room temperature and then immediately transferred to a bath of liquid air, in which their critical resolved shear stresses were measured by bending. Specimen P15, treated in this way and tested immediately, gave a

critical stress of 400 gm/mm^2. By comparison, specimen P17, rested for two hours at room temperature after quenching and before cooling to liquid air, gave a critical stress in liquid air of 740 gm/mm^2. Again the material is softer in the freshly quenched state than in the quenched and aged state. Although these results support the vacancy theory they do not completely rule out the theories of quenching strains and of quenched-in jogs, since the freshly quenched specimens are also fairly hard. This immediate hardening could be caused by quenching strains, by quenched-in jogs, or by a partial condensation of the vacancies during quenching. A technique for faster quenching is needed to explore this point further.

§ 4. Discussion

The evidence presented above favours the condensation of quenched-in vacancies as the cause of part, at least, of the hardening produced by quenching. Condensation on existing dislocations appears to be the more important process in this particular case, rather than the clustering of vacancies, since the slip lines become longer and coarser after quench hardening. This coarsening of slip is to be expected when the *nucleation* of a slip band is made more difficult, e.g. by the formation of jogs on dislocations in Frank–Read sources, whereas when the *growth* of slip lines is made more difficult, e.g. by dispersed obstacles such as voids or rings of sessile dislocations, the slip lines ought to become shorter, finer and more numerous. Consistent with this view is the fact that the rate of work hardening in the quenched crystal is low ; a low rate is typical of materials such as alpha brass in which nucleation of slip is difficult.

The resistance to movement of jogs on screw dislocations is well known. That a jog on an edge dislocation is also difficult to move can be seen in the following way. The atomic structure on the expanded side of an edge dislocation resembles, in the re-entrant corner of a jog, a vacant atomic site. Each time the jog moves with the gliding dislocation by one atomic spacing, the ' vacancy ' at the jog makes one jump and the energy of activation, J, for this jump is dissipated. If the spacing of jogs along the dislocation is l the stress needed to move the dislocation rapidly, i.e. without help from thermal fluctuations, is approximately J/b^2l, where b is the length of the Burgers vector. Very roughly, one may say that the drag of a jog is due, in the case of a screw dislocation, to the energy needed to form vacancies, and in the case of an edge dislocation, to the energy needed to move vacancies.

Acknowledgments

The authors are pleased to acknowledge the help of Mr. P. H. Thornton and Mr. M. A. Claridge in the experiments on the commercial purity aluminium. The advice and help of Dr. C. D. Graham, Jr. and Mr. R. J. Stokes are greatly appreciated. Many useful discussions with Dr. P. L. Pratt aided materially to the analysis of the data. The zone-refined

Fig. 3 (*a*)

Fig. 3 (*b*)

Fig. 3 (*c*)

(*a*) slip lines (×340) on crystal P1 after an elongation of 7·2%;
(*b*) slip lines (×340) on crystal P2 after an elongation of 7·5%;
(*c*) as (*b*) but ×1000.

aluminium was kindly given by Professor F. C. Frank and Mr. S. Marshall, University of Bristol.

The authors would like to thank the University of Birmingham and The Johns Hopkins University for arranging the exchange lectureship for one of them (R. M.).

References

Blank, F., 1930, *Zeit Phys.*, **61,** 727.

Jamison, R. E., and Blewitt, T. H., 1953, *Phys. Rev.*, **91,** 236.

Kunz, F. W., and Holden, A. N., 1954 a, *Phys. Rev.*, **94,** 1417 ; 1954 b, *Acta Met.*,**2,** 816.

Li, Choh Hsien, Washburn, J., and Parker, E. R., 1953, *Trans. Amer. Inst. Min. Met. Engrs*, **197,** 1223.

Paxton, H. W., and Cottrell, A. H., 1954, *Acta Met.*, **2,** 3.

Pratt, P. L., 1955, *Report of* 1954 *Bristol Conference* (London : Physical Society).

Pratt, P. L., and Kear, B. H., 1954, private communication.

LXXXIV. *The Specific Heats of Magnesium and Zinc*

By P. L. Smith
Clarendon Laboratory, Oxford *

[Received March 5, 1955]

Abstract

Specific heat measurements have been made on magnesium from 1°K to 20°K and on zinc from 4°K to 20°K. The magnesium data agree with the most recent measurements above 15°K, whilst the results on zinc confirm one set of earlier data.

The shape of the curve of the Debye θ versus temperature for magnesium is found to be similar to that for beryllium. The θ value rises from a constant value of 326° above 30°K to 406° at absolute zero. The θ value for zinc rises much more sharply from a value of 195° at 20°K to 291° at absolute zero.

§ 1. Introduction

The specific heat of magnesium has been measured by Craig *et al.* (1954), Clusius and Vaughen (1930) and Friedberg and Estermann (1952). The latter authors' work is in the helium range only, while the other measurements extend down to 12°K. Comparison of the values of the Debye θ at 4°K and 12°K shows that it must reach a maximum before attaining the value of 342° at the absolute zero. This would contrast strongly with the behaviour of beryllium, and further investigation was felt to be warranted.

Measurements on zinc are more complete. The more recent data are those of Daunt and Silvidi (1950) and Keesom and v. d. Ende (1932) and Clusius and Harteck (1928). At 20°K, however, the data given in the latter two references disagree by about 15%, so that some experiments to clarify the position were desirable.

The axial ratio of the magnesium lattice is 1·623, whilst the ratio for close-packed spheres is 1·633. The zinc lattice, however, has an axial ratio of 1·856 and its lattice may be considered as approaching a layer type structure. Thus the representation of the specific heat by one value of a Debye θ may be expected to be less applicable for zinc than for magnesium.

The present measurements agree with those of Keesom and v. d. Ende in the case of zinc and, on correcting for the electronic term, a sharp rise of about 50% in the value of the Debye θ is found. The data on magnesium give a higher value of the Debye θ at absolute zero than that given by Estermann and Friedberg, and the variation of θ with temperature is

* Communicated by the Author.

found to be very similar to the variation found for beryllium. When a correction for the electronic specific heat is made to the C_v values of Craig *et al.*, it is found that the specific heat of magnesium above 30°K is closely represented by a Debye θ of 326°.

§ 2. Experimental

The magnesium was measured in a calorimeter similar to that described by Parkinson *et al.* (1951), except that it was fitted with a phosphor bronze thermometer in place of the leaded brass wire. The measurements extend from 1·3°K to 20°K.

A different technique was employed for zinc. A high purity sample was put at the author's disposal by the Metallurgy Department, University of Oxford, was fitted with a heater and a thermometer and suspended in the working space of a conventional Simon expansion helium liquefier. The method of measurement and thermometer calibration is the same as that described by Hill and Smith (1953) and will not be enlarged upon here.

§ 3. Results

(*a*) *Magnesium*

The heat capacities in the range 1°K to 20°K are shown in fig. 1. A plot of C/T *vT*^{2} is also given in fig. 2, showing that the electronic term is $3{\cdot}15\times10^{-4}$ cal mol^{-1} deg^{-2}. The θ value taken for the slope of this line is 406°, with an uncertainty of ±10°K. The lattice specific heat is at 2°K less than one-tenth of the total measured and it is impossible to assign a greater precision to the Debye θ.

(*b*) *Zinc*

The measurements of Keesom and v. d. Ende are in good agreement with those of Daunt and Silvidi below 4°K, and it was considered unnecessary to extend the present measurements below 4°K. The specific heat values given here join smoothly on to those of Daunt and Silvidi and are in good agreement with the Leiden work in the whole range 4°K to 20°K. The results of Clusius and Harteck lie above the present values at 12°K and are 15% lower at 20°K. The results of the latter authors above 25°K, however, appear to fit smoothly on to the present data. It is impossible to derive a value of the electronic term from the data above 4°K since the lattice specific heat is already out of the T^3 region. The measured values are shown in fig. 3.

§ 4. Discussion

(*a*) *The lattice specific heats*

(i) *Magnesium.* Given the electronic specific heat and the value of the correction for C_p-C_v, the true value of the lattice specific heat is found, from which θ may be calculated. The θ values for magnesium taken from the present work are given in the table with those found by Craig *et al.*, corrected for the electronic contribution. Even in the region of $T=\frac{1}{2}\theta$

Fig. 1

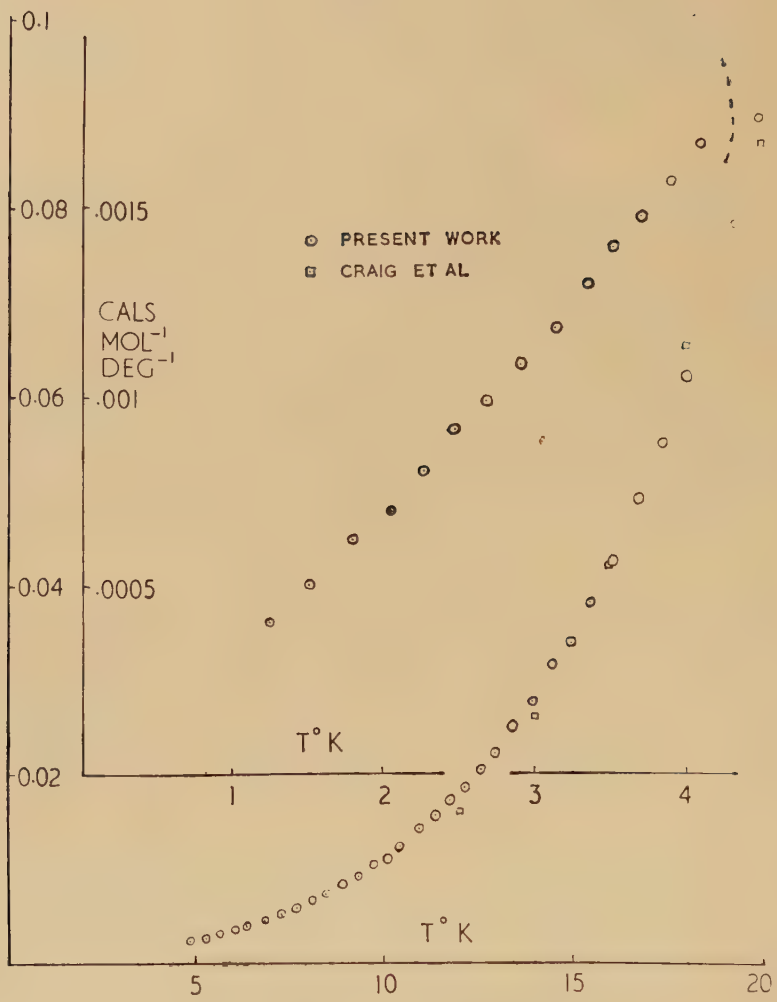

The specific heat of magnesium.

Fig. 2

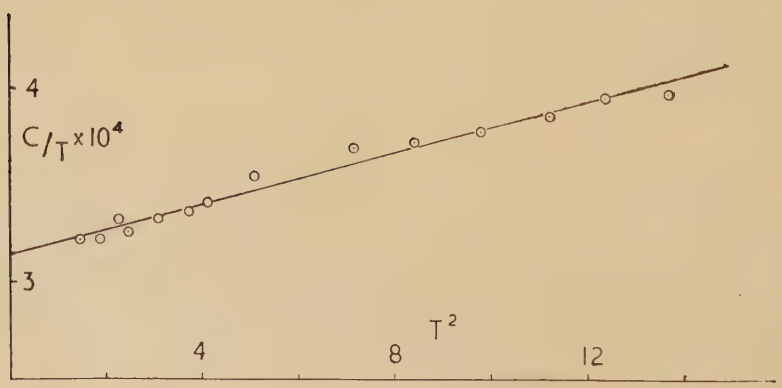

C_p/T against T^2 for magnesium.

the electronic term markedly affects the θ value since the Debye function in this range is very sensitive to small changes in C_v. It is, however, seen that above 30°K the lattice specific heat of magnesium is closely represented by the Debye model with a $\theta_D = 327°$.

Fig. 3

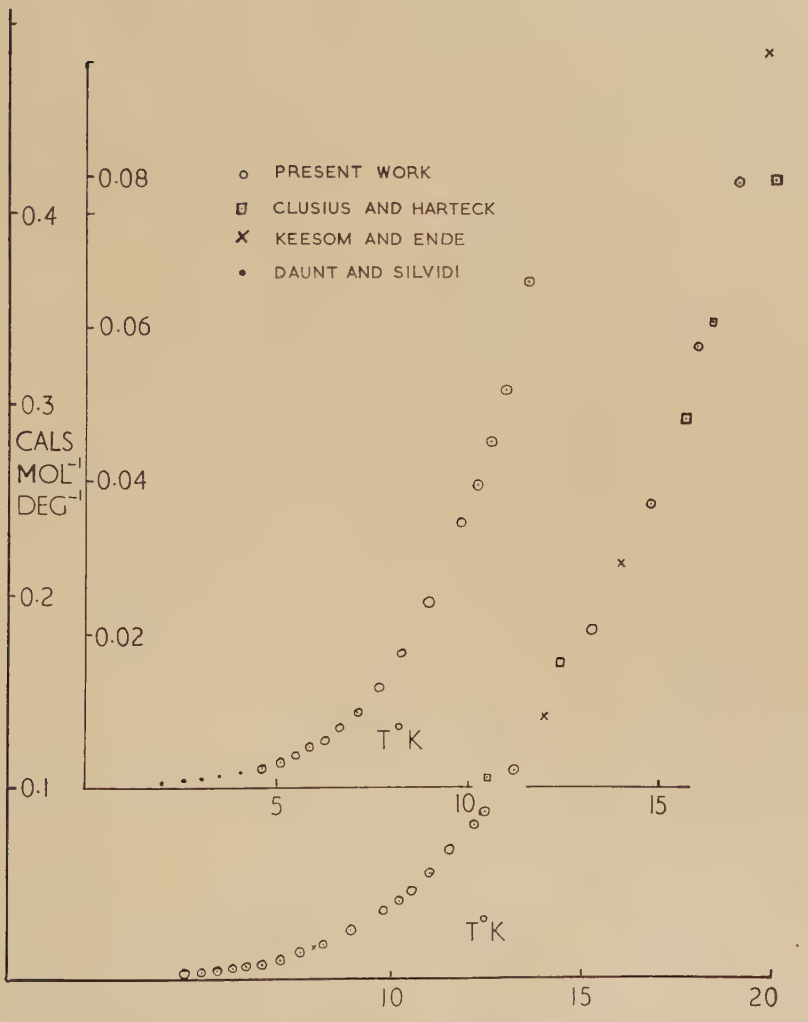

The specific heat of zinc.

(ii) *Zinc.* This metal presents a strong contrast to magnesium. Taking the present data together with those of Clusius and Harteck above 26°K, and using Daunt and Silvidi's value of $1{\cdot}50 \times 10^{-4}$ cal mol^{-1} deg^{-2} for the electronic term, values of θ are found which show a marked fall from 291°

at 4°K to 194° at 20°K. At 90°K the θ value has risen to 243°, but it falls to 220° at 180°K. The work of Clusius and Harteck on zinc, however, dates from 1928, and it must be borne in mind that the precision of their data will not equal that obtained by Craig *et al.* on magnesium.

The θ values for the two metals are given in the table, but comparison of the two is best effected by plotting a reduced θ–T curve, i.e. θ/θ_∞ versus T/θ_∞ for each metal. This has been done in fig. 4 together with corresponding values for beryllium, using $\theta_\infty = 220°$ for zinc, 326° for magnesium and 920° for beryllium.

The Debye Characteristic Temperatures for Magnesium and Zinc

T	Mg	Zn	*T*	Mg	Zn
0	406	306	25	342	209
4	406	300	30	334	209
6	400	280	40	326	216
8	393	250	50	325	220
10	389	235	75	325	236
12	383	220	100	327	244
16	372	207	125	326	228
20	355	195	150	327	220

Fig. 4

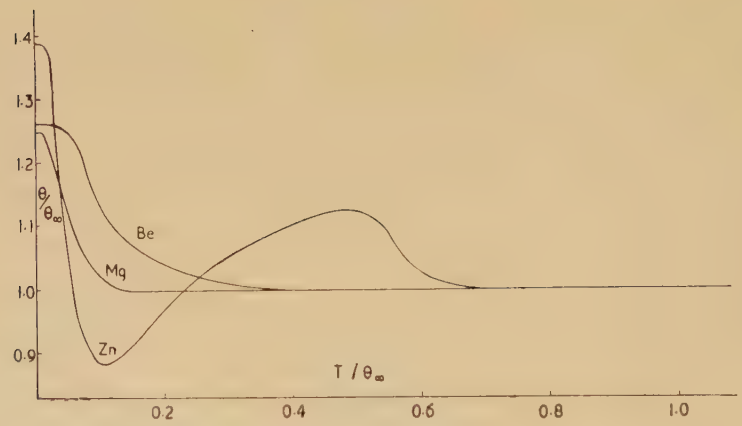

Reduced Debye θ's against reduced temperature.

With an axial ratio of 1·623, magnesium closely approximates to the ideal hexagonal lattice of close-packed spheres (c/a = 1·633). The reduced θ–T curve for magnesium is very similar in shape to the reduced θ–T curve given by Leighton (1948) for the face centred cubic lattice. Leighton predicts a change in θ of about 17%, whilst for magnesium a change of 20% is observed. Here, however, the resemblance ceases since if an attempt is made to calculate Leighton's parameter β, using room temperature elastic data, a value of β equal to 129° is found. This

leads to a value of θ/β of 3·1 against Leighton's value of 2·09 for the face centred lattice at that absolute zero. It seems apparent, therefore, that calculations for the face-centred lattice may not be applied even to a nearly ideal hexagonal lattice.

It is interesting to note that a value of $\theta=390°$ for magnesium has been predicted by Kohler (1939) from the low temperature elastic constants. Room temperature elastic data for zinc have been used by Honnefelder (1923) to determine a value of 305° for θ. If, however, the low temperature elastic data were to be used, the θ value would undoubtedly be higher.

Thus, whilst the anisotropy of the zinc lattice (c/a=1·856) is strongly reflected in the sharp drop in θ, it appears that a genuine T^3 region is reached at the lowest temperatures for both magnesium and zinc, and that moreover the thermal θ value agrees fairly well with that determined from the elastic constants.

(*b*) *The electronic specific heats*

The value of $3{\cdot}15\times10^{-4}$ cal mol^{-1} deg^{-2} for the temperature coefficient of the electronic specific heat of magnesium is lower than that given by Estermann and Friedberg. The free electron value of this coefficient, γ, is given in the same units by $3{\cdot}26\ (A/\rho)^{2/3}\ n^{1/3}\times10^{-5}$ where A is the atomic weight, ρ the density and n the number of electrons per atom. This value for magnesium is $2{\cdot}38\times10^{-4}$. The corresponding values for beryllium are in contrast to these, since the measured value of γ is less than half the calculated value. An explanation of this is to be found by considering the Brillouin zone for the hexagonal lattice, described, for example, by Hume-Rothery (1948). For an axial ratio less than that for close-packed spheres (1·633), the density of states rises sharply after a minimum caused by the overlap of the s and p bands. The Fermi surface for beryllium occurs just at this minimum, whilst for magnesium it occurs beyond it. Owing to the sharp rise in the curve of the density of states, $N(E)$, as a function of the energy E, the density of states at the Fermi surface for magnesium is considerably greater than that for beryllium, giving a correspondingly higher value for γ.

In the case of zinc, a γ value of $1{\cdot}5\times10^{-4}$ cal mol^{-1} deg^{-2} is less than the free electron value for this metal ($1{\cdot}72\times10^{-4}$ cal mol^{-1} deg^{-2}), showing that the Fermi surface for zinc occurs at a point where the density of states curve falls below the free electron value. Since the axial ratio of the zinc lattice is much greater than 1·633, the p states overlap the s states in an essentially different manner from the overlap for magnesium and beryllium. The $N(E)$ curve is believed to have no steep proportion in the region of the Fermi surface.

Acknowledgement

The author is indebted to the Department of Scientific and Industrial Research for a maintenance grant, during the tenure of which this work was carried out.

References

Clusius, K., and Harteck, P., 1928, *Zeits. fur Phys. Chem.*, **134**, 243.
Clusius, K., and Vaughen, J. V., 1930, *J. Amer. Chem Soc.*, **52**, 4686.
Craig, R. G., Krier, C. A., Coffer, L. W., Bates, E. A., and Wallace, W. E., 1954, *J. Amer. Chem. Soc.*, **76**, 238.
Daunt, J. G., and Silvidi, A. A., 1950, *Phys. Rev.*, **77**, 125.
Estermann, I., Friedberg, S. A., and Goldman, J. E., 1952, *Phys. Rev.*, **87**, 582.
Hill, R. W., and Smith, P. L., 1953, *Phil. Mag.*, **44**, 636.
Honnefelder, K., 1933, *Zeits. fur Phys. Chem.*, B **21**, 53.
Hume-Rothery, W., 1948, *Atomic Theory for Students of Metallurgy* (London : Institute of Metals).
Keesom, W. H., and v. d. Ende, J. N., 1932, *Leid. Comm.* 219 b and *Proc. Roy. Soc. Amsterdam*, **35**, 143.
Kohler, M., 1939, *Ann. der Phys.*, **36**, 227.
Leighton, R. B., 1948, *Rev. Mod. Phys.*, **20**, 105.
Parkinson, D. H. Simon, F. E., and Spedding, F. H., 1951, *Proc. Roy. Soc.* A, **207**, 137.

LXXXV. *The Specific Heats of Lithium Fluoride, Sodium Chloride and Zinc Sulphide at Low Temperatures**

By Douglas L. Martin†
Department of Physics, Queen Mary College, University of London ‡

[Received March 8, 1955]

Abstract

The specific heats of lithium fluoride, sodium chloride and zinc sulphide have been measured within the temperature range 2°K to 30°K using a calorimeter of a novel type, upon which the crystal specimens were stuck with silicone grease. Ideally, these three substances have only a lattice contribution to their specific heats so that a direct comparison of the results with the theoretical predictions of the lattice theory of specific heats is possible. Good agreement between theory and experiment is found. The existence of a 'T^3' region extending up to a temperature of about 20°K is shown clearly in the case of lithium fluoride.

§ 1. Introduction

The specific heats of lithium fluoride, sodium chloride and zinc sulphide are all of interest because ideally the only contribution to their specific heat is that due to the lattice, so that a direct comparison is possible between the experimental results and the theoretical predictions of the lattice theory of specific heats. Such a comparison is made more significant because these salts have comparatively high Θ_D values. They are also of interest individually for other reasons. Previous measurements by Clusius and co-workers (Clusius 1946, Clusius, Goldman and Perlick 1949) had shown that lithium fluoride has the greatest variation of Θ_D over the Debye T^3 region so far observed for any substance, the Θ_D value rising from a minimum of 607°K at a temperature of about 80°K to 750° at 18·8°K. This latter Θ_D value is of the same order as that estimated from the elastic constants at absolute zero and therefore the course of the variation of Θ_D below 18·8°K was of some interest. Sodium chloride formed a particularly suitable experimental material because the vibration spectrum had already been worked out (Kellermann 1940) and detailed predictions of the specific heat exist (Kellermann 1941). Zinc sulphide was chosen because there is a very large discrepancy between the Θ_D value obtained by Clusius and Harteck (1928) from specific heat measurements at 20°K and that estimated by them from the elastic constants.

* Some of the work described here was included in a thesis submitted for the Ph.D. degree of the University of London.

† At present Postdoctorate Fellow, National Research Council of Canada, Ottawa.

‡ Communicated by Professor G. O. Jones.

§ 2. Experimental

The apparatus was designed specifically for the measurement of the thermal capacity of crystals having good thermal conductivity but relatively small specific heat (i.e. large Θ_D value). The need to measure small thermal capacities made unadvisable the use of the conventional type of low-temperature calorimeter with the specimen enclosed. In any case, unless great care is taken, the use of a specimen in powder form involves the possibility of errors due to lack of thermal equilibrium or to adsorption of the necessary ' exchange gas '. The most suitable method which has hitherto been used employs a heater and thermometer wound directly upon a large crystal of the salt. A correction for the thermal capacity of the wires and lacquer is involved in this method and the only alternative to the use of exchange gas (which is best avoided at helium temperatures) in cooling the ' calorimeter ' and calibrating the thermometer is to wait a very long time for thermal equilibrium to be established.

For these reasons a novel type of low temperature calorimeter has been designed in which the thermal capacity is kept to a minimum and the objections to the methods cited above are avoided. The calorimeter consists of a thin copper tray below which are attached a thermometer, heater and cooling device, and upon which the crystal specimen can be stuck with a vacuum grease. (Dow–Corning silicone grease was found to form a stronger bond at low temperatures than Apiezon greases.) The cooling device consists of a small vessel through which cold gas can be circulated. The carbon resistance thermometer used (Allen Bradley Co. radio resistor, 56Ω, 1 watt) was calibrated by condensing an appropriate liquid in this vessel. Below 20°K the calibration was referred to the vapour pressures of normal hydrogen and helium (using the data collected by Linder (1950)) and above 20°K the oxygen triple and transition points were also used. The interpolation formula given by Clement and Quinnell (1952) was employed, although the thermometer was not found to be as reproducible as they claim—a variation of up to 1% in the calculated temperature at 4°K being found after a number of warmings to room temperature. Thus frequent recalibrations of the thermometer were necessary.

The heater consisted of a thin roll of constantan-nylon resistance tape lacquered in a thin copper tube which was soldered to the copper tray. The heater resistance was high (10 000Ω) so that the correction for the heat dissipated in the necessarily thin lead wires was as small as practicable. Instead of using an external voltage divider in order to determine the voltage applied to the heater, the heater itself was tapped so that a known fraction of the voltage across it could be measured directly. The method of discrete heating was used, the heater being switched on for accurately known periods by a semi-automatic device operated from a chronometer, which also gave audio signals at the times when temperature readings were due to be taken.* A ' dummy heater ' was also used to

* This device was developed in collaboration with Mr. B. F. Figgins.

ensure that the current drain from the batteries was constant whether the real heater was switched on or off.

All wires leading to the calorimeter were of 40 S.W.G. ' Lewmex ' insulated Eureka, and one metre in length between the point on the radiation shield at which they were thermally ' anchored ' and the calorimeter. The two tubes leading to the vessel on the calorimeter were also one metre in length and of German silver (1 mm o.d. ; 0·05 mm wall thickness).

The radiation shield surrounding the calorimeter was attached to the liquid helium vessel contained in the vacuum space of a miniature liquefier-cryostat of the type described by Chester and Jones (1953). For work at the higher temperatures employed hydrogen could be liquefied in the same vessel. All measurements were made with the radiation shield near 4°K or 20°K. The fact that the spread of results in the region of 10°K, where measurements were made with the shield at either of the above temperatures, was no greater than elsewhere, showed that the method employed of correction for heat losses (extrapolation of the curves of temperature drift before and after heating to the mid point of the heating period) was essentially satisfactory. Nevertheless the main source of random error in the results lay in the determination of the temperature rise during a heating period. (This error could have been reduced had separate potentiometers been available for the measurement of heat input and temperature.) The accuracy was limited at the lowest temperatures by the rapid drift rate of the calorimeter and at higher temperatures by the insensitivity of the carbon thermometer. Over most of the temperature range covered the random error of the specific heat results was less than $\pm 3\%$, leading to a scatter of less than $\pm 1\%$ in the derived Θ_D values. It is estimated that possible systematic errors are much smaller than the random errors.

No correction was necessary for the thermal capacity of the silicone grease used for establishing thermal contact because measurements on the ' empty ' calorimeter were made with the grease already applied. The correction necessary to obtain values of C_v from the results of the measurements (at constant pressure) is negligibly small for all the materials studied. The results are most conveniently expressed in terms of the Debye Θ_D, obtained through use of the relation $C_v = 464{\cdot}5\ (T/\Theta_D)^3$.

§ 3. Results and Discussion

Lithium Fluoride

These results have already been briefly reported (Jones and Martin 1954). An artificial crystal weighing 197 gm was used. The results obtained in four separate experimental runs are shown in fig. 1 in terms of Θ_D and temperature. A T^3 law is obeyed quite well up to a temperature of about 20°K. Above this temperature the Θ_D value falls off in good agreement with the previous results of Clusius and co-workers. The

mean Θ_D value for the 51 experimental points below 20°K is 737°K and the root mean square deviation from this value is ±9°K.

A criterion that the T^3 region has been reached is that the value of Θ_D obtained from the elastic constants at absolute zero should agree with that obtained from specific heat measurements. Unfortunately different workers have obtained widely differing results for the elastic constants of lithium fluoride and only measurements at room temperature have been

Fig. 1

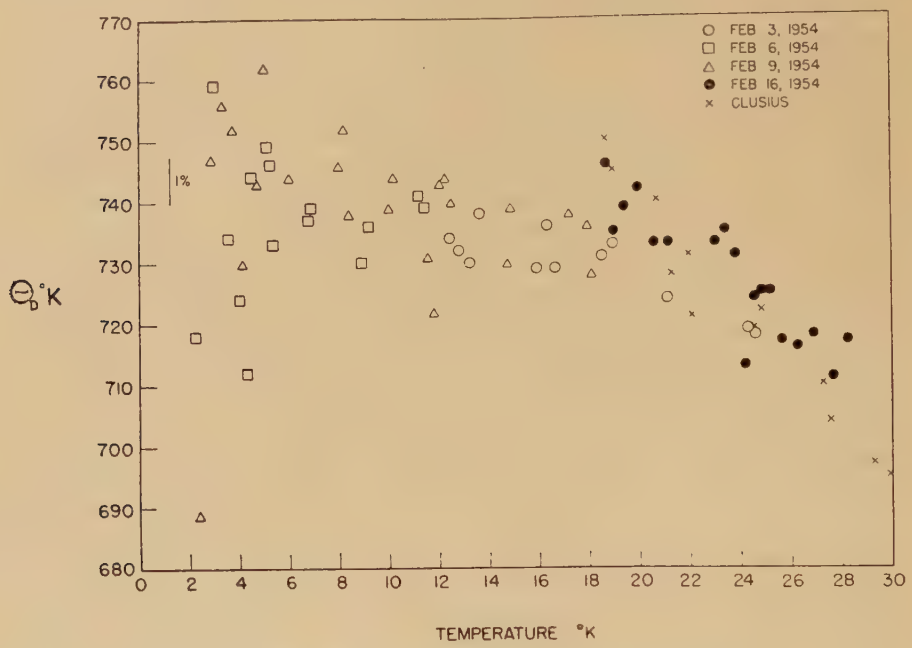

The Debye temperature of lithium fluoride below 30°K.

reported. These results are summarized in table 1. The discrepancies may be genuine, since Ballard, Coombes and McCarthy (1951) have shown that specimens of lithium fluoride can have differing physical properties, the method of growth apparently having some bearing upon them.

Table 1. Elastic Constants of Lithium Fluoride

Source	c_{11}	c_{12}	c_{44}
	(in units of dyne cm^{-2} × 10^{11})		
Bergmann (1938)	11·8	4·34	6·28
Huntingdon (1947)	9·74	4·04	5·54
Sundara Rao (1949)	11·9	4·58	5·42
Seshagiri Rao (1949)	11·9	5·38	5·34
Hoerni and Wooster (1952)	9·9	4·3	5·4

It is necessary to obtain estimates of the elastic constants at the absolute zero in order to calculate the required Θ_D. Durand (1936) has measured the variation of the elastic constants of magnesium oxide, sodium chloride and potassium chloride with temperature and has shown

that the variation may be represented by an empirical formula. These salts have the same crystal structure as lithium fluoride and a comparison of the Θ_D values, molecular weights and ionic radii show that lithium fluoride is most similar to magnesium oxide. Using the results of the measurements of elastic constants due to Huntingdon (1947) and extrapolating by comparison with Durand's results for magnesium oxide the following estimates are obtained for the elastic constants of lithium fluoride at absolute zero :—$c_{11}=10{\cdot}0$, $c_{12}=4{\cdot}0$, $c_{44}=5{\cdot}6(\times 10^{11}$ dyne cm$^{-2})$.

The most suitable method for computing Θ_D seemed to be that recently proposed by Quimby and Sutton (1953) and, using the values of the elastic constants just given, the value of 714°K is obtained for Θ_D. A simple formula proposed by Blackman (1951) also gives the same result. Using the other values of the elastic constants given above (uncorrected for temperature) and Blackman's simple formula, Θ_D values in the range 670°K to 770°K are obtained. Values of the coefficient of thermal expansion given by Sharma (1950) indicate that the change of density with temperature is very small and, since in any case the value of density is rather uncertain, the room-temperature value quoted in the Landolt–Börnstein tables has been used in the above calculation.

In view of the uncertainty of the experimental results for the elastic constants the only conclusion that can be drawn at present is that there is no evidence of a discrepancy between the thermal and elastic values of Θ_D in the T^3 region, which extends up to about 20°K—a temperature rather close to the value of $\Theta_D/50$ predicted by Blackman (1935). It is of interest to note that this is probably the only case in which the existence of a T^3 region has emerged clearly from experimental results without the necessity for making corrections to allow for other factors such as the electronic specific heat.

Sodium Chloride

An artificial crystal weighing 52 gm was used. The results are shown graphically in fig. 2. It will be noted that the Θ_D values are slightly higher than those found by Clusius and co-workers (Clusius, Goldman and Perlick 1949). The results are however in good agreement with the recent results of Morrison, Patterson and Dugdale (1955) except at temperatures below about 6°K where the two sets of results diverge. Both sets lead to values which are higher than the theoretical estimate (313°) due to Kellerman (1941) and the estimate (293°) from measurements of elastic constants by Overton and Swim (1951), but Morrison, Patterson and Dugdale have shown that a value of about 320°K is obtained from the results of Overton and Swim if the method of Bhatia and Tauber is used to calculate the Θ_D. The method of Quimby and Sutton also leads to a Θ_D value of this order, as did the earlier measurements of Durand (1936). The present experimental results do not give any indication of the start of a T^3 region but the large scatter of the results at the lowest temperatures precludes any definite conclusions being drawn on this point.

Fig. 2

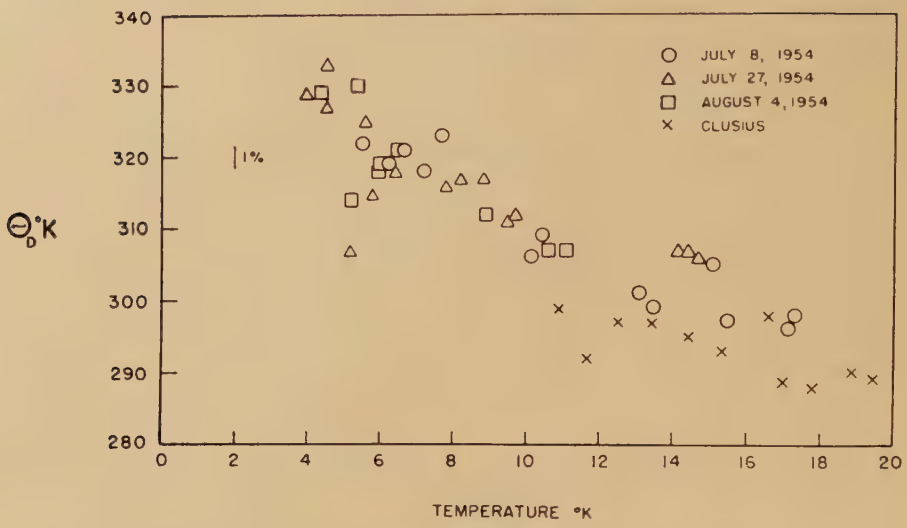

The Debye temperature of sodium chloride below 20°K.

Fig. 3

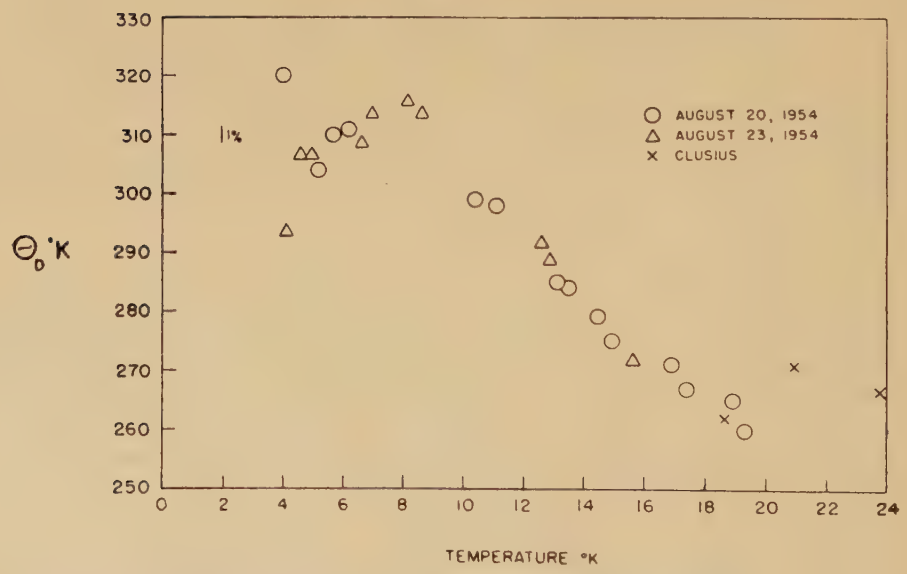

The Debye temperature of zinc sulphide below 24°K.

Zinc Sulphide

The sample used was a natural crystal of zinc-blende (from Santander, N. Spain) weighing 94 gm and consisting of an irregularly shaped transparent mass, of which a part was tinted slightly brown and the remainder with a pale green coloration. The zinc-blende structure was confirmed

by electron diffraction measurements. A spectrographic analysis showed that the only impurity present in any appreciable amount was cadmium, the amount being of the order of 0·1%. The resistivity at room temperature was greater than 10^{12} ohm cm, a value which would appear to rule out the possibility of any significant electronic contribution to the specific heat. (Zinc sulphide is a semi-conductor with a high activation energy.) The results of the measurements of specific heat are shown in fig. 3. Below 20°K the Θ_D value begins to rise with falling temperature, as predicted by Blackman (1935), reaching a value of about 315°K at 8°K, and subsequently remaining constant or even falling slightly.

There is again considerable uncertainty in the values of elastic constants, as will be seen from the data summarized in table 2. Moreover, there appear to be no data available to assist in the extrapolation of these

Table 2. Elastic Constants of Zinc Sulphide

Source	c_{11}	c_{12}	c_{44}
	(in units of dyne cm$^{-2} \times 10^{11}$)		
Voigt (1918)	9·43	5·68	4·37
Bhagavantam and Suryanarayana (1944)	10·79	7·22	4·12
Prince and Wooster (1951)	10	6·5	3·4

constants to absolute zero. Previous estimates of Θ_D reported by Clusius and Harteck (1928), and by Blackman (1938), are about 350°K and 325°K respectively. A calculation by the method of Bhatia and Tauber, using the room temperature elastic constant values of Prince and Wooster (1951), yields a result of 306°K. There would thus again appear to be no discrepancy between the values of Θ_D estimated from elastic and thermal data at very low temperatures.

§ 4. Conclusion

A direct experimental investigation of the lattice contribution to specific heats has been made, the results confirming theoretical predictions due to Blackman. As well as adding to the very small amount of data on the low-temperature thermal capacities of solids having only a lattice contribution to their specific heats, the results for lithium fluoride show clearly for the first time the existence of a T^3 region, without the necessity for invoking corrections for other contributions.

Acknowledgments

I am indebted to Professor G. O. Jones for suggesting the problem and for his constant interest and advice, to Dr. M. Blackman, Dr. R. O. Davies and Mr. B. F. Figgins for many helpful discussions and to Dr. J. A. Morrison, Dr. D. Patterson, and Dr. J. S. Dugdale of the National Research Council of Canada for allowing me to see some results before publication. The lithium fluoride crystal was kindly supplied by Dr. D. A. Jones and Dr. D. M. Finlayson of the University of Aberdeen and the sodium chloride by Dr. M. Blackman. Electron diffraction

measurements on the zinc-blende were made by Mr. R. B. Kehoe and Mr. R. C. Newman at Imperial College and the electrical resistance measurements by Dr. W. Ehrenberg at Birkbeck College. I acknowledge with thanks the careful workmanship of Mr. W. A. G. Baldock and the willing assistance of Mr. W. Eagers. The work was assisted by the loan of apparatus from the Central Research Fund of the University of London and by grants from the Department of Scientific and Industrial Research.

References

Ballard, S. S., Coombes, L. S., and McCarthy, K. A., 1951, *J. Opt. Soc. Amer.*, **41**, 772.
Bergmann, L., 1938, *Ultrasonics* (London : Bell).
Bhagavantam, S., and Suryanarayana, D., 1944, *Proc. Ind. Acad. Sci.* A, **20**, 304.
Bhatia, A. B., and Tauber, G. E., 1954, *Phil. Mag.*, **45**, 1211 ; 1955, *Ibid.*, **46**, 108.
Blackman, M., 1935, *Proc. Roy. Soc.* A, **149**, 117 ; 1938, *Ibid.*, **164**, 62 ; 1951, *Phil. Mag.*, **42**, 1441.
Chester, P. F., and Jones, G. O., 1953, *Proc. Phys. Soc.* B, **66**, 296.
Clement, J. R., and Quinnell, E. H., 1952, *Rev. Sci. Inst.*, **23**, 213.
Clusius, K., 1946, *Z. Naturforschg.*, **1**, 79.
Clusius, K., Goldman, J., and Perlick, A., 1949, *Z. Naturforschg.*, **4a**, 424 ; 1954, *Ibid.*, **9a**, 1054.
Clusius, K., and Harteck, P., 1928, *Z. Phys. Chem.*, **134**, 243.
Durand, M. A., 1936, *Phys. Rev.*, **50**, 449.
Hoerni, J., and Wooster, W. A., 1952, *Acta Crystallogr.*, **5**, 386.
Huntingdon, H. B., 1947, *Phys. Rev.*, **72**, 321.
Jones, G. O., and Martin, D. L., 1954, *Phil. Mag.*, **45**, 649.
Kellermann, E. W., 1940, *Phil. Trans. Roy. Soc.* A, **238**, 513 ; 1941, *Proc. Roy. Soc.* A, **178**, 17.
Linder, C. T., 1950, *Research Report* R-94433-2-A, Westinghouse Research Laboratories, Pittsburg.
Morrison, J. A., Patterson, D., and Dugdale, J. S., 1955, *Canad. J. Chem.*, **33**, 375.
Overton, W. C., and Swim, R. T., 1951, *Phys. Rev.*, **84**, 758.
Prince, E., and Wooster, W. A., 1951, *Acta Crystallogr.*, **5**, 386.
Quimby, S. L., and Sutton, P. M., 1953, *Phys. Rev.*, **91**, 1122.
Seshagiri Rao, T., 1949, *Curr. Sci.*, **18**, 436.
Sharma, S. S., 1950, *Proc. Ind. Acad. Sci.* A, **32**, 268.
Sundara Rao, R. V. G., 1949, *Curr. Sci.*, **18**, 336.
Voigt, W., 1918, *Gottinger Nach.*, 424.

LXXXVI. *Fields around Impurity Atoms in Metals*

By L. C. R. Alfred and N. H. March
Department of Physics, The University, Sheffield*

[Received March 9, 1955]

Abstract

Detailed calculations of the potential around impurity atoms with valency $Z+1$ dissolved in a monovalent metal are reported. The first order or linearization approximation usually employed is avoided, and the basic Thomas–Fermi equation must then be solved numerically. The potentials thus obtained differ significantly from those predicted by the first order approximation. The differences are always in the direction of a more effective shielding of the point charge Ze. The shielding depends appreciably on the valency of the dissolved impurity, whereas the first order result is a screened potential with a screening radius independent of Z. The connection between the present results and Friedel's second order approximation is briefly discussed. The calculations have then been extended to cover the case when we are dealing with a finite concentration of impurities, using the model of Friedel. Again we find that the results given by the first order approximation are appreciably in error. In all the numerical calculations we have taken copper as the solvent metal; the essential conclusions will however hold more generally.

§ 1. Introduction

In quite a number of important problems one requires a knowledge of the potential surrounding an impurity atom in a metal. For example, such knowledge is essential for an understanding of the experimental results on the electrical resistivity of various alloys (Mott 1936), and has recently been shown by Lazarus (1954) to be of importance in developing a theory of solute diffusion in metals. Mott first showed how the problem could be tackled by using the Thomas–Fermi (TF) model and his results have formed the basis of a number of more recent investigations. Besides using the TF approximation, however, it was also found necessary to introduce a further approximation amounting to the linearization of the basic equation, in order to obtain a solution in terms of known functions. We shall refer to this procedure in what follows as the first order approximation (cf. Friedel 1954, where an excellent review of the whole subject of impurities in metals is presented). This linearization, whilst important in leading to a tractable equation which can be solved in a form of

* Communicated by the Authors.

considerable generality, leads to some results which fairly clearly must be peculiar to the mathematical approximation made. For example, the potential is found to be of the screened Coulomb form, but with a screening radius which is independent of the valency of the dissolved impurity, and dependent only on the Fermi energy of the solvent metal, whereas the equation before linearizing clearly will not give such a result. One purpose of the present work is to examine how serious any deviation from this prediction of the first order treatment may be. Friedel has previously given a partial answer to this question, using a so-called second order approximation, but this depends on assuming the basic form obtained from the first order treatment and thus is not completely convincing. We are concerned here with avoiding these approximations altogether, as it seemed to us that the results of the TF model in this problem were of sufficient importance to warrant a more careful examination than has hitherto been made.

In this paper we shall restrict ourselves to the ordinary TF approximation, that is we shall neglect exchange, and we shall not be concerned with the generalized TF approximation of Friedel.

§ 2. The TF Equation for the Potential around an Impurity

We assume, following Mott, that the solvent atom is monovalent, whilst the solute atom has $Z+1$ valence electrons. We adopt the approximation of a free electron gas, and then we have the usual relation between the number of electrons (or atoms in the case of the monovalent metal considered here) per unit volume, n_0 say, and the maximum momentum k_M (we shall use atomic units throughout),

$$n_0 = \frac{k_M^3}{3\pi^2}. \qquad (1)$$

The Fermi energy E_M is of course given in terms of k_M by

$$E_M = \frac{k_M^2}{2} \qquad (2)$$

for free electrons, when we neglect exchange and correlation effects as we shall do throughout this paper.

When we perturb the metal by the introduction of impurity atoms then we have in general a shift of the Fermi level, and using Friedel's notation we shall denote the Fermi energy by $E_M + \Delta E_M$. Then, in the usual way, we have the TF approximation for the electron density $n(r)$ as

$$n(r) = \frac{2^{3/2}}{3\pi^2}(E_M + \Delta E_M - V_P)^{3/2} \qquad (3)$$

where V_P is the perturbing potential energy. Using Poisson's equation we can calculate a self-consistent potential V_P from

$$\begin{aligned} -\nabla^2 V_P &= 4\pi[n(r) - n_0] \\ &= \frac{2^{7/2}}{3\pi}[(E_M + \Delta E_M - V_P)^{3/2} - E_M^{3/2}]. \qquad (4) \end{aligned}$$

In the case of infinite dilution, the change in the Fermi energy ΔE_M will be zero, but for a finite concentration of impurities this will not be so.

§ 3. A Single Impurity in an Infinite Metal

In this case, putting $\Delta E_M = 0$, the TF equation becomes

$$-\nabla^2 V_P = \frac{2^{7/2}}{3\pi}[(E_M - V_P)^{3/2} - E_M{}^{3/2}]. \quad . \quad . \quad . \quad . \quad (5)$$

The appropriate boundary conditions are

$$\left.\begin{aligned} V_P &\to -\frac{Z}{r} \quad \text{as} \quad r \to 0 \\ V_P &\to 0 \quad \text{as} \quad r \to \infty \end{aligned}\right\} . \quad . \quad . \quad . \quad . \quad . \quad (6)$$

It has been customary to solve eqn. (5) assuming $E_M \gg |V_P|$. We see from the boundary conditions (6) however that this is obviously not true as r tends to zero and the linearization previously adopted is evidently not completely justifiable. When the first order approximation is nevertheless made, eqn. (5) simplifies to

$$\nabla^2 V_P = \frac{4k_M}{\pi} V_P \quad . \quad . \quad . \quad . \quad . \quad . \quad . \quad . \quad (7)$$

and with the boundary conditions (6) the solution is

$$V_P = -\frac{Z}{r}\exp(-qr) \quad . \quad . \quad . \quad . \quad . \quad . \quad . \quad (8)$$

where

$$q^2 = \frac{4k_M}{\pi}.$$

We have now dealt with eqn. (5) exactly by numerical methods, which clearly must be used unless some approximation such as that leading to eqn. (7) is made. To solve numerically it is convenient to make the substitution

$$V_P = -\frac{Z}{r}\phi \quad . \quad . \quad . \quad . \quad . \quad . \quad . \quad . \quad (9)$$

in order to remove the singularity at the origin. Since we now have to deal with a problem in which the boundary conditions are at the two extremes of the range, the usual step-by-step methods are not very suitable and we have made use in this work of the relaxation method. For a clear account of this method reference should be made to a paper by Fox (1949). In the present application it is necessary to transform to a new independent variable w defined by

$$r = w^2. \quad . \quad . \quad . \quad . \quad . \quad . \quad . \quad . \quad (10)$$

The resulting equation for $\phi(w)$ can be written in the form

$$\frac{d^2\phi}{dw^2} - \frac{1}{w}\frac{d\phi}{dw} = \frac{2^{11/2}}{3\pi}\frac{w^4}{Z}\left[\left(E_M + \frac{Z\phi}{w^2}\right)^{3/2} - E_M{}^{3/2}\right]. \quad . \quad . \quad (11)$$

Obviously we have to solve this equation separately for each solvent metal we wish to investigate and throughout this paper we shall present results for copper. Besides this we have to solve eqn. (11) for each value of Z, and we have chosen to investigate the cases $Z=1$, 2, 3 and 4. (The first order approximation given in eqns. (7) and (8) leads to $\phi = \exp(-qw^2)$, independent of Z.) $Z<0$ also has physical significance, for a vacancy can be treated as an impurity with zero valency (cf. Dexter 1952), but we shall confine ourselves to cases for which $Z>0$ in this paper. The results obtained by carrying through the relaxation procedure are shown in fig. 1, where we plot ϕ against r. Curves 1 to 4 show the results we have obtained, whilst curve 5 shows for comparison the results obtained from the first order treatment.

Fig. 1

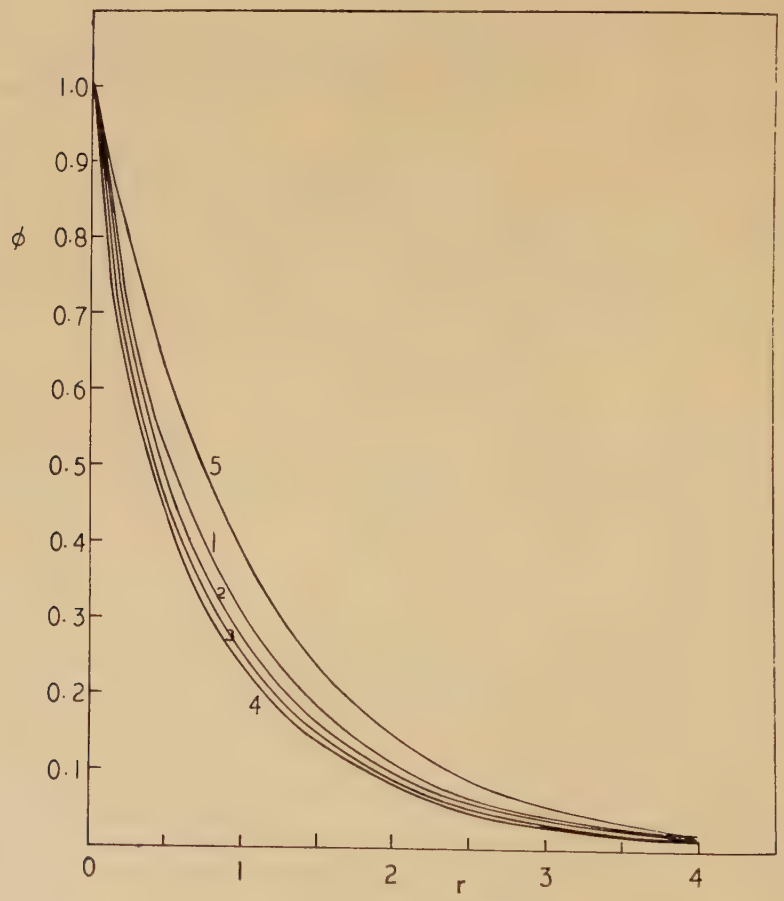

$\phi(=-rV_P/Z)$ plotted against r.
Curves 1 to 4. $Z=1$, 2, 3 and 4, respectively.
Curve 5. First order results.

§ 4. Case of Finite Concentration of Impurities

So far we have been concerned with the case of infinite dilution, where the Fermi energy is unchanged. Before discussing the results we have obtained in this case, however, it is of interest to examine the situation when we have a finite concentration of impurity atoms. Friedel (1954) has proposed a model by means of which we can deal with this case,

Fig. 2

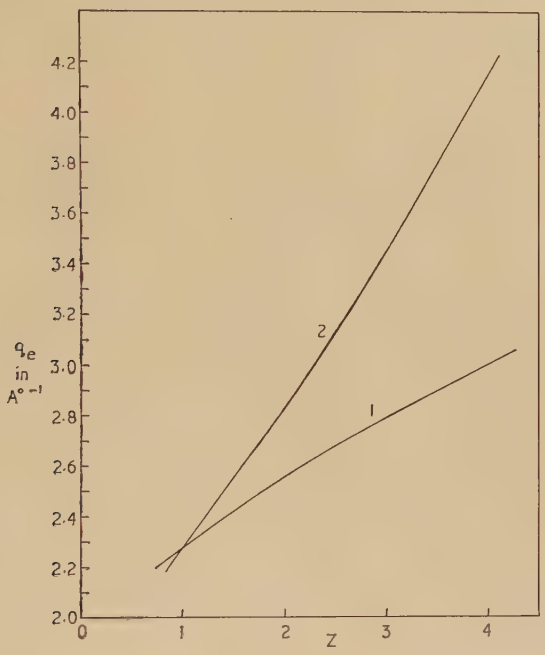

Variation of reciprocal of effective screening radius with Z.

Curve 1. Accurate numerical results.
Curve 2. Results of second order approximation.

and has obtained results using again a first order approximation. The assumption is made that the impurity atoms are well dispersed in the matrix, so that each can be surrounded by its own polyhedron. This can then be replaced by a sphere of equal volume to a reasonable approximation, all the spheres having the same radius R. The appropriate boundary conditions in this case are then (Friedel 1954)

$$\left.\begin{aligned} V_P &\to -\frac{Z}{r} \quad \text{as} \quad r \to 0 \\ V_P(R) &= 0 \\ \left(\frac{dV_P}{dr}\right)_R &= 0 \end{aligned}\right\} \quad . \quad . \quad . \quad . \quad . \quad (12)$$

Making the first order approximation again, we obtain from eqn. (4)

$$\nabla^2 V_P = q^2(V_P - \Delta E_M) \quad . \quad . \quad . \quad . \quad . \quad . \quad . \quad (13)$$

with solution due to Friedel

$$V_P - \Delta E_M = -\frac{Z}{r}\frac{qR\cosh\{q(R-r)\} - \sinh\{q(R-r)\}}{qR\cosh qR - \sinh qR}, \quad . \quad (14)$$

$$\Delta E_M = Zq/(qR\cosh qR - \sinh qR). \quad . \quad . \quad . \quad . \quad (15)$$

This time, since the boundary conditions are less precise, it is convenient to use step-by-step methods, and to integrate out from the origin. We make the substitution

$$\Delta E_M - V_P = \frac{Z}{r}\phi \quad . \quad . \quad . \quad . \quad . \quad . \quad . \quad (16)$$

and work in terms of the original variable r rather than w. The procedure adopted was to develop a series expansion around the origin. This takes the form

$$\phi = 1 + a_2 r + a_3 r^{3/2} + a_4 r^2 + \ldots \quad . \quad . \quad . \quad . \quad . \quad (17)$$

where the higher coefficients can be obtained in terms of a_2, E_M and Z. Coefficients up to and including a_{11} are given in the table. This series is then used to calculate starting values for a number of convenient initial slopes a_2. We have restricted ourselves to the case of $Z=1$, and we show two representative solutions in curves 1 and 2 of fig. 3. The values of R for these solutions are 3·6 and 4·4 respectively. For the case $R=3{\cdot}6$ we also show for comparison the results obtained using eqn. (14). The boundary values of ϕ are also of some interest as they determine ΔE_M defined through eqn. (16), and we plot ΔE_M as a function of concentration in fig. 4, using the five solutions we have computed.

Table. Coefficients in Series Expansion around Origin*

$$\alpha = \frac{2^{7/2}Z^{1/2}}{3\pi}, \qquad \epsilon = \frac{E_M}{Z}.$$

$a_3 = \frac{4}{3}\alpha$	$a_6 = \frac{\alpha^2}{3} - \frac{\alpha\epsilon^{3/2}}{6}$	$a_9 = \frac{2}{27}\alpha^3 - \frac{1}{63}\cdot\alpha^2\epsilon^{3/2} - \frac{1}{252}\cdot\alpha(a_2+\epsilon)^3$	
$a_4 = 0$	$a_7 = \frac{3}{70}\alpha(a_2+\epsilon)^2$	$a_{10} = \frac{1}{175}\cdot\alpha^2(a_2+\epsilon)^2$	
$a_5 = \frac{2}{5}\alpha(a_2+\epsilon)$	$a_8 = \frac{2}{15}\alpha^2(a_2+\epsilon)$	$a_{11} = \frac{31}{1485}\alpha^3(a_2+\epsilon) - \frac{1}{198}\cdot\alpha^2\epsilon^{3/2}(a_2+\epsilon) + \frac{1}{1056}\cdot\alpha(a_2+\epsilon)^4.$	

* Putting $\alpha=1$ and $\epsilon=0$, these reduce to coefficients in Baker's expansion for the usual dimensionless TF equation $d^2\phi/dx^2 = \phi^{3/2}/x^{1/2}$.

§ 5. Discussion of Results

We shall consider first the results shown in fig. 1 for infinite dilution. The main points which emerge from these may be summarized as follows :

(1) There are significant differences between the exact numerical results and those obtained by making the first order approximation.

Fig. 3

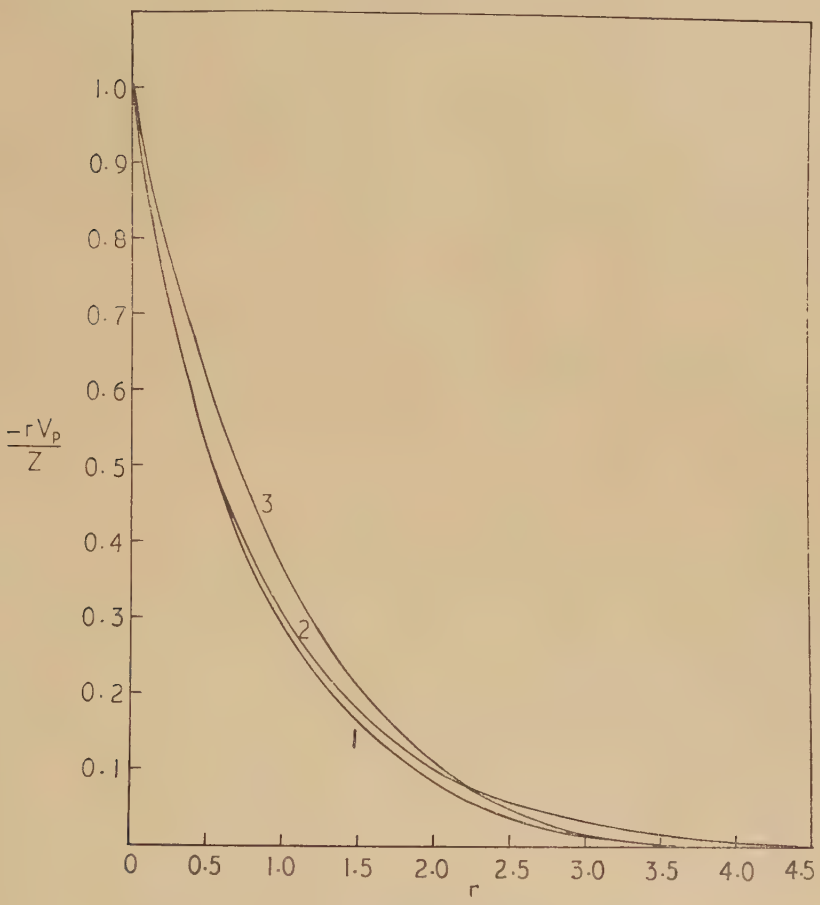

$-(r/Z)V_P$ plotted against r.

Curve 1. $R=3{\cdot}6$.
Curve 2. $R=4{\cdot}4$.
Curve 3. Results of first order approximation for $R=3{\cdot}6$.

(2) As a plot of $\log_e \phi$ against r shows, it is not possible to represent the results of our work very satisfactorily by a screened potential as in eqn. (8), although of course our potentials are roughly of this form as can be seen from fig. 1. We can say however that our results definitely indicate a more effective shielding of the point charge Z than is predicted by the first order approximation.

(3) The shielding obviously varies with Z as we see from a comparison of curves 1 to 4 of fig. 1, whereas from eqn. (8) the screening radius q^{-1} is given to be independent of Z and determined solely by the Fermi energy.

With regard to point (3) above, a comparison with previous results is not completely clear-cut except by a direct comparison of potentials because, as we have mentioned, our results cannot be fitted very accurately by a screened Coulomb potential. However, if we choose to define an effective screening radius q_e^{-1} to be that value of r at which the function ϕ has fallen to e^{-1} of its initial value, then we obtain the results shown in curve 1 of fig. 2. The decrease of the screening radius with Z has been predicted previously by Friedel (1954) by considering a second order approximation, and curve 2 shows the results of his treatment. We see that the variation with Z which we find is considerably less than that given by the second order approximation.

Fig. 4

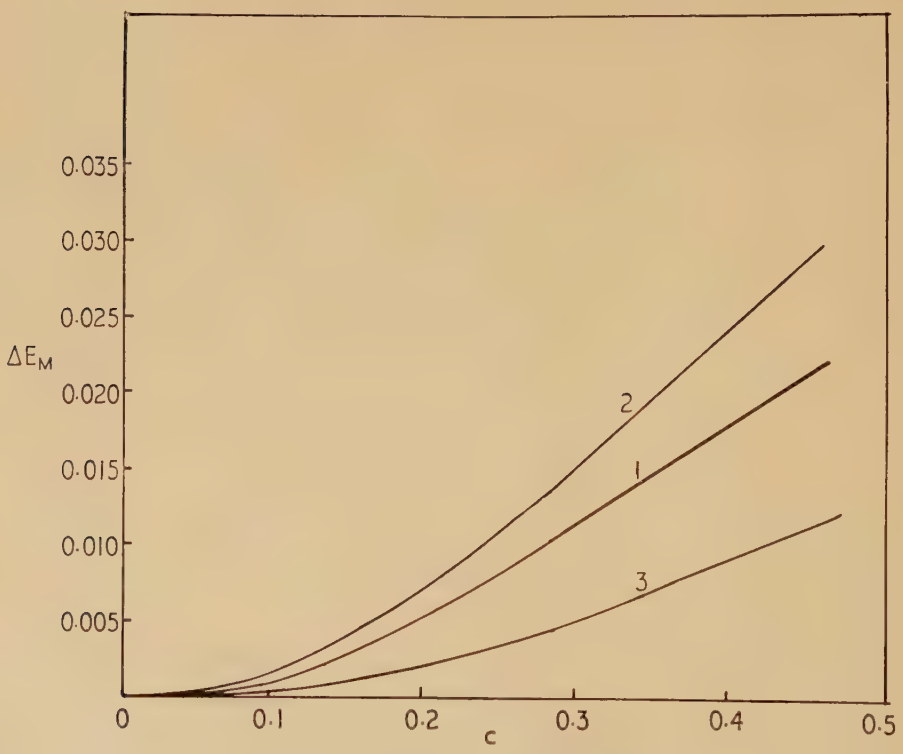

ΔE_M plotted against concentration c.

Curve 1. Accurate numerical results.
Curve 2. First order results.
Curve 3. Second order results.

We turn now to the results when we have a finite concentration of impurities. Figure 3 shows both the exact and first order potentials and it can be seen that the same sort of discrepancies arise as in the infinite dilution case. Further it is clear that the differences will become more marked as Z is increased, just as in fig. 1.

Whilst the main object of this paper, that of calculating in a completely self consistent manner the fields around impurities, both for infinite dilution and for finite concentrations, and hence assessing the reliability of the existing approximate treatments, has now been achieved, it is perhaps of interest finally to make a few remarks concerning the results we have obtained for ΔE_M in the course of this work. These are shown in curve 1 of fig. 4, as a function of concentration. Curve 2 shows the results obtained using the first order approximation, whilst curve 3 has been calculated from the second order approximation (Friedel 1954, eqns. (50) and (51)). The following points are worth recording :

(1) In all three cases the general type of variation with concentration is the same, although rather marked quantitative differences exist.

(2) As Dr. J. Friedel has pointed out to us, when one goes beyond the first order approximation the results should really be corrected because we count twice the potential energy of interaction of the displaced charge with itself, a general difficulty when using the Hartree approximation.

§ 6. Conclusions

The work reported in this paper makes it quite clear that nontrivial errors are introduced by solving the TF equation for an impurity by means of the first order approximation. Removing this, we find in general smaller screening radii, the potential falling off more rapidly than predicted by the first order treatment. Most of the essential features of the first order method are verified, however, but the shielding depends quite appreciably on the valency of the dissolved impurity, as was anticipated by Friedel using his second order approximation. This does not seem particularly reliable quantitatively however. The case of a finite concentration of impurities has also been considered, although in less detail, and the same general conclusions apply.

It seems that the reduction of the effective screening radii which we have found by accurate numerical solution of the TF equation is a step in the right direction to improve agreement with experiment. It should be remembered however that we have here neglected exchange, and that the somewhat rough estimates which have been made (see, for example Friedel 1954 ; § 3.7.3) indicate that this may well be of some importance. Finally, the accurate numerical results presented here have all been for the case when the solvent metal is copper ; the essential conclusions will however obviously be true more generally.

Acknowledgment

It is a pleasure to thank Dr. J. Friedel for reading a preliminary manuscript of this paper and for his valuable comments.

References

Dexter, D. L., 1952, *Phys. Rev.*, **87,** 768.
Fox, L., 1949, *Proc. Camb. Phil. Soc.*, **45,** 50.
Friedel, J., 1954, *Advances in Physics*, **3,** 44.
Lazarus, D., 1954, *Phys. Rev.*, **93,** 973.
Mott, N. F., 1936, *Proc. Camb. Phil. Soc.*, **32,** 281.

LXXXVII. *Polarization in Nucleon Scattering at Various Energies*

By Richard Wilson
Clarendon Laboratory, Oxford*

[Received March 18, 1955]

Abstract

The polarization of nucleons elastically scattered from nuclei is discussed on the optical model. Analytical formulae are used to illustrate the differences between various approximations.

A uniform spin–orbit potential is shown to be at variance with experiment, unless the magnitude varies with the nuclear radius, and it is shown that the polarization may change sign at an energy close to that for which the total cross section is a maximum.

§ 1. Introduction

Polarization of protons by elastic scattering from nuclei has been studied experimentally and theoretically (Oxley 1953, Dickson 1954, Chamberlain 1954, Marshall 1954, de Carvalho 1954, Malenka 1954, Fermi 1954, Sternheimer 1954, Watson 1954, and Adair 1954). The theoretical calculations so far published have either used Born approximation, which is often inadequate, or used a phase shift analysis which obscures the physics of the problem.

Tamor (1954) has discussed the polarization in terms of the impulse approximations and has shown that all α-particle nuclei should show the same polarization. The application of the impulse approximation, to carbon and heavier elements, is doubtful. It implies that, if we calculate upon the optical model, the absorption of the wave representing the nucleon in the nucleus is small. In carbon the wave is absorbed by a factor of about 2 at energies from 50–400 Mev so that this is not likely to be accurate. For low energies, moreover, this approach neglects the phase shift of the wave in passing through the nucleus which is the subject of this paper.

Malenka (1954) has suggested analytical formula which extend the optical model of Fernbach (1949) to include a spin–orbit potential. These may be directly derived by the same optical analogy as that of Fernbach or by the Born Series summation of Glauber (1953). The optical analogy omits the phase factor of i which is correctly included in the calculations of this paper. With this as a starting point we propose to discuss some features of the polarization as a function of energy. This will be done exactly for the unrealistic case of a cylindrical nucleus and indications given of the deviations from this case in order to suggest the directions in which exact calculations and further experiments can best proceed.

* Communicated by the Author.

It will be shown that the usual fit to the total cross sections (e.g. Taylor 1954) may have to be modified to include the effects of the spin–orbit potential. Two forms of spin–orbit potential will be assumed; one uniformly distributed throughout the nucleus, the other, originally suggested by Fermi, located at the surface. It will be shown that there are distinct differences between the predictions of the two models which favour the latter.

§ 2. Optical Model

Following Malenka we express the nuclear potential as

$$V(\rho, z)(1+i\epsilon)+U(\rho, z)\tfrac{1}{2}\vec{\boldsymbol{\sigma}} \cdot \vec{\mathbf{r}}\times(-i)\vec{\nabla} \quad . \quad . \quad . \quad (1)$$

with cylindrical coordinates ρ and z, and derive the scattering amplitudes in the form $f(\theta)+\vec{\boldsymbol{\sigma}} \cdot \vec{\mathbf{n}}g(\theta)$ where suitable spin functions are assumed, and $\vec{\mathbf{n}}$ is a unit vector normal to the scattering plane.

Then the polarization

$$P(\theta)=\frac{f^*(\theta)g(\theta)+g^*(\theta)f(\theta)}{|f(\theta)|^2+|g(\theta)|^2} = \frac{2\{Imf(\theta)\,Img(\theta)+Ref(\theta)Reg(\theta)\}}{|f(\theta)|^2+|g(\theta)|^2} \quad . \quad . \quad . \quad (2)$$

where

$$f(\theta)=ik\int_0^\infty \rho d\rho\{1-\exp(2i\delta_0)\cos(\rho k\cos\tfrac{1}{2}\theta\delta_1)\}J_0(2k\rho\sin\theta/2) \quad . \quad . \quad (3)$$

$$g(\theta)=ik\int_0^\infty \rho d\rho\exp(2i\delta_0)\sin(\rho k\cos\tfrac{1}{2}\theta\delta_1)J_1(2k\rho\sin\theta/2) \quad . \quad . \quad . \quad (4)$$

and

$$\delta_0(\rho)=-\frac{(1+i\epsilon)}{\hbar v}\int_0^\infty V(\rho, z)\,dz \quad . \quad . \quad . \quad . \quad . \quad (5)$$

$$\delta_1(\rho)=-\frac{1}{\hbar v}\int_0^\infty U(\rho, z)\,dz. \quad . \quad . \quad . \quad . \quad . \quad . \quad (6)$$

These formulae tend to the Born approximation formulae when the assumptions are made that $\delta_0 \ll 1$ and $\delta_1 \ll 1$. As will be easily seen from what follows, the former assumption is never valid.

The optical model is not expected to be accurate to better than 10% at energies below 100 Mev but is as good as the WKB method used in calculating the phase shifts by Fernbach (1954).

§ 3. Uniform Spin–Orbit Potential

We now assume that the spin–orbit potential U is uniform throughout the nucleus and so is V; we will assume further that the nucleus is spherical. Then

$$\left.\begin{aligned} V(\rho, z)&=-V_0(r<R)\\ &=0(r>R)\\ U(\rho, z)&=-U_0(r<R)\\ &=0(r>R). \end{aligned}\right\} \quad . \quad . \quad . \quad . \quad . \quad . \quad (7)$$

For convenience we define parameters K and k_1 as used by Fernbach,

$$\left.\begin{aligned} k_1/k&=(1+V_0/E)^{1/2}-1\simeq V_0/2E \\ K/k&=\epsilon V_0/E. \end{aligned}\right\} \quad . \quad . \quad . \quad . \quad . \quad (8)$$

Further we will approximate $k\rho\delta_1 \cos\theta/2 \ll 1$. Then $f(\theta)$ is the usual optical model form

$$f(\theta)=ik\int_0^R \rho d\rho\{1-\exp[-K\sqrt{(R^2-\rho^2)}]\exp[2ik_1\sqrt{(R^2-\rho^2)}]\}J_0(k\rho\theta), \quad (9)$$

$$g(\theta)=ik\int_0^R \rho d\rho \exp[-K\sqrt{(R^2-\rho^2)}]\exp[2ik_1\sqrt{(R^2-\rho^2)}] \times U_0k^2\sqrt{(R^2-\rho^2)}/2EJ_1(k\rho\theta). \quad . \quad . \quad . \quad . \quad . \quad . \quad (10)$$

On the optical model these integrals are readily recognized as integrations over the impact parameter ρ.

§ 4. Cylindrical Approximation

We now assume that the nucleus is a cylinder of radius R and length $2L$ with axis along the beam direction.

Then we have from an analogous optical calculation

$$f(\theta)=ik\{1-\exp(-KL)\exp(2ik_1L)\}\int_0^R \rho d\rho J_0(k\rho\theta)$$

$$=iR\{1-\exp(-KL)\exp(2ik_1L)\}\frac{J_1(kR\theta)}{\theta}, \quad . \quad . \quad . \quad (11)$$

$$g(\theta)=ik\{\exp(-KL)\exp(2ik_1L)\}\int_0^R \frac{k^2}{2E}UL\rho^2\, d\rho J_1(k\rho\theta)$$

$$=ik^2R^2LU_0/2E\frac{J_2(kR\theta)}{\theta}\exp(-KL)\exp(2ik_1L). \quad . \quad . \quad (12)$$

If we assume that U_0 is constant with energy and we use small angles, then

$$\frac{J_1(k\rho\theta)}{\theta}\simeq\frac{k}{2}p, \qquad \frac{J_2(k\rho\theta)}{\theta}\simeq k^2\rho^2\frac{\theta}{8},$$

so that $f(\theta)$ varies as k and $g(\theta)$ as k^2.

The cylindrical approximation may be regarded as an approximation to the integrals (9) and (10) by inserting an average L in place of $\sqrt{(R^2-\rho^2)}$ in the exponent. As will be discussed in more detail later, the average L involved can be appreciably different in the two cases although here it is treated as the same.

The significant feature about these formulae which give the qualitative features of the following predictions is that $Imf(\theta)$ is always the same sign as $iJ_1(k\rho\theta)$ regardless of the parameters K and k_1, whereas $g(\theta)$ changes phase and sign.

§ 5. Thomas Form of Spin–Orbit Interaction

Fermi and others have considered an interaction of the form of the Thomas correction

$$U(r)=-\alpha\lambda\!\!\!^{-2}\frac{1}{r}\frac{d}{dr}V(r) \quad . \quad . \quad . \quad . \quad . \quad . \quad (13)$$

with this interaction δ_1 for a spherical nucleus and a square well becomes

$$\begin{aligned}\delta_1(\rho)&=\frac{1}{\hbar v}\alpha\lambda\!\!\!^{-2}\int_0^\infty \frac{dV(r)}{dr}\frac{dr}{\sqrt{(r^2-\rho^2)}}\\ &=\frac{k\lambda\!\!\!^{-2}}{2E}\frac{V_0}{\sqrt{(R^2-\rho^2)}} \qquad \rho<R\\ &=0 \qquad\qquad\qquad \rho>R. \quad . \quad . \quad . \quad . \quad . \quad (14)\end{aligned}$$

One part of the approximation is to put $k\rho\delta_1 \ll 1$, in spite of the infinity at $\rho=R$. Then

$$\begin{aligned}g(\theta)=ik\int_0^R \rho d\rho \exp\left[-K\sqrt{(R^2-\rho^2)}\right]\exp\left[2ik_1\sqrt{(R^2-\rho^2)}\right]\\ \times\frac{V_0}{2E}\frac{\rho}{\sqrt{(R^2-\rho^2)}}J_1(k\rho\theta). \quad . \quad . \quad . \quad . \quad . \quad (15)\end{aligned}$$

A possible cylindrical spin–orbit potential is

$$\begin{aligned}U(\rho,z)&=-\alpha\lambda\!\!\!^{-2}\frac{1}{z}\frac{d}{dz}V(\rho,z) \qquad \rho<R\\ &=-\alpha\lambda\!\!\!^{-2}\frac{1}{\rho}\frac{d}{d\rho}V(\rho,z) \qquad \rho=R. \quad . \quad . \quad . \quad (16)\end{aligned}$$

Then

$$\begin{aligned}\delta_1(\rho)&=\frac{\alpha V_0}{2E}\frac{\lambda\!\!\!^{-}}{L} \qquad \rho<R\\ &=\infty \qquad\qquad \rho=R\\ &=0 \qquad\qquad \rho>R. \quad . \quad . \quad . \quad . \quad . \quad . \quad (17)\end{aligned}$$

The infinity introduces no contribution to $f(\theta)$ or $g(\theta)$ because $\sin(k\rho\delta_1)$ remains finite.

This is equivalent to approximating in (15) the terms

$$\exp\left[-K\sqrt{(R^2-\rho^2)}\right] \text{ by } \exp(-KL)$$

and $$\exp\left[2ik_1\sqrt{(R^2-\rho^2)}\right] \text{ by } \exp(2ik_1L)$$

and in addition the $\sqrt{(R^2-\rho^2)}$ in the denominator by L. Then

$$\begin{aligned}g(\theta)&=ik\exp(-KL)\exp(2ik_1L)\frac{\alpha}{L}\frac{V_0}{2E}\int_0^R \rho^2\, d\rho J_1(k\rho\theta)\\ &=iR^2\exp(-KL)\exp(2ik_1L)\frac{V_0}{2E}\frac{\alpha}{L}\frac{J_2(kR\theta)}{\theta}, \quad . \quad . \quad . \quad . \quad . \quad . \quad (18)\end{aligned}$$

$f(\theta)$ varies as k. $g(\theta)$ has no direct variation with E so that polarization goes as $1/\sqrt{E}$ apart from the energy dependent terms V, K, k_1 and possibly α.

§ 6. Polarization as a Function of R

(*a*) *Uniform spin–orbit coupling*

For small θ we may expand the J_1 and J_2 in our formulae for $f(\theta)$ and $g(\theta)$. Then for a uniform

$$U(r)f(\theta)=iR^2k/2\{1-\exp(-KL)\exp 2ik_1L\} \quad . \quad . \quad . \quad (19)$$

$$g(\theta)=iR^4L(\theta/4)[\exp(-KL)\exp 2ik_1L]M^2U_0E. \quad . \quad . \quad (20)$$

For high energies we put $\exp 2ik_1L=1$. Then for small θ $g(\theta)\ll f(\theta)$ and $g(\theta)$ and $f(\theta)$ are total imaginaries

$$P(\theta)=\frac{g(\theta)}{f(\theta)}=\frac{R^2L\exp(-KL)}{1-\exp(-KL)}\left(\frac{k\theta U_0M}{4}\right) \quad . \quad . \quad . \quad (21)$$

which increases rapidly with R, unless U_0 is considered to be a function of R, in disagreement with experiment (Dickson 1955).

(*b*) *Thomas correction form of spin–orbit coupling*

$$f(\theta)=iR^2\frac{2}{k}\{1-\exp(-KL)\exp(2ik_1L)\}. \quad . \quad . \quad (22)$$

$$g(\theta)=\frac{iR^4}{L}\exp(-KL)\exp(2ik_1L)\frac{MV_0\alpha\theta}{8}. \quad . \quad . \quad . \quad (23)$$

So that for small $g(\theta)$ and small k_1

$$P(\theta)=\frac{g(\theta)}{f(\theta)}\frac{R^2}{L}\frac{\exp(-KL)}{1-\exp(-KL)}\frac{MV_0\alpha\theta}{4k}. \quad . \quad . \quad . \quad (24)$$

Since L varies as R, this falls slowly with R in agreement with experiment.

The variation of $P(\theta)$ with R thus decides against the uniform spin–orbit coupling and in favour of the Thomas correction coupling unless the magnitude of the spin–orbit coupling term U_0 is dependent upon R.

§ 7. Parameters from other Experiments

The parameters K and k_1 may be determined as functions of energy from other experiments.

If the nuclear radius R is assumed, K is determined with little ambiguity from total inelastic cross section measurements because the real part of the potential V_0 and the spin–orbit potential have little effect on these measurements (DeJuren 1950, Ball 1953, Voss 1955). K varies little as a function of energy from 50 Mev to 300 Mev and $\exp(-KL)$ varies from 0·4 for light nuclei to 0·15 for heavy nuclei.

k_1 may be determined from the position of the peak in the total cross section measurements as a function of energy (Taylor 1953, Lawson 1953) or from small angle scattering measurements (van Zyl 1955). k_1 decreases from 0·3 to $0{\cdot}1\times10^{13}$ cm^{-1} from 80 Mev to 150 Mev.

For heavy nuclei therefore $f(\theta)$ is mostly imaginary, particularly when $\sin 2k_1L=0$ and always the same sign as $iJ_1(k\rho\theta)$ which is $+i$ for small θ. Thus if $g(\theta)$ is totally imaginary there will be a maximum polarization and if $g(\theta)$ is totally real then the polarization is near zero. If $g(\theta)$ changes sign then so does the polarization.

The total cross section is given by a well-known theorem

$$\sigma_{\text{tot}}=4\pi k Imf(0)=2\pi R^2\{1-\exp(-KL)\cos(2k_1L)\}. \quad . \quad . \quad (25)$$

This is a maximum for $2k_1L=\pi$ and a minimum for $2k_1L=2\pi$.

Table

k_1L	Total	P +ve	Energy for Pb (Mev)
$\pi/4$		zero	170
$\pi/2$	max.	−ve max.	85
$3\pi/4$		zero	60
π	min.	+ve max.	40

The situation is summarized in the table. The energies in the fourth column are fitted to the experimental maximum for 85 and a smooth variation of k_1 with energy as predicted by Taylor (1954).

This correspondence between the total cross section maximum and the polarization is approximately true for a spherical nucleus, though small deviations are expected because of the integration over the parameter ρ as discussed below.

For light nuclei it is not possible to say that the scattering amplitude $f(\theta)$ is mainly imaginary; in the cylindrical approximation it is still easy to deduce the value for the energy at which the polarization is zero. For small θ, $g(\theta)\ll f(\theta)$ and we find that the variation with energy is

$$\frac{[\cos 2k_1L-\exp(-KL)]E^{\pm 1/2}}{[1-\exp(-KL)\cos 2k_1L]^2+[\exp(-KL)\sin 2k_1L]^2}$$
$$=\frac{[\cos 2k_1L-\exp(-KL)]E^{\pm 1/2}}{1+\exp(-2KL)-2\exp(-KL)\cos 2k_1L} \quad . \quad . \quad . \quad . \quad (26)$$

with the + sign in the exponent for a uniform spin–orbit coupling, and the − sign for the Thomas correction form.

If $L/R=\pi/4$ and values for K and k_1 are taken from Taylor (1954) then the polarization in scattering by carbon is zero at 90 Mev. Experimentally, Dickson (1955) finds that the polarization at 90 Mev, though small, is still the same sign as at high energies. This is hard to explain if a uniform spin–orbit coupling is assumed, but can be explained as a failure of the approximations for a Thomas correction form of spin–orbit coupling, which leads to a shift of the zero to a lower energy.

§ 8. Effects of the Approximations

The approximations have consisted in taking $F=k\rho\delta_1\cos\frac{1}{2}\theta\ll 1$; taking a uniform nucleus with sharp edges; and putting L in place of $\sqrt{(R^2-\rho^2)}$ in the integrals for $f(\theta)$ and $g(\theta)$.

(*a*) *Small spin–orbit coupling*

If the first approximation is not correct, then the replacement of cos F by unity in the formula (9) for $f(\theta)$ is not correct. The integrand in (9) tends to zero for large ρ, so that the approximation need only be accurate for $\rho<0{\cdot}8R$. If $\cos F=-1$ for $\rho<0{\cdot}8R$ then the interpretation of the peak in the plot of total cross section versus energy must be different from that given by Lawson and Taylor. Instead of a cross section maximum for $k_1R=2$ there is a cross section minimum. The peak at 85 Mev for the lead total cross sections would then have to be interpreted as given by $k_1R=4$, and $V_0=40$ Mev ; then a dip would be expected in the total cross section near 150 Mev, which is not found. It is reasonable to suppose therefore, that such a drastic failure of the approximation $F\ll 1$ does not take place.

For the uniform spin–orbit coupling $F=U_0(k^2\rho/2E)\sqrt{(R^2-\rho^2)}$ which, as a function of $\rho<R$, reaches a maximum value of $U_0/E(k^2R^2/2\sqrt{3})$ which depends upon energy only as U_0. For $U_0=1$ Mev we find that $F_{\max}=0{\cdot}2$ for carbon and $1{\cdot}1$ for lead ; the approximation, therefore is beginning to fail (though not drastically) for lead. Since F varies as R^2, this reduces the predicted variations of polarization with R, more nearly, but not sufficiently, in conformity with experiment.

For the Thomas correction form of the spin–orbit coupling we have

$$F=\frac{\alpha V_0}{2E}\frac{1}{[\sqrt{(R/\rho)^2-1}]} \quad . \quad . \quad . \quad . \quad . \quad . \quad (29)$$

which, as already pointed out, goes to infinity as $\rho\to R$. If again we take V_0 from Taylor's paper and then take $\alpha=15$ as used by Fermi and Malenka, we find for $E=100$ Mev, $V_0=20$ Mev,

$$F=\frac{1}{[\sqrt{(R/\rho)^2-1}]}=1{\cdot}33 \quad \text{for} \quad \rho/R=0{\cdot}8. \quad . \quad . \quad . \quad . \quad (30)$$

For ρ greater than this, F increases rapidly and cos F and sin F oscillate. The consequent failure of the approximation $F\ll 1$ has a small effect on $f(\theta)$ reducing slightly the maximum in the total cross section. The effect on $g(\theta)$ is large, especially since large ρ are favoured in the integral for $g(\theta)$.

It is possible to make a preliminary estimate by cutting off the integral at the value of ρ for which $F=\pi$, and assuming that the oscillation of sin F makes contributions to $g(\theta)$ from values of ρ greater than this cancel. If $\alpha=15$ the cut off varies from $\rho/R=0{\cdot}82$ at $E=50$ Mev, to $\rho/R=0{\cdot}93$ at $E=200$ Mev.

(*b*) *Assumption of sharp nuclear boundary*

From the formulae for $f(\theta)$ and $g(\theta)$ it is seen that sharp diffraction maxima and minima are predicted ; $f(\theta)$ changes sign as $J_1(k\rho\theta)$, whereas $g(\theta)$ changes sign as $J_2(k\rho\theta)$. It is clear that there exists regions of angle θ at which the polarization goes negative. This was predicted by Malenka and Sternheimer. It is well known from ordinary optical

considerations that the sharp maxima and minima, and therefore the regions of negative polarization associated with them, are directly related to the unrealistic assumption of a sharp nuclear boundary. If a more realistic assumption (Hofstadter 1954) is made the regions of negative polarization disappear (Sternheimer 1954, Heckrotte 1954).

At the diffraction minimum $f(\theta)$ becomes zero by a cancellation of the effects of different ρ in eqn. (9). Clearly the exact value of $f(\theta)$ is critically dependent on all the approximations and the arguments of this paper cannot apply to such a region.

(c) *Failure of cylindrical approximation*

The cylindrical approximation may be regarded as replacing $\sqrt{(R^2-\rho^2)}$ in the formulae for $f(\theta)$ and $g(\theta)$ by an appropriate average L. As $\rho/R \to 1$ then the integrand in the formula for $f(\theta)$ tends to zero. That in the formula for $g(\theta)$ tends to a maximum, for the Thomas correction spin–orbit coupling, and tends to zero more slowly for the uniform spin–orbit coupling. It is clear therefore that the average appropriate to $f(\theta)$ is a value of ρ *smaller* than that appropriate to $g(\theta)$. This means that the correspondence between the maxima in the total cross sections and the negative polarization is not exact, and the region of negative polarization is shifted to smaller energies. For the uniform spin–orbit coupling this is a small effect, particularly for the heavy nuclei where the correspondence could be established, but for the Thomas correction type of spin–orbit coupling the shift is considerable. For the low energies and large spin–orbit coupling the shift is small because of the cut-off necessary to allow for the oscillation in sin F mentioned earlier. Thus for 50 Mev and $\alpha=15$ the phase shift is approximately the same in $f(\theta)$ as $g(\theta)$ and the cylindrical approximation is valid; but for 200 Mev, the phase shift is less for $g(\theta)$ than the cylindrical approximation predicts.

It has been pointed out to the author (Solmitz 1955) that if F is everywhere small and a Thomas correction type of spin–orbit coupling is assumed, the polarization can be shown to be independent of the magnitude and shape of the potential $V(r)$, and does not change sign as the energy is reduced.

This discrepancy with the predictions of eqn. (28) can be explained in two complementary ways. Firstly, the potential (15) is not the Thomas form in cylindrical coordinates, and the general argument cannot apply. Secondly, the infinite value of F at $\rho=R$ is neglected in the derivation of eqn. (16). This was justified by the observation that sin F must be finite.

For a real nucleus, which has not sharp edges, F will not be infinite. The prediction of eqn. (28) that the polarization changes sign at low energies is critically dependent on the failure of the approximation $F \ll 1$ at the edge of the nucleus. Otherwise the main contribution to $g(\theta)$ comes from large values of ρ. The average phase shift in $g(\theta)$ is small, and the polarization becomes the same as the Born approximation value as Solmitz predicts.

§ 9. Illustration of Approximations

A special case where (15) can be integrated analytically is when $K=0$ and $J_1(k\rho\theta)=k\rho\theta/2$.

$$g(\theta)=\frac{\alpha V_0 k^2\theta}{2E}\,i\left(\frac{\sin 2k_1R-2k_1R\cos 2k_1R}{4k_1{}^3}\right)$$
$$+\frac{\alpha V_0 k^2\theta}{2E}\left(\frac{\cos 2k_1R}{4k_1{}^3}+\frac{R\sin 2k_1R}{2k_1{}^2}-\frac{R^2}{2k_1}-\frac{1}{4k_1{}^3}\right) \qquad (31)$$

the upper limit is taken to be R and the infinity in $1/\sqrt{(R^2-\rho^2)}$ disappears in the integration. The neglect of the infinity gives an error in the opposite direction from the cylindrical approximation. A more realistic approximation (still keeping small enough angles so that $J_1(k\rho\theta)=(k\rho\theta/2)$ is to take

$$\sin\frac{\alpha V_0}{2E}\,\frac{\rho}{\sqrt{(R^2-\rho^2)}}=\frac{\alpha V_0}{2E}\,\frac{\rho}{R}. \qquad (32)$$

This is a very close approximation in the range of parameters

$$\tfrac{1}{2}<V_0/2E<2$$

and is better if the nucleus has not a sharp boundary.

Then $g(\theta)$ may be integrated graphically for various values of KR and k_1R.

$$g(\theta)=\frac{k^2\alpha V_0R^3\theta}{2E}\,(Q+iP) \qquad (33)$$

where values of P and Q are plotted as a function of k_1R in fig. 1. The curves P_0 and Q_0 refer to values for $KR=0$ and $P_{1\cdot5}$ and $Q_{1\cdot5}$ for $KR=1\cdot5$ (corresponding to Taylor's value for lead).

Also plotted in fig. 1 is the equivalent $P_{1\cdot5}$ which is the value of P from the cylindrical approximation from formula (16); and the equivalent value P_0'' from formula (31) (the last with the ordinate divided by 3).

The effects qualitatively discussed are illustrated. The maximum in the negative polarization which corresponds to the negative maximum in P, is shifted to larger k_1R (lower energy) by the failure of the cylindrical approximation. The negative polarization still persists, but relative to the polarization at high energies, the value may be considerably reduced; in the most realistic case to 1/3. The polarization at low energies may be slightly increased due to the decreased values for $f(\theta)$ at small angles, and the possibility of obtaining larger angles before entering upon the first minimum in the diffraction pattern.

It is of interest to note that the exact calculations of Culler (1955) using a uniform spin–orbit coupling at 14 Mev also show this negative polarization.

Fig. 1

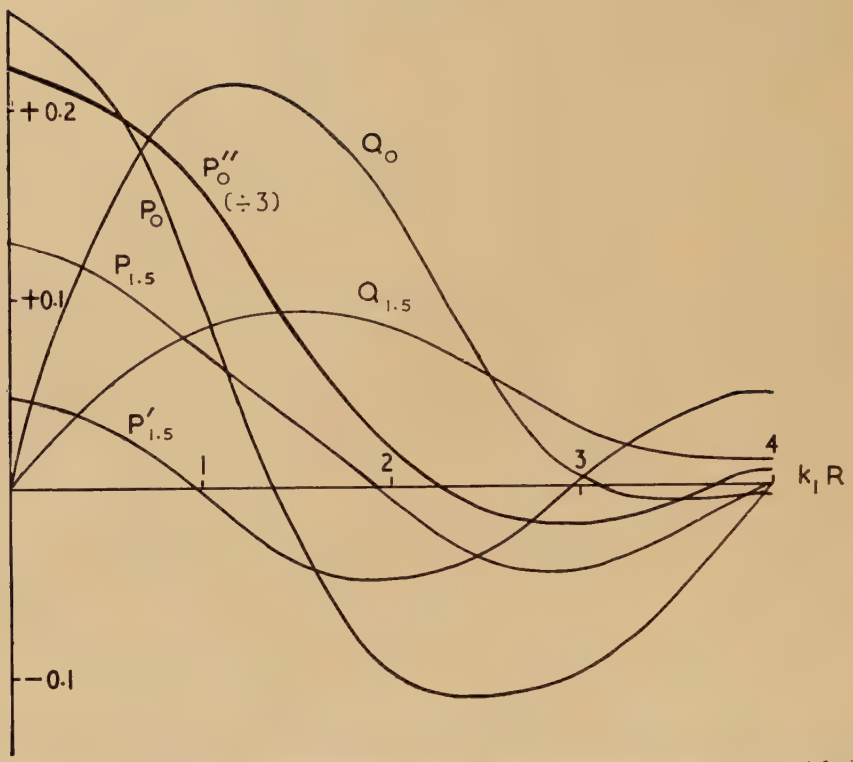

The variation of the spin dependent part of the scattering amplitude with k_1. The functions P and Q are defined by eqn. (33).

§ 10. Coulomb Interference

These formulae have been derived for neutrons. For protons we must add a coulomb scattering term to the scattering amplitude.

The scattering of protons may be solved exactly (Chase 1954). When the number of phase shifts is large, the method of the optical model may still be used if a coulomb potential Ze^2/r to the potential (1) and using the same general formulae (3) and (4). It is easy to show that if $\eta = Ze^2/\hbar v$ is small, then a common phase factor may be taken outside the expressions for $f(\theta)$ and $g(\theta)$ to yield a formula for $g(\theta)$ as before, and for $f(\theta)$ with the addition of a coulomb term

$$-\eta \operatorname{cosec}^2 \theta/2 \exp(-2i\eta \ln \sin \theta/2). \quad . \quad . \quad . \quad . \quad (34)$$

This corresponds to equating the coulomb phase shifts σ_1 to σ_2 in the exact formulae of Chase.

In what follows η will be assumed sufficiently small that this is possible, and further that $2i\eta \ln \sin \frac{1}{2}\theta$ is small in the coulomb interference region. This will hold approximately only for the lightest nuclei; it is under these conditions that the coulomb amplitude may be regarded as real,

as stated by Malenka. The coulomb amplitude is of the opposite sign to the nuclear scattering amplitude so that at one angle these will cancel.

For high energies where the phase shift in $g(\theta)$ is small, $Reg(\theta)=0$. Then

$$P(\theta)=\frac{2Imf(\theta)Img(\theta)}{|f(\theta)|^2+|g(\theta)|^2} \quad . \quad . \quad . \quad . \quad . \quad . \quad (35)$$

the denominator being the unpolarized differential cross section $I(\theta)$. $f(\theta)$ and $g(\theta)$ are slowly varying functions of angle, so that $P(\theta)$ is a maximum when $|f(\theta)|^2+|g(\theta)|^2$ is a minimum.

This prediction is represented graphically in fig. 2 where $P(\theta)$ and $I(\theta)$ is plotted for no coulomb scattering (dotted), and with coulomb scattering (full line). On these plots are also shown the values of $P(\theta)$, P_1 and P_2, at $\theta_{\min}$ for no coulomb interaction and including the coulomb interaction and similarly for I_1 and I_2. The predicted relationship is

$$\frac{P_1}{P_2}=\frac{I_2}{P_1} \quad . \quad . \quad . \quad . \quad . \quad . \quad . \quad . \quad . \quad (36)$$

P_1 and I_1 can be found from a suitable extrapolation from experiment.

The situation is different for the point where $g(\theta)$ has a $\pi/2$ phase shift and becomes totally real. There is now little polarization at most angles, the only contribution being from the term $Re\ g(\theta)\ Re\ f(\theta)$ which is negative. The polarization becomes zero at the interference minimum $\theta_{\min}$ and becomes positive for a very small range of angles less than this minimum fig. 3. The positive value which is reached should be slightly *less* than the value predicted at this angle for no coulomb scattering and no phase shift in $g(\theta)$.

In these calculations the spin dependent interaction due to the magnetic moment of the proton is neglected. The calculation for neutrons (Schwinger 1948) suggest that this is less than 0·1% of the nuclear or coulomb scattering at the angles of 5° at which the coulomb interference appears at 150–300 Mev. At higher energies, however, the calculations of Mott (1929) show that there can be polarization in the coulomb scattering alone. For heavy nuclei η is not sufficiently small and the coulomb scattering affects the scattering at all angles.

When the coulomb amplitude begins to have an appreciable imaginary component, then from (34) it can be seen that the numerator in the formula (35) is reduced. This will *reduce* the peak in the polarization to a smaller value than that given by (33). The preliminary results of Rose suggest a *higher* peak than given by (36). This may be evidence for a phase shift in $g(\theta)$ giving it already a real component.

§ 11. Conclusions

Evidence exists that favours the Thomas correction spin–orbit coupling over the uniform spin–orbit coupling. The former gives a variation of polarization with nuclear radius that is in agreement with

experiment, whereas the latter does not. The rapid fall off of polarization as the energy is reduced from 150 Mev to 60 Mev (Rose 1955) is qualitatively explained ; it is further predicted that for heavy elements the polarization may change sign to give a maximum in the negative polarization near the peak in the total cross section.

Fig. 2

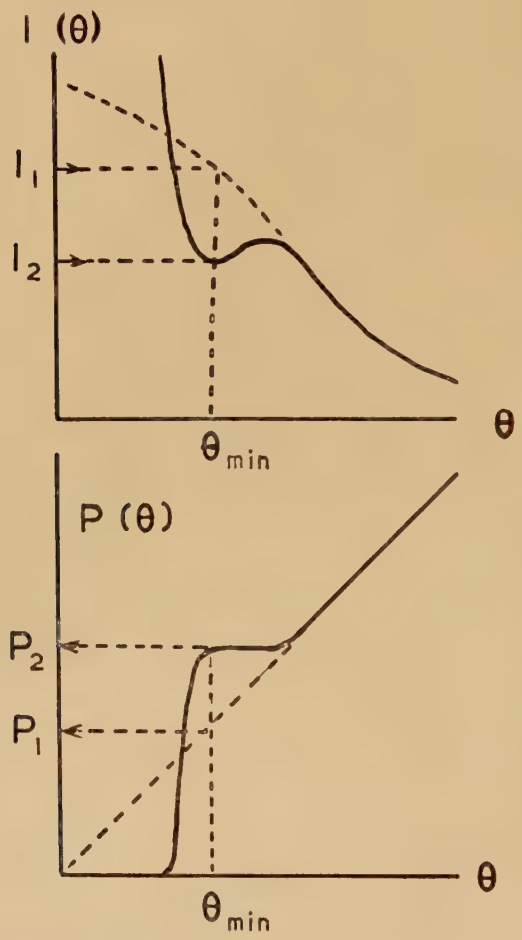

The relation between the polarization as a function of angle and the unpolarized cross section. This for the limit of high energies. Illustrative only.

Several experimental points suggest themselves ; it is of interest to determine the polarization at small angles such that the exact shape of the nuclear potential is relatively unimportant ; yet angles sufficiently large that coulomb interference does not affect the polarization. It is of interest to determine the coulomb interference effects at various energies

in order to obtain information about the phase of $g(\theta)$, to determine to what extent the phase change discussed in this paper is correct. It is also of interest to determine the dependence of polarization upon atomic radius R to check the conclusion that the Thomas correction type of spin–orbit coupling is that which is operative.

Fig. 3

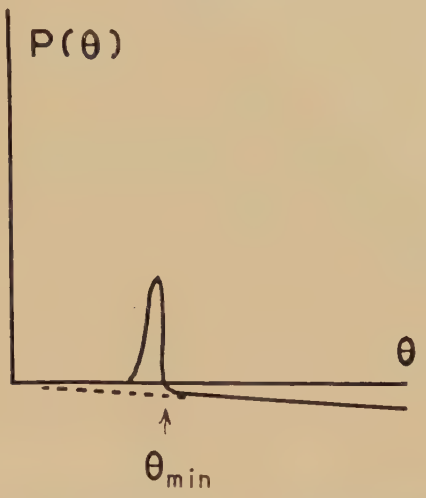

The behaviour of the polarization at the coulomb interference minimum for a $\pi/2$ phase shift in $g(\theta)$.

The relative phases of $f(\theta)$ and $g(\theta)$ can also be determined in triple scattering experiments, as discussed by Wolfenstein (1954).

Acknowledgments

It is a pleasure to acknowledge helpful discussions with Dr. Blin-Stoyle, Dr. Cassels and Mr. Rose, particularly about coulomb interference. Dr. Solmitz kindly pointed out an oversight in the original manuscript.

References

Adair, R. K., Darden, S. E., and Fields, R. E., 1954, *Phys. Rev.*, **96,** 503.
Ball, W. P., 1953, *U.C.R.L. Report* 1938, unpublished.
Chamberlain, O. G., Segre, E., Tripp, R., Wiegand, C., and Ypsilantis, T., 1954 a, *Phys. Rev.*, **93,** 1430.
Chase, D. M., and Rohrlich, F., 1954, *Phys. Rev.*, **94,** 81.
Culler, G., Fernbach, S., and Sherman, N., 1955, *U.C.R.L.* 4446.
De Carvalho, H. G., Marshall, J., and Marshall, L., 1954, *Phys. Rev.*, **96,** 1081.
DeJuren, J. A., 1950, *Phys. Rev.*, **80,** 27.
Dickson, J. M., and Salter, D. C., 1954, *Nature, Lond.*, **173,** 46.
Dickson, J. M., Rose, B., and Salter, D. C., 1955, *Proc. Phys. Soc.*, **68,** 361.
Fermi, E., 1954, *Nuovo Cimento*, **11,** 407.
Fernbach, S., Serber, R., and Taylor, T. B., 1949, *Phys. Rev.*, **75,** 1352.

Fernbach, S., Heckrotte, W., and Lepore, J. V., 1954, *U.C.R.L.*, 2749.
Glauber, R. J., 1953, *Phys. Rev.*, **91,** 459.
Heckrotte, W., and Lepore, J. V., 1954, *Phys. Rev.*, **95,** 1109.
Hofstadter, R., Hahn, B., Knudsen, A. W., and MacIntyre, J. A., 1954, *Phys. Rev.*, **95,** 512.
Lawson, J. D., 1953, *Phil. Mag.*, **44,** 102.
Malenka, B. J., 1954, *Phys. Rev.*, **95,** 522.
Marshall, J., Marshall, L., and Carvalho, H., 1954, *Phys. Rev.*, **93,** 1431.
Mott, N. F., 1929, *Proc. Roy. Soc.* A, **124,** 1929.
Oxley, C. L., Cartwright, W. F., and Rouvina, J., 1954, *Phys. Rev.*, **93,** 806.
Snow, C. P., Sternheimer, R. M., and Yang, C. N., 1954, *Phys. Rev.*, **94,** 1073.
Solmitz, F., private communication.
Sternheimer, R. M., 1954, *Phys. Rev.*, **95,** 587.
Tamor, S., 1954, *U.C.R.L. Report* 2710, unpublished.
Taylor, A. E., and Wood, E., 1953, *Phil. Mag.*, **44,** 95.
Taylor, T. B., 1954, *Phys. Rev.*, **94,** 785.
van Zyl, C. P., Voss, R. G. P., and Wilson, R., 1955, to be published.
Voss, R. G. P., and Wilson, R., 1955, to be published.
Wolfenstein, L., 1954, *Phys. Rev.*, **96,** 1654.

LXXXVIII. *Calculation of Viscous Flow around Spheres at Low Reynolds Numbers*

By T. Pearcey and B. McHugh
Division of Radiophysics, C.S.I.R.O., Sydney, Australia*

[Received in revised form April 13, 1955]

Abstract

Detailed computations have been carried out, on the basis of Oseen's approximation to the hydrodynamic equations of motion, of the flow pattern around a uniformly translated sphere at Reynolds numbers, R, of 1, 4 and 10. A strongly marked wake is apparent even at the lowest Reynolds number. The boundary of the wake becomes more marked as R increases and is bounded by a thin layer in which the fluid motions are particularly small and of rapidly changing direction.

No vortex is attached to the rear of the sphere even at $R=10$, although the presence of a ' boundary layer ' to the front is well indicated.

§ 1. Introduction

A knowledge of the flow velocities to be expected of a viscous medium surrounding a uniformly translated sphere is essential to any, even approximate, theoretical study of effects due for instance to the interaction between two neighbouring droplets falling freely under gravity through air. To facilitate such a study computations have been made of the fluid velocity impressed upon an otherwise stationary viscous medium of infinite extent by a sphere moving with uniform velocity at the relatively low Reynolds numbers of 1, 4 and 10. The computations were based upon the solution of Oseen's (1910) approximation to the hydrodynamic equations of a viscous medium, and the resulting flow patterns are shown in the accompanying figures. The main computations covered in detail the range from the surface of the sphere to a distance of 10 sphere radii (see figs. 1, 2, 3), and additional computations using only the most important terms of the solution continue the description of the flow fields to greater distances (see figs. 4, 5, 6).

A number of questions may be asked about the nature of the flow field and its manner of change with increasing Reynolds number :

(1) At what stage of increasing Reynolds number does a clearly defined wake become established ?

(2) Is a vortex formed immediately to the rear of, and attached to, the sphere ; if so at what stage of increasing Reynolds number does it arise ?

* Communicated by the Authors.

(3) At what stage of increasing Reynolds number does a boundary layer type of flow become established to the front of the sphere ?

Some answer to these questions is given by the results of these computations. Firstly, a distinct wake is established having well-defined properties. Its establishment is apparent at a Reynolds number as low as 1 and is clearly defined at Reynolds' numbers of 4 and 10, and although well defined becomes narrower at higher Reynolds numbers. Secondly, no evidence of the presence of an attached vortex is found even at a Reynolds number as high as 10. This is in disagreement with less extensive computations previously reported by Tomotika and Aoi (1950). Thirdly, the main properties of a boundary layer type of flow at the front of the sphere are clearly marked at a Reynolds' number as low even as 10.

In addition to the two regions of motion distinguished by predominance in one case of irrotational flow, and by vorticity in the other, that is, the wake, the presence of a third region separating the former two is indicated. This new region is one of transition from solenoidal to irrotational flow and is distinguished by particularly small velocities and rapid change in direction of flow.

The transition from one type of flow to the other becomes more rapid as the Reynolds number increases and the region of transition becomes thinner at a somewhat greater rate than does the thickness of the wake.

It seems likely that the flow around smooth surfaced bodies of other shapes than spheres would exhibit similar effects where change from solenoidal to irrotational flow takes place.

§ 2. The Analytical Solution

The complete analytical solution of Oseen's approximation to the flow around a sphere at low Reynolds numbers was given in the comprehensive work by Goldstein (1929 a, b), who however quoted only a table of values for the drag coefficient as a function of Reynolds numbers up to 20. Tomotika and Aoi (1950) have shown that the solution may be given the form of a Stokes type of stream function, from which they computed the pattern of streamlines for a low Reynolds number, namely 1. However, the Stokes' type of stream function is not particularly suitable for showing up the details of the variations which occur in the flow as the Reynolds number varies. The stream function shows only the total flow of fluid, and in any application which needs the actual velocities, a space differentiation must be performed with a consequent loss of precision. All computations have therefore been carried out for the velocities.

All the calculations were made using the basic analytical expressions, suitably adjusted for computing purposes, due to Goldstein ; the details of the expressions and computing techniques are given in the final section.

§ 3. The Coefficients A_n and B_n

The behaviour of the coefficients A_n and B_n† as functions of the Reynolds number determines the manner in which the flow pattern changes from that corresponding to Stokes' flow for very small Reynolds numbers to a state in which a boundary layer type of flow may be expected for larger Reynolds numbers.

The values of the A_n and B_n found for the cases $R=1$, 4, 10 are listed in the table, where it will be seen that all the B_n are positive, the sequence of values as a function of n converging less rapidly to zero as R increases. This applies also to the A_n except for an alteration in sign and an anomaly in the case of A_1 which differs in magnitude from the others by an additional $+\frac{1}{2}$.

For small values of R the B_n decrease very rapidly with increasing n and it may be shown that these satisfy a simple recurrence relation in the limit as R tends to zero, namely

$$B_0 = \frac{3}{2\pi} \cdot \frac{R}{4}(1+0(R^2))$$

$$B_n = \frac{R^2}{16} \frac{B_{n-1}}{(2n+3)(2n+1)}(1+0(R^2)).$$

Their rapid rate of decrease justifies the determination of these coefficients by solution of a finite set of linear equations truncated beyond some suitable values of n and m, which may be determined to provide sufficient precision in all the B_n significant enough to affect the calculations. In fact the ratios of the B_n's of the table closely satisfy this condition for the later values of n. The A_n's do not satisfy such a convenient relationship, but it is well known that for small R

$$A_0 = \frac{3}{R} + \frac{9}{16} + 0(R)$$

and

$$A_1 = +\tfrac{1}{2} + 0(R).$$

In particular, A_0 is related to the B_n's by a simple relationship :

$$A_0 = \frac{2\pi}{R^2} \sum_{m=0}^{\infty} (-1)^m B_m.$$

The leading terms of A_0 and B_0 combine to provide flow velocities which, close to the sphere, correspond to those given by the Stokes solution. Further, from table 1, the A_n decrease with increasing n except A_1 which possesses the main component of $+\frac{1}{2}$: it is precisely this component which would be expected to provide the non-viscous irrotational flow in the case of negligible viscosity.

---

† Here the coefficients A_n and B_n differ from those of Goldstein by a factor $(2n+1/2)$, and due to a slight change of coordinate system the signs of B_n, where n is odd, are changed.

Values of the Coefficients A_n and B_n for $R=1$, 4 and 10

n \ R	1		4		10	
	A_n	B_n	A_n	B_n	A_n	B_n
0	3·5262716	0·1478152	1·217482	1·3890845	0·71690	32·027532
1	$-0·0492207+0·5$	$0·7561227\times10^{-2}$	$-0·120739+0·5$	0·6755315	$-0·17239+0·5$	42·73042
2	$0·221590\times10^{-2}$	$0·5202745\times10^{-4}$	$0·151916\times10^{-1}$	$0·6388151\times10^{-1}$	$0·3363\times10^{-3}$	23·741437
3	$-0·700443\times10^{-4}$	$0·1299286\times10^{-6}$	$-0·132298\times10^{-2}$	$0·2408187\times10^{-3}$	$-0·402\times10^{-2}$	2·982743
4	$0·17260\times10^{-5}$	$0·1656737\times10^{-9}$	$0·8610\times10^{-4}$	$0·4771995\times10^{-4}$	$0·22\times10^{-3}$	0·3219339
5	$-0·3496\times10^{-7}$	$0·1278097\times10^{-12}$	$-0·421\times10^{-5}$	$0·5788223\times10^{-6}$	$-0·1\times10^{-4}$	$0·217858\times10^{-1}$
6	$0·60\times10^{-9}$	$0·660063\times10^{-16}$	$0·14\times10^{-6}$	$0·472712\times10^{-8}$		$0·103724\times10^{-2}$
7		$0·244\times10^{-19}$		$0·2022\times10^{-10}$		$0·36098\times10^{-4}$
8				$0·12\times10^{-12}$		$0·9458\times10^{-6}$
9						$0·17\times10^{-7}$

The total drag force upon the sphere predicted by the theory depends upon A_0 only. The values computed are found to agree with those of Goldstein.

§ 4. Properties of the Flow Velocities

The flow velocities of figs. 1 to 6 show an increasingly strong asymmetry as R increases, and is apparent even at the relatively low value of $R=1$. Further, the rate of decrease of the magnitude of the velocity with distance is much slower to the rear of the sphere than to the front, and a distinct wake occurs.

We may divide the regions of the flow field into two different parts, a distant part in which the properties of flow are distinctly and simply defined, and a region immediately surrounding the sphere.

(*a*) *The Distant Flow*

The flow at great distances from the sphere shows three distinctly different regions : that to the rearward of the sphere and close to the axis of motion comprising the wake ; a region outside the wake extending to the region ahead of the sphere ; and a narrow region of transition separating these two regions.

(i) *The Wake*

Vorticity is shed steadily from the surface of the sphere as it moves through the fluid. into the wake of the sphere close to the axis of motion, and steadily diffuses into the surrounding medium. At great distances, x, from the centre of the sphere along the wake, and at distance y from the axis of motion, the components of fluid velocity become

$$u_r=-RA_0(2x)^{-1}\exp(-Ry^2/8x), \qquad u_\theta=yu_r/2x.$$

It will be noticed that u_θ is proportional to u_r and thus both components, and hence the magnitude, of the velocity vary exponentially as the square of the distance y from the axis of motion in addition to a further slow decrease with distance down the wake as x^{-1}.

The direction of the flow in the wake is generally toward the sphere, and is directed toward the axis of motion at an angle approximately of $(\pi-\theta)/2$, except near the boundary of the wake, the angle θ being measured from the axis of forward motion.

The magnitude of the flow velocity in the wake varies with the Reynolds' number as the factor RA_0, and increases steadily from 3·0 at $R=0$ through 3·526 at $R=1$ and 4·870 at $R=4$ to 7·169 at $R=10$. Presumably thereafter it continues to increase with R somewhat more slowly than linearly. At $R=40$ an estimate of RA_0 gave a value of 20·4.

These properties of the flow may be seen in the figures.

(ii) *The Irrotational Region*

The region well outside the wake exhibits a type of flow which is essentially irrotational. This region extends to the forward axis of motion ahead of the sphere, and the velocity components are

$$u_r \doteq A_0/r^2, \qquad u_\theta=A_1\sin\theta/r^3$$

where θ is the angle between the radius vector and the axis of forward motion. This type of flow differs radically from that in the wake and is almost entirely radial, i.e. $u_r \gg u_\theta$ for large distances. The decrease of velocity with distance is as r^{-2}, instead of r^{-1} as in the wake, and consequently irrotational motions at great distances are much smaller than those in the wake.

Further, there is an additional decrease in velocity of this type as R increases, as may be seen from the decreasing trend of the values of A_0 in the table. Thus the magnitude of flow in this region decreases as A_0, as distinct from the increase as RA_0 in the wake.

These properties are exhibited by the figures where the lines of constant u_r differ little from arcs of circles centred about the sphere. The relative ranges of the rotational and irrotational flows may be compared by inspecting the points on the axis of motion which correspond to velocities of 1% of the sphere velocity. These distances, expressed as a ratio of distance along the wake to the distance forward, are 9·389 for $R=1$, 22·068 for $R=4$, and 42·335 for $R=10$. These figures may be taken as a measure of the asymmetry of the flow, and even at $R=1$ the 'length' of the wake extends to nearly 10 times the range of the flow to the front.

(iii) *The Transition Region*

A region of transition marks the boundary between the regions of rotational and irrotational flow. This possesses again a flow of character. Both u_r and u_θ change sign upon passing from one region to the other. This occurs in the transition region which contains the curves $u_r=0$ and $u_\theta=0$ defined approximately by

$$Rr(1+\mu)/4 \doteqdot \ln (rR/2) \qquad \text{for} \quad u_r=0$$

and

$$Rr(1+\mu)/4 \doteqdot 2 \ln (rR/2)+\ln 2A_0/RA_1 \qquad \text{for} \quad u_\theta=0.$$

The former of these expressions is the more important since u_r is normally an order greater than u_θ and because of the slow variation of the logarithm, represents a nearly parabolic curve about the axis of the wake. In the immediate neighbourhood the flow is further reduced in size to the size of u_θ at least, and this varies at least as rapidly as r^{-3}, that is, more rapidly than in either of the neighbouring regions. Associated with the reduction in velocity is rapid change of direction of flow caused principally by the reversal of sign of u_r. For large R this amounts to almost a complete reversal of direction. These effects are apparent in figs. 4, 5 and 6.

The 'thickness' of the region of transition, Δy say, is determined by the rate of change of the vorticity at the boundary of the wake and so at large distances

$$\Delta y \propto y\,(\ln Rr)^{-1} \propto (2r/R \ln Rr)^{1/2}$$

where y takes approximately the value for which $u_r=0$. Thus this region is a layer which decreases in thickness somewhat more rapidly

than does the wake as both the Reynolds number and the distance increase. In particular, this implies the wake to appear sharply bounded as the Reynolds number increases.

(*b*) *Flow Close to the Sphere*

Figures 1, 2 and 3 show the flow close to the sphere, that is, up to $r=10$. A steady transition of the flow from $R=1$ to $R=10$ is clear ; in particular the line $u_\theta=0$, not evident in the case $R=1$, approaches the sphere from

Fig. 1

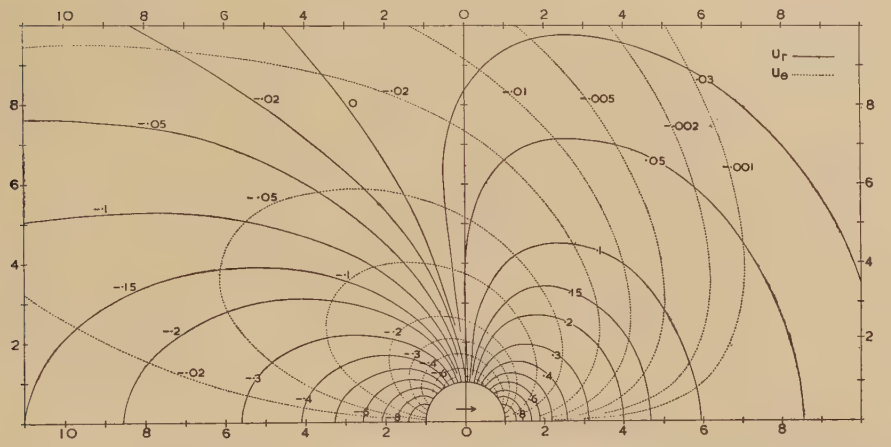

Flow around a sphere at $R=1$. Contours of fluid velocity in radial and angular directions, u_r and u_θ, referred to the velocity of the sphere moving from left to right. Dimensions are referred to the radius of the sphere.

Fig. 2

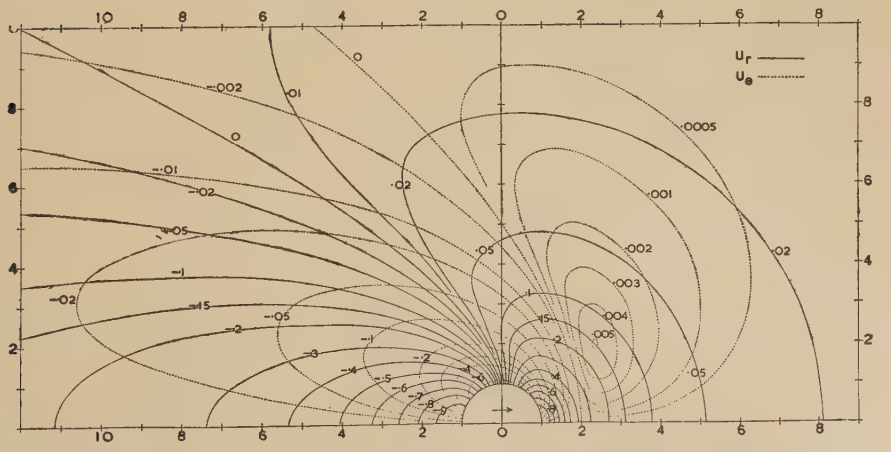

Flow around a sphere at $R=4$. Contours of fluid velocity in radial and angular directions, u_r and u_θ, referred to the velocity of the sphere moving from left to right. Dimensions are referred to the radius of the sphere.

the forward region and is apparent at $R=4$ and 10. This curve meets the forward axis of motion orthogonally, while the curve $u_r=0$ meets the surface of the sphere at $\theta=\pi/2$ for all R. As R increases, these curves approach each other.

Fig. 3

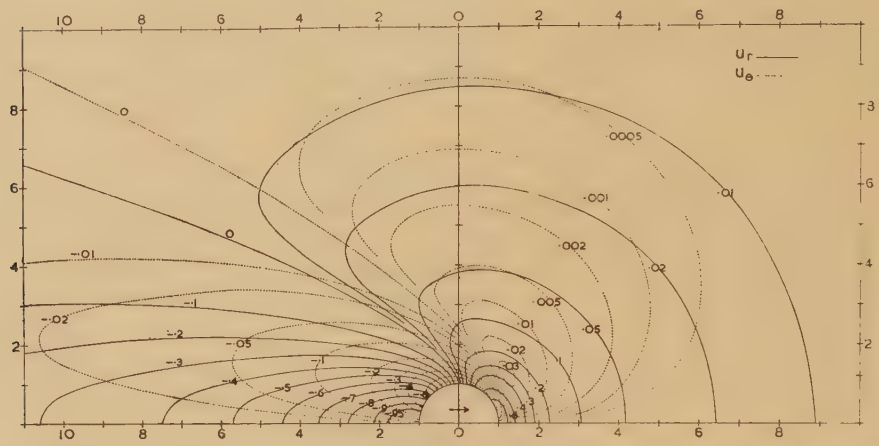

Flow around a sphere at $R=10$. Contours of fluid velocity in radial and angular directions, u_r and u_θ, referred to the velocity of the sphere moving from left to right. Dimensions are referred to the radius of the sphere.

(i) *Flow to the Front*

The diffusion of vorticity from the surface affects the flow immediately to the front of the sphere. As the Reynolds number increases, the vorticity is swept rearward more rapidly than it diffuses forward. Roughly, the boundary between the rotational flow near the surface and the irrotational flow well forward is delineated by the line $u_\theta=0$. This curve approaches the surface of the sphere as R increases, and the gradient of velocity at the surface becomes large. In fact a boundary layer is formed. This is apparent at $R=10$ in fig. 3, and the thickness of this layer is also of the expected order of magnitude, i.e. $R-\frac{1}{2}\times$ (diameter of sphere).

Thus, even at such a low Reynolds number as 10, there is clear evidence of the establishment of a boundary layer.

(ii) *Flow to the Rear*

Computations of the stream function by Tomotika and Aoi indicated the establishment of a stationary vortex situated at, and attached to, the rear of the sphere. Our calculations show no evidence of such a vortex even at $R=10$. To the immediate rear of the sphere is that region where the computation of the velocities is most difficult because of the slowness of the convergence of the series. Our calculations, at $R=10$, we believe to be correct to about a unit or two in the third decimal, and better for $R=4$ and 1. If Tomotika's calculations are correct at

$R=1$, the only case attempted by him, there should have been, within the accuracy of the present computations, a clear indication of the presence of the vortex. The disagreement is probably due to the truncation of the series to $n=1$ previously adopted by Tomotika.

It may also be argued on physical grounds that the vortex should not exist, for it may be easily possible for the volume vacated by the motion of the receding surface to be filled with fluid which can approach from all directions along the surface of the sphere. This is distinctly different from the case of the moving cylinder in which fluid can move to fill up the vacated space from two directions only. It is well known that a clearly defined vortex is attached to the rear of a cylinder (Thom 1933).

It seems clear, however, that some form of attached vortex must eventually arise, since in a well-established boundary layer at the surface of a sphere separation does take place. Presumably, at some Reynolds number greater than 10, a vortex is formed which must spread over the surface as R increases. It is of course not clear that solutions of Oseen's approximation would predict such a separation. A solution of the full hydrodynamic equations would seem to be required.

No estimates of the errors due to the use of Oseen's approximation have been made, but the term omitted from the equations of motion is $(\mathbf{u} \cdot \nabla)\mathbf{u}$ and is large where either $\mathbf{u}$ is large or $\nabla\mathbf{u}$ is large. For large R this is particularly serious close to the surface of the sphere where both $\mathbf{u}$ and $\nabla\mathbf{u}$ are large. Although at the surface the usual boundary conditions are satisfied and thus the error in $\mathbf{u}$ must be small, the error in $\nabla\mathbf{u}$ may be large, and may in fact affect the solution so far as to fail to show a separation which could be indicated by a solution of the complete equations of motion.

§ 5. Method of Computation

The computations were carried out largely by automatic methods with the assistance of Hollerith and I.B.M.-type punched-card machines, suitable checks for precision and freedom from error being made at each stage. The computations proceeded in four main stages, first the evaluation of the matrices of coefficients α_{nm} and λ_{nm} in preparation for the determination of the A_n and B_n which followed. Tables of the necessary functions of r and θ were constructed ; and final multiplication by the A_n and B_n and summation provided the values of u_r and u_θ. From tables of these values figs. 1, 2 and 3 were drawn, those of figs. 4, 5 and 6 being obtained from the asymptotic expressions for u_r and u_θ at large distances using the A_0 and A_1 previously obtained.

The expressions used correspond closely to those of Goldstein (1929 b) except for small changes made to assist computation. Thus our A's and B's correspond to those of Goldstein multiplied by $(2n+1/2)$. The angle θ is measured from the axis of forward motion.

The $\psi_n(z)$'s and $\psi'_n(z)$'s were computed from their known recurrence relations in descending order of n, those for the two highest values of n

Fig. 4

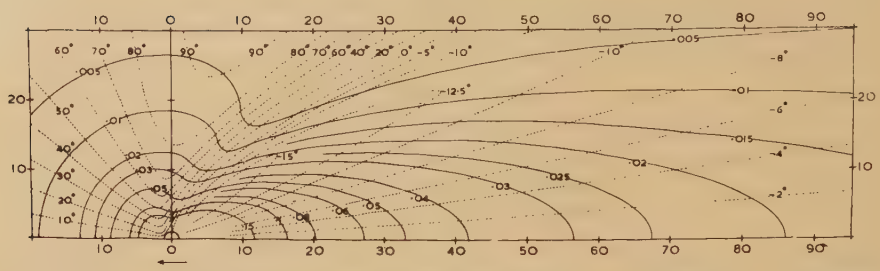

Flow around a sphere at great distances at $R=1$. Contours of constant magnitude and direction of flow velocities. The magnitude, full lines, is referred to the velocity of the sphere ; the lines of constant direction, dotted, indicate direction away from the axis of motion. Dimensions are referred to the radius of the sphere, which moves from right to left.

Fig. 5

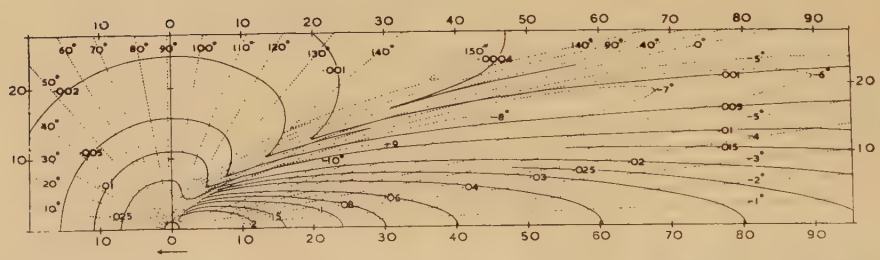

Flow around a sphere at great distances at $R=4$. Contours of constant magnitude and direction of flow velocities. The magnitude, full lines, is referred to the velocity of the sphere ; the lines of constant direction, dotted, indicate direction away from the axis of motion. Dimensions are referred to the radius of the sphere, which moves from right to left.

Fig. 6

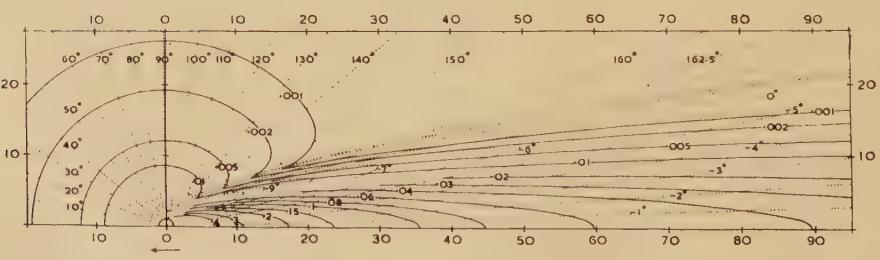

Flow around a sphere at great distances at $R=10$. Contours of constant magnitude and direction of flow velocities. The magnitude, full lines, is referred to the velocity of the sphere ; the lines of constant direction, dotted, indicate direction away from the axis of motion. Dimensions are referred to the radius of the sphere, which moves from right to left.

being specially computed to sufficient accuracy for the three values of z. This method was adopted to avoid the progressive loss of precision which occurs upon repeated application of the recurrence formulae when n is greater than z. From these ψ'_n's the values of the Ψ_{nm}, Ψ'_{nm} and X_{nm} were obtained for $n>m$, extension to values of $n<m$ being readily obtained from the symmetry properties of these functions.

The χ_n and χ'_n needed were computed by use of recurrence relations from the specially computed values of χ_0 and χ_1, for ascending values of n. From the results of these computations the matrices of values of α_{nm} and λ_{nm} were then computed, retaining 10 significant figures, and extending to $n=8$, $m=7$ for $R=1$, to $n=9$, $m=8$ for $R=4$ and to $n=10$, $m=9$ in the case $R=10$.

The solution of the three sets of linear equations for the B's was carried out on a 602A-type punched-card calculator, using a specially devised programme. The method of solution adopted was equivalent to that of progressive pivotal condensation about the successive terms of the leading diagonal of the matrix of coefficients. Owing to the great variation in the magnitude of the λ_{nm} in any one matrix, a system of floating point arithmetic was adopted, each number being represented as a 15-digit fraction, together with an integral number denoting the index which was allowed to vary by multiples of 5 units. The programme of the computation was devised to maintain the fractional component within the range 1·0 and 10^{-5}, appropriate 5-place shifts and adjustments to the index being made to ensure this. Checks were made on the accuracy of the resulting B's by substitution into the original equations.

The final tabulation of the flow velocities was completed also by the use of standard punched-card machines. For this purpose, tables of the required functions were produced, which by correct manipulation could provide the values of the flow velocities. Some simplification of the computation was attained by extracting the exponential function from the χ_n and associating it with the factor $\exp -Rr\mu/4$ as $\exp -Rr(1+\mu)/4$ and then using $\kappa_n(Rr/4)$ defined by writing

$$\chi_n(z)=\exp(-z)\kappa_n(z).$$

From tables of $\kappa_0(z)$ and $\kappa_1(z)$, similar tables for $\kappa_n(z)$ were obtained by recurrence, thus

$$\kappa_0(z)=\frac{1}{2z}, \qquad \kappa_1(z)=\frac{1}{2z}\left(1+\frac{1}{z}\right), \qquad \kappa_{n+1}(z)=\frac{\kappa_n(z)}{z}-\kappa_{n-1}(z).$$

Then the expressions for u_r and u_θ become

$$\left.\begin{aligned} u_r&=\sum_{n=0}^{\infty}\{A_n(1+n)/r^{n+2} \\ &\quad +\exp[-z(1+\mu)][\beta_n\kappa_{n-1}(z)+\beta_{n+1}\kappa_{n+1}(z)]\}P_n(\mu) \\ u_\theta&=\sin\theta\sum_{n=1}^{\infty}\{A_n/r^{n+2} \\ &\quad -\exp[-z(1+\mu)][\gamma_{n-1}\kappa_{n-1}(z)+\gamma_n\kappa_{n+1}(z)]\}P_n'(\mu) \end{aligned}\right\} z=Rr/4$$

where the β_n and γ_n depend upon the B_n's previously obtained, $z=Rr/4$, and $\cos\theta=\mu$; thus

$$\beta_n=n\left[\frac{B_n}{2n+1}+\frac{B_{n-1}}{2n-1}\right], \qquad \gamma_n=\frac{B_n}{2n+1}-\frac{B_{n+1}}{2n+3}.$$

Tables of $\exp -(1+\mu)z$ were formed on card decks for values of θ from 0 to 180° in 10° intervals and at varying intervals of z from 0·2 to 25 ; from 0·1 for small z and increasing toward the upper limit of the range. Tables of the remaining radial function were then formed, and their products with regard to the $P_n(\mu)$ and $P_n'(\mu)$ were obtained. These products were again multiplied by the exponential function. Tables of the remaining terms in r^{-n-2} were obtained separately. After selection of the appropriate values of z corresponding to the particular case of R from the card decks, the values of both components were summed in n and the final totals for u_r and u_θ obtained.

In the final stages a precision of five figures was retained in the case $R=1$. In the case $R=4$, five figures were retained except close to the rear of the sphere where convergences of the series are slow, and four figures only were obtained. In the case $R=10$, four figures were retained except at the rear of the sphere where, after some careful extrapolation of the series to improve convergence, three figures were kept.

Acknowledgments

The authors wish to express their appreciation of the assistance of Mr. J. Telford and Miss M. Adamson, the former for assistance in devising the methods of computation and the latter for the extensive and very detailed work involved in the final tabulation.

References

Goldstein, S., 1929 a, *Proc. Roy. Soc.* A, **123**, 216 ; 1929 b, *Ibid.*, **123**, 226.
Oseen, 1910, *Ark. Mat. Ast. Fys.*, **6**, No. 29.
Thom, A., 1933, *Proc. Roy. Soc.* A, **141**, 658.
Tomotika, S., and Aoi, I., 1950, *Quart. J. Mech. and App. Math.*, **3**, 140.

LXXXIX. *The Selection of Potentials in Nucleon–Nuclear Scattering Problems*

By G. C. Morrison, H. Muirhead and P. A. B. Murdoch
Department of Natural Philosophy, University of Glasgow*

[Received April 10, 1955]

Summary

It is shown that the magnitudes of the real and imaginary potentials employed in nucleon–nuclear scattering problems may be qualitatively predicted with the aid of data on free nucleon–nucleon scattering, and a Fermi gas model of the nucleus.

§ 1. Introduction

Feshbach, Porter and Weisskopf (1953, 1954, referred to henceforward as F.P.W.) have suggested that the magnitude of the imaginary potential in their ' cloudy crystal ball ' model of the nucleus may be interpreted in terms of a relatively long mean free path for nucleons in nuclear matter, before their incorporation in the compound nucleus. They have estimated that for neutrons with energies $\sim$1 mev the mean free path is about 2×10^{-12} cm in nuclear matter. A mean free path $\sim10^{-12}$ cm for nucleons in the same energy range was obtained by members of this laboratory (Morrison, Muirhead and Rosser 1953) during the course of a calculation on the development of a nucleon cascade inside a nucleus.

In view of the successful extension of the model of F.P.W. to other energies (Woods and Saxon 1954), with an apparent necessity to modify the imaginary part of the potential in the manner predicted by our earlier calculation, we have estimated the potentials expected on the basis of a very simplified free particle model of the nucleus. In this model we have assumed that, since the nuclear potential well is comparatively deep ($\sim$40 mev), when even a slow nucleon enters nuclear matter it will possess a wavelength of roughly inter-nucleon dimensions, and so it may be considered to move as a free particle through that matter. This assumption allows a description of the absorption of a nucleon in a nucleus to be made in terms of a model which has been successfully applied at much higher energies (Fernbach, Serber and Taylor 1949). A similar approach to the problem has been made by Lane and Wandel (private communication).

§ 2. Method of Calculation

F.P.W. expressed their nuclear potential in the form $V_0(1+i\zeta)$. We have assumed a nucleus to consist of two Fermi gases of neutrons and protons. We have defined the depth V_0 to be the maximum Fermi

* Communicated by Professor J. C. Gunn.

energy plus the binding energy of the last nucleon. The binding energies were obtained from the tables of Feather (1953). The radius, R, of the neutron gas was assumed to be given by $1{\cdot}37A^{1/3}\times 10^{-13}$ cm, where A represents the atomic weight of the nucleus ; with this assumption we obtain a value for V_0 of about 38 Mev for $A\sim 100$. This figure is almost insensitive to A in the range of A from 50 to 200. The further assumption was made that the real potential was the same for the proton as for the neutron gas. This placed the proton gas within a sphere of radius $\sim 1{\cdot}18A^{1/3}\times 10^{-13}$ cm.

An expression relating the mean free path, λ, of a particle in nuclear matter and the imaginary potential, ζV_0, has been given by Francis and Watson (1953),

$$\zeta V_0 = \frac{\hbar}{\lambda\sqrt{(2m)}}(E+V_0)^{1/2}$$

where E represents the kinetic energy of the incident nucleon, and m its mass. We now assume, on our free particle model, that the mean free path, λ, can be expressed in terms of the cross sections for free particle scattering modified by the restrictions of the Pauli exclusion factor in the manner first described by Fernbach, Serber and Taylor (*loc. cit.*)

$$1/\lambda = \alpha_{Np}\sigma_{Np}\rho_p + \alpha_{Nn}\sigma_{Nn}\rho_n$$

where α_{Np}= Pauli exclusion factor for a nucleon, N, in collision with a proton inside the nucleus, σ_{Np}= free nucleon–proton scattering cross section, ρ_p=proton density in the nucleus, and the other three terms represent the corresponding quantities related to a collision with a neutron.

The term α has been calculated by Goldberger (1948) for nucleons whose energies are greater than twice the maximum Fermi energy. We have extended this calculation to particles of lower energies and have included rough correction factors for the difference in binding energy of the last proton and neutron, and the non-isotropy of neutron–proton scattering in the centre of mass system for energies greater than $\sim$ 20 Mev.

§ 3. Results

Using published data on n–p and p–p scattering and assuming that the latter is equivalent to n–n scattering, the imaginary potentials may be estimated to be

$$\zeta V_0 \sim (3{\cdot}0+0{\cdot}35E) \text{ Mev for neutrons}$$
$$\sim (1{\cdot}3+0{\cdot}35E) \text{ Mev for protons,}$$

where E is expressed in Mev units. This calculation was carried out for values of E lying between 0 and 24 Mev and for a nucleus in the middle of the periodic table : like the calculation for V_0, it is fairly insensitive to the nucleus involved, over the range $A=50$–200. It should also be noted that the calculation represents the potential in the interior of the nucleus.

In the table we have compared the imaginary potentials with those used by various authors in successful applications of the ' cloudy crystal ball ' model (F.P.W., *loc. cit.*, Culler, Fernbach and Sherman 1955, Woods and Saxon *loc. cit.*).

Incident particle	Scattering nucleus, radius $\times 10^{13} \times A^{-1/3}$ cm^{-1} and potential used	$V_0(1+i\zeta)$ this calculation
0·1–400 ev neutrons	A=100–250 1·45 (42+1·2i) Mev (42+2i) Mev	(38+3·0i) Mev
50 kev–3 Mev neutrons	A=10–250 1·45 (42+1·2i) Mev (42+2i) Mev	(38+3·5i) Mev
14 Mev neutrons	A=12–208 (1·22$A^{1/3}$+0·74) ~1·4 (42+11i)	(38+8i) Mev
18 Mev protons	Nickel 1·36 (40+10i) Mev	(39+8i) Mev
22 Mev protons	Platinum 1·42 (38+9i) Mev	(37·5+9·7i) Mev

The values of the potential given for 18 and 22 Mev protons in the last column of the table differ slightly from those quoted earlier, in that account has been taken of the binding energies of the last nucleons in the main isotopes of nickel and platinum.

In addition, the potential obtained by us for neutrons at very low energies, (38+3·0i) Mev, has been used to evaluate the ratio of reduced neutron widths to level spacing, $\bar{\Gamma}_n^0/\bar{D}$, (Γ_α^0/D in the notation of F.P.W.). This calculation has been carried out for a square potential well, and a rounded well of the type used by Woods and Saxon (*loc. cit.*)

$$V(r) = \frac{(38+3\cdot0i)}{1+\exp{(r-R)/a}}$$

where a value of $0\cdot49\times10^{-13}$ cm was used for a. This figure represents a rough mean of the two values quoted by these authors for nickel and platinum. The result of this calculation is compared with that obtained using the parameters of F.P.W. in figs. 1 and 2.

Fig. 1

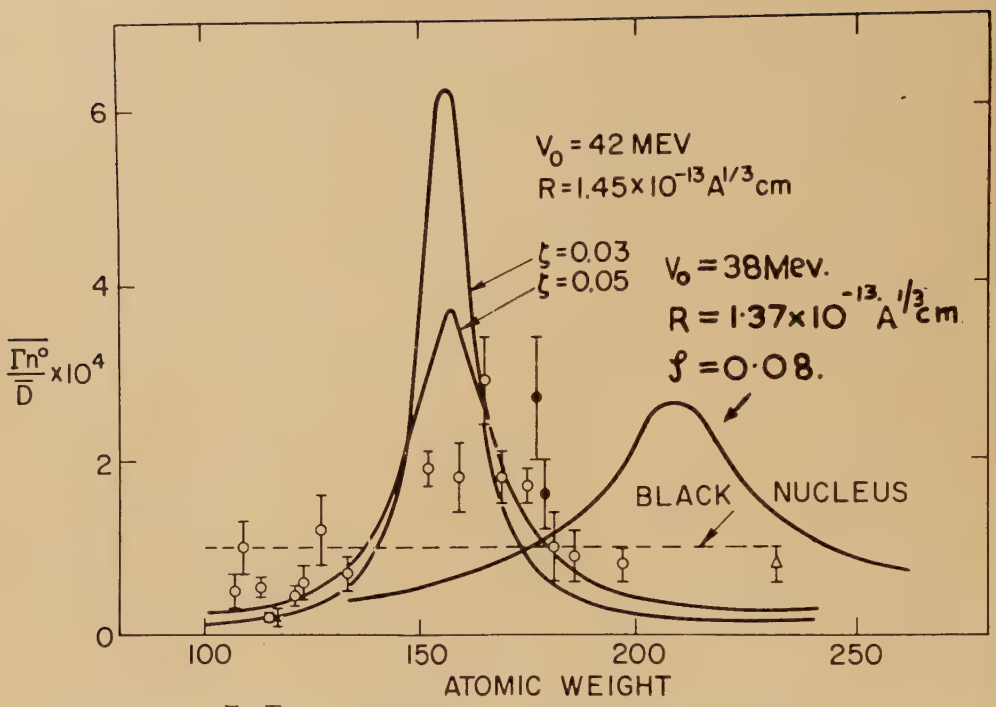

$\bar{\Gamma}_n^0/\bar{D}$ as a function of A for square potential well.

Fig. 2

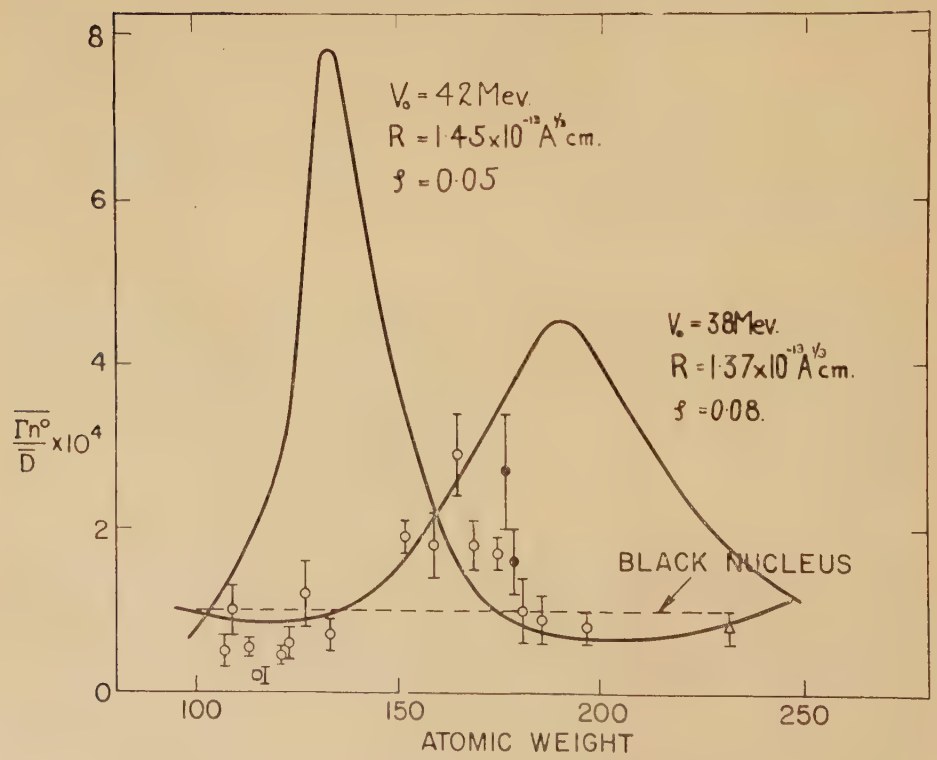

$\bar{\Gamma}_n^0/\bar{D}$ as a function of A for a rounded potential well.

§ 4. Discussion

It can be seen that, when our potential is applied, the maximum value of $\bar{\Gamma}_n^0/\bar{D}$ is displaced to values for A which are too large when compared with the experimental data. The maximum value of $\bar{\Gamma}_n^0/\bar{D}$ is mainly dependent on the mean free path, λ, for the nucleons, whilst its position is sensitive to the product of $V_0^{1/2}R$. In performing the calculation for a rounded potential well, we have not taken into account that the rounding of the well will also change its depth. The work of Scott (1954) has indicated that if a Fermi gas model is abandoned in favour of a shell model with a rounded potential well, then the depth of the well must be increased in order to confine the nucleons. An effect of this type would cause the maximum value of $\bar{\Gamma}_n^0/\bar{D}$ to occur at a lower value of A.

In order to obtain satisfactory agreement with the magnitude of $\bar{\Gamma}_n^0/\bar{D}$, it would be necessary to increase ζV_0 by a factor of 2 when employing a rounded potential well. Such an increase does not appear possible for this model.

An examination of the table indicates that our simplified free particle model gives rise to values for the imaginary potential, which are, qualitatively, in satisfactory agreement with those derived from successful applications of the ' cloudy crystal ball ' model to the analysis of scattering experiments at different energies. This approach gives rise to the possibility of calculating the magnitude of the direct interaction effects at intermediate energies in nuclear reactions involving medium and heavy nuclei. Such an approach could yield information on the distributions in energy and angle of the products of these interactions, if suitable assumptions could be made concerning the penetration of the surface of the nucleus by the outgoing particles.

Acknowledgment

The authors wish to express their gratitude to Professor J. C. Gunn for many valuable discussions during the course of this work.

References

Culler, G., Fernbach, S., and Sherman, N., 1955, *UCRL Report*, 4436.
Feather, N., 1953, *Adv. in Phys.*, **2**, 141.
Fernbach, S., Serber, R., and Taylor, C., 1949, *Phys. Rev.*, **75**, 1352.
Feshbach, H., Porter, C. E., and Weisskopf, V. F., 1953, *Phys. Rev.*, **90**, 166 ; 1954, *Ibid.*, **96**, 448.
Francis, N. C., and Watson, K. M., 1953, *Amer. J. Phys.*, **21**, 659.
Goldberger, M. L., 1948, *Phys. Rev.*, **74**, 1269.
Morrison, G. C., Muirhead, H., and Rosser, W. G. V., 1953, *Phil. Mag.*, **44**, 1326.
Scott, J. M. C., 1954, *Phil. Mag.*, **45**, 751.
Woods, R. D., and Saxon, D. S., 1954, *Phys. Rev.*, **95**, 577.

XC. *A Note on the Branching Ratio of the* D–D *Reactions*

By K. G. McNeill

Department of Natural Philosophy, The University, Glasgow, Scotland*

[Received March 3, 1955]

Abstract

Recently two papers have been published which contain results on the branching ratio of the two D–D reactions at variance with those of earlier workers. In this note it is suggested that this disagreement is due to the acceptance by the latter of incorrect values for the angular asymmetries of the reactions. On this assumption the experimental results have been recalculated using more recent data on the angular distribution, and it is found that the corrected values are in agreement with those of the more recently published results; that is, the 90° c.m. branching ratio, $\sigma D(dn)^3He/\sigma D(dp)^3H$, does not vary with deuteron energy, but the ratio of the total cross sections rises from 1·01 at 14 kev to 1·20 at 466 kev deuteron energy.

§ 1. Introduction

In recent years several research groups have studied the D–D reactions

$$D+D \rightarrow {}^3He+n+3{\cdot}3 \text{ Mev} \qquad (a)$$

$$\rightarrow {}^3H+p+4{\cdot}0 \text{ Mev} \qquad (b)$$

in the deuteron energy region 0–300 kev. Particular attention has been given to the variation with deuteron energy of the branching ratio, that is, the ratio of the cross section for reaction (*a*) to the cross section for reaction (*b*).

McNeill and Keyser (1950), and Arnold, Phillips, Sawyer, Stoval and Tuck (1954) (hereinafter referred to as MK and APSST respectively), measured the yields of the reaction products from a gas target at an angle to the deuteron beam of 90° in the laboratory frame of reference. After conversion of their experimental results to the more instructive centre of mass frame of reference, these two sets of authors published mutually consistent results which showed that, at all detection angles in the c.m. frame, the branching ratio $^3He/^3H$ increased from 0·93 at 13 kev to 1·06 at 250 kev.

Similar experiments on the yields of the charged particles from the D–D reactions were performed by Eliot, Roaf and Shaw (1953), and Preston, Shaw and Young (1954). Both these groups measured the branching ratio at more than one detection angle. Their mutually

* Communicated by the Author.

consistent results indicate that the 90° c.m. branching ratio does not vary appreciably with energy (having at all energies a value of about 0·96), but that the total branching ratio, that is, the ratio of the total cross sections of the two reactions, increased from 1·01 at 14 kev to 1·20 at 466 kev.

The D–D reaction is of considerable theoretical interest, and therefore the results of the various authors have been investigated to determine whether the disagreement between them is a fundamental one, or whether it has arisen in the course of the interpretation of the experimental results.

§ 2. The Angular Anisotropies of the Reactions

As previously stated, MK and APSST measured the yields of the reactions at an angle to the deuteron beam of 90° in the laboratory frame of reference. The effective angle of measurement in the centre of mass system therefore changed with deuteron energy, and at a particular energy was different for the two reactions. For purpose of comparison, it is necessary either to calculate the yields corresponding to a particular angle in the c.m. system, for example 90° c.m., or to determine the total cross section from the measured differential cross section at 90° in laboratory coordinates. Both alternatives require a knowledge of the angular anisotropies of the two reactions.

In the low energy region, the angular anisotropies of both reactions may be represented by an equation of the form $\sigma_\theta = \sigma_{90}(1+A(E)\cos^2\theta)$, where $A(E)$ is the asymmetry coefficient, corresponding to a deuteron energy E, for the reaction under consideration. Then the 90° c.m. yields are obtained from the $90°_{\text{lab}}$ results by multiplying the latter by the factor $g(\phi)/(1+A(E)\cos^2\phi)$, where ϕ is the c.m. angle corresponding to $90°_{\text{lab}}$, and $g(\phi)$ is a solid angle correction term depending only on the c.m. and laboratory detection angles.

It is clear that a knowledge of the actual values of the angular anisotropies is necessary for converting the experimental results. At the time of the work of MK and APSST, the results of Bennett, Mandeville and Richards (1946), Hunter and Richards (1949), and Bartholdson (1950), all appeared to indicate that the anisotropy coefficients at a given deuteron energy were the same for both reactions. Both MK and APSST therefore used the accurately known values for the anisotropy coefficients for the proton reaction when converting both the D(dn)^{3}He and D(dp)^{3}H experimental results to the centre of mass coordinate system. In particular, MK used the values of $A(E)$ given by Manning, Huntoon, Myers and Young (1941), while APSST used the values of Wenzel and Whaling (1952). These two sets of values are in agreement with one another and with later results.

However, during the course of the work previously quoted, Eliot, Roaf and Shaw (1953), and Preston, Shaw, and Young (1954) measured the angular distributions of the ^{3}He and ^{3}H nuclei from the two reactions and both concluded that at all deuteron energies (between 0 and 466 kev)

the asymmetry coefficient for reaction (*a*) was greater than the corresponding coefficient for reaction (*b*). Both these groups naturally used their own values for the asymmetry coefficients when converting their experimental results to the c.m. frame. As Preston, Shaw and Young (1954) point out, the earlier workers on the angular distribution for reaction (*a*) made their measurements on the emitted neutrons, and none of them measured the proton angular distribution at the same time. The difficulties associated with fast neutron detection suggest that the measurements of Eliot, Roaf and Shaw, and of Preston, Shaw and Young should be accepted in preference to the earlier results.

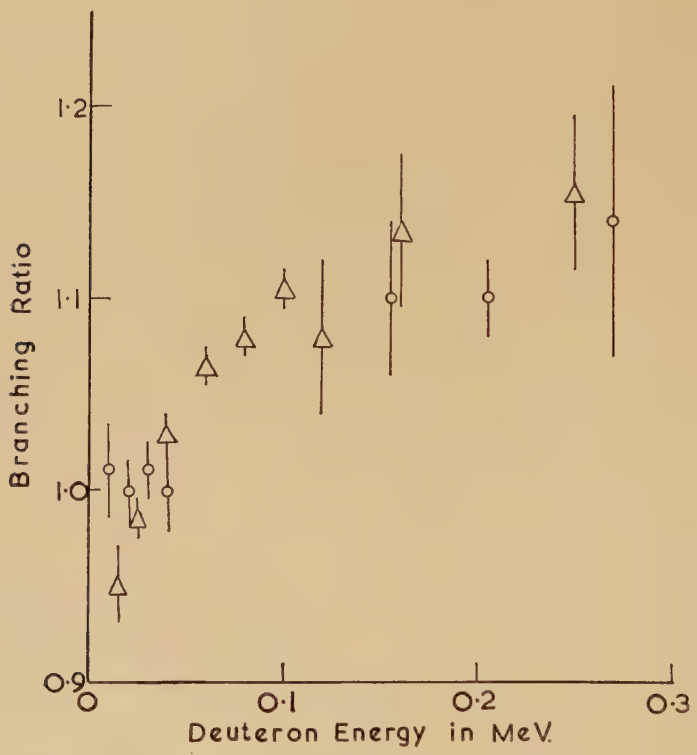

The branching ratio (ratio of the total cross section for the reaction D(dn)^{3}He to that for the reaction D(dp)^{3}H) as a function of deuteron bombarding energy. ♀ Preston, Shaw and Young (1954), and Eliot, Roaf and Shaw (1953), the values being taken from fig. 4 of the former paper. ♙ The corrected values of Arnold *et al.* (1954), and McNeill and Keyser (1951). These values are given in the table of the present paper.

In this connection it is of interest to note that experiments on the angular distributions of the neutrons at incident deuteron energies between 200 and 700 kev are being carried out at Glasgow by A. Ward. In this work the fast neutrons are being detected by plastic scintillators.

§ 3. Recalculation of the Experimental Results

The acceptance by MK and APSST of wrong values for the asymmetry coefficients for the He reaction appears to be a possible reason for the disagreement between their branching ratio results and those of the later authors. To test whether this is so, the experimental results of MK and APSST have been recalculated using the more recent data.

In the first place the 90° c.m. results have been recalculated. The values of the branching ratios given by McNeill and Keyser have therefore been multiplied by the factor $(1+A(b)\cos^2\phi)/(1+A(a)\cos^2\phi)$. $A(a)$ and $A(b)$ are the asymmetry coefficients for reactions (a) and (b) respectively at the particular energy under consideration. Typical points on the branching ratio versus deuteron energy curve published by APSST have been treated similarly. The numerical values of $A(a)$

Author	Deuteron energy kev	$\cos^2\phi_{cm}$	$A(b)$	$A(a)$	90° c.m. branching ratio		Corrected total branching ratio
					Uncorrected	Corrected	
APSST	13·0	0·006	0·20	0·25	0·93 ± 0·02	0·93 ± 0·02	0·95
	25	0·011	0·25	0·40	0 95 ± 0·01	0·95 ± 0·01	0·985
	40	0·018	0·31	0·60	0·95 ± 0·01	0·945 ± 0·01	1·03
	60	0·027	0·37	0·75	0·96 ± 0·01	0·95 ± 0·01	1·065
	80	0·036	0·43	0·88	0·97 ± 0·01	0·96 ± 0·01	1·08
	100	0·045	0·50	1·05	0·985 ± 0·01	0·96 ± 0·01	1·105
MK	120	0·054	0·57	1·17	0·95 ± 0·04	0·92 ± 0·04	1·08
	140	0·062	0·64	1·23	1·00 ± 0·07	0·96 ± 0·07	1·12
	160	0·071	0·70	1·31	1·00 ± 0·04	0·95 ± 0·04	1·135
	250	0·11	1·00	1·78	1·06 ± 0·04	0·96 ± 0·04	1·155

were taken from Preston, Shaw and Young (1954). The values of $A(b)$, those used by MK for both reactions, were taken from Manning, Huntoon, Myers and Young (1941). This calculation gives the corrected 90° c.m. branching ratio.

Secondly, as $\sigma_{total}=4\pi\sigma_{90}(1+\frac{1}{3}A)$, the ratios of the total cross sections at different deuteron energies have been obtained from the results of MK and APSST by multiplying the corrected 90° c.m. values by $[1+\frac{1}{3}A(a)]/[1+\frac{1}{3}A(b)]$. It may be noted here that as MK and APSST always used a value of $A(a)$ equal to $A(b)$, their total branching ratios were naturally always equal to their 90° c.m. ratios.

The results of these two calculations are given in the table, and the total cross section branching ratios are graphically compared with the results of other authors in the figure. As will be seen from the table and the graph, there is complete accord between the corrected values and the results of Eliot, Roaf and Shaw, and of Preston, Shaw and Young, both in the constancy of the 90° c.m. branching ratio and in the increase of the total branching ratio with deuteron energy.

It may be concluded, therefore, that there is agreement between the experimental results of the various authors quoted, and that the orginal apparent disagreement was due to the acceptance by MK and APSST of values for the asymmetry coefficients of the D(dn) ^{3}He reaction which later work has shown to be incorrect.

References

Arnold, W. R., Phillips, J. A., Sawyer, G. A., Stovall, E. J., and Tuck, J. L., 1954, *Phys. Rev.*, **93**, 483.

Bartholdson, I., 1950, *Ark Fys.*, **2**, 271.

Bennett, W. E., Mandeville, C. E., and Richards, H. T., 1946, *Phys. Rev.*, **69**, 418.

Eliot, E. A., Roaf, D., and Shaw, P. F. D., 1953, *Proc. Roy. Soc.* A, **216**, 57.

Hunter, G. T., and Richards, H. T., 1949, *Phys. Rev.*, **76**, 1445.

McNeill, K. G., and Keyser, G. M., 1951, *Phys. Rev.*, **81**, 602.

Manning, H. P., Huntoon, R. D., Myers, F. E., and Young, V. J., 1942, *Phys. Rev.*, **61**, 371.

Preston, G., Shaw, P. F. D., and Young, S. A., 1954, *Proc. Roy. Soc.* A, **226**, 206.

Wenzel, W. A., and Whaling, W., 1952, *Phys. Rev.*, **88**, 1149.

XCI. CORRESPONDENCE

An Accurate Determination of the Energy of the D(d, n)^{3}He *Reaction*

By Sonja Subotić and Bogdan Maglić*
Institute of Nuclear Sciences, ' Boris Kidric ', Belgrade

[Received April 28, 1955]

This paper describes a method of measuring the Q-value of the reaction D(d, n)^{3}He using C2 nuclear emulsions, which have been widely employed in the precise measurements of neutron energies. Three determinations of the Q-value of this reaction by measuring the neutron energy have been previously reported: Bonner (1941) using a cloud chamber, Livesey and Wilkinson (1945) using old type emulsions (' half-tone ') and Bichsel *et al.* (1952) using a Boron-10 ionization chamber. They differ in value and accuracy (see table below) from the result of Tollestrup *et al.* (1949) and Argo (1948) who measured the energy of the ^{3}He recoil. The only result obtained using C2 plates, that of Dyer and Bird (1953) has an experimental error of ± 60 kev; this error is greater than that which can be obtained by the emulsion technique, due to the presence of the neutrons from beryllium (which were the main object of their measurement), probably low number of tracks (number not mentioned) and higher bombarding energy than the one in the present measurement.

Deuterons of $0{\cdot}0852 \pm 0{\cdot}020$ Mev energy from an H.T. set bombarded a thick heavy ice target inclined at an angle of 45° to the direction of the incident beam. The target assembly, in which the heavy ice has a translatory motion and is continuously renewed, has been described previously (Maglić 1954). Six plates, with Ilford C2 emulsions 100 microns thick, were mounted vertically around the target, on a ring 10 inches in radius at angles −90°, −45°, 0°, 45°, 90° and 135° in the laboratory system. Exposures of over 1000 microampere hours were made.

The plates were analysed using a Zeiss binocular microscope (×1250). A mechanical device (to be published) was used which allows for the direct measurement of the vertical components of recoil proton tracks.

A strip 0·05 cm wide in the middle of each of the plates was analysed giving about 650 tracks per plate. Three measurements were made on each track: (1) horizontal component, (2) vertical component and (3) angle of projection of the scattered proton in the plane of the emulsion. Only those protons scattered within an angle less than 5° to the neutron

* Now at Nuclear Physics Research Laboratory, University of Liverpool.

direction were accepted. Since Rotblat's range–energy data (1951) for dry emulsions were used, the correction for the moisture of the air in the target room was applied for each track. The resulting neutron energies corresponding to each proton track were grouped into intervals of 30 kev and then the spectra were corrected (*a*) for change of n–p cross-section with energy and (*b*) for escape of recoil protons from the emulsion (Richards 1940). Experimental differential curves, so obtained, were translated into neutron energy curves and then integrated, to obtain the extrapolated energy. The mean energy is determined from the extrapolated energy by calculating : (1) range straggling, (2) apparent range straggling, (3) angular straggling and (4) thick target straggling as defined by Mandeville (1947). Translated into energy scale these being : 0·056, 0·017, 0·010 and 0·070 MEV respectively. Because of the very low bombarding energy used, the uncertainties arising from target thickness and variation of bombarding energy were substantially less than in previously reported experiments. The total error includes : (1) statistical probable error, (2) error which involves Rotblat's range–energy curve, (3) error in measurement of the range by the instrument, (4) error in the bombarding energy and (5) fluctuation of the relative moisture, giving a total error of $\pm 0{\cdot}024$ MEV for the Q-value. The neutron energy most accurately obtained was at 135° (thick target effects are less serious at backward angles) being $2{\cdot}258 \pm 0{\cdot}017$ MEV, thus giving a value of $Q = 3{\cdot}276 \pm 0{\cdot}024$ MEV.

Of the reaction emitting fast monoenergetic neutrons D(d, n) is one for which the Q-value could be derived from three well-known quantities : (1) the energy of protons (Tollestrup *et al.* 1947, Argo 1948) from the concurrent D(d, p) reaction, (2) the end point energy of tritium β-rays (Li, *et al.* 1951) (both these having been accurately measured) and (3) the neutron–proton mass difference, which is very well established (Li, *et al.* 1951). These values lead to the derived Q-value of

$$3{\cdot}272 \pm 0{\cdot}023 \text{ MEV},$$

which is to be compared with values obtained by various methods, given on the table below.

The Comparison of Values obtained by Various Methods

Author	Year	Method	Q (MEV)
Bonner	1941	Neutrons, cloud chamber	$3{\cdot}31 \pm 0{\cdot}03$
Livesey	1945	Neutrons, ' half-tone ' emulsions	$3{\cdot}23 \pm 0{\cdot}02$
Argo	1948	^{3}He-recoil, electrostatic analyser	$3{\cdot}30 \pm 0{\cdot}01$
Tollestrup	1949	^{3}He-recoil, double focus magnetic spectrometer	$3{\cdot}265 \pm 0{\cdot}018$
Bichsel	1952	Neutrons, boron-10 ionization chamber	$3{\cdot}24 \pm 0{\cdot}04$
Dyer	1953	Neutrons, C2 emulsions	$3{\cdot}25 \pm 0{\cdot}06$
Present result		Neutrons, C2 emulsions	$3{\cdot}276 \pm 0{\cdot}024$

The authors are thankful to Professor P. Savić and Dr. R. J. Walen.

References

Argo, H. V., 1948, *Phys. Rev.*, **74**, 1293.
Bichsel, H., Hälg, W., Huber, P., and Stobler, A., 1952, *Helv. Phys. Acta*, **25**, 119.
Bonner, T. W., 1941, *Phys. Rev.*, **59**, 237.
Dyer, A. J., and Bird, J. A., 1953, *Australian Journal of Physics*, **6**, 45; *Nucl. Sci. Abstract*, **7**, 86.
Li, C. W., *et al.*, 1951, *Phys. Rev.*, **83**, 512.
Livesey, D. L., and Wilkinson, D. H., 1949, *Proc. Roy. Soc.* A, **195**, 123.
Maglić, B. C., 1954, *Atomics*, March, p. 85.
Mandeville, C., 1947, *J. Franklyn Institute*, **24**, 385.
Richards, H., and Hudspeth, E., 1940, *Phys. Rev.*, **58**, 382.
Rotblat, J., 1951, *Nature, Lond.*, **167**, 550.
Tollestrup, A. V., *et al.*, 1949, *Phys. Rev.*, **75**, 1947.

An Analysis of the Neutrons from ^{7}Li(dn)^{8}Be *at* 880 kev

By W. M. Gibson
Physics Department, Queen's University of Belfast

and D. J. Prowse
H. H. Wills Physical Laboratory, University of Bristol

[Received May 20, 1955]

In view of the considerable interest shown recently (Malm and Inglis 1953, Treacy 1953, Titterton 1954, 1955) in the energy levels of ^{8}Be, we describe in this letter the results of an analysis of the neutrons emitted at an angle of 120° by a lithium target, 100 kev thick, bombarded with deuterons of 930 kev. The photographic plate method was used to obtain the energy spectrum of the neutrons (Powell 1940). Only 'knock-on' protons making an angle of less than 12° with the incident neutron direction were measured. Proton tracks having a range of less than 200μ were ignored as these could be due to neutrons from reactions other than ^{7}Li(dn)^{8}Be, or to highly excited states of ^{8}Be which could not be resolved without great difficulty.

After correction of the observed distribution of neutron energies for the loss to the surfaces of the 400μ-thick emulsion (Gibson and Livesey 1948), and for the variation of the n–p scattering cross section with energy (Sleator 1947), the histogram shown in the figure was obtained. The relative number of tracks in each 0·2 mev interval is plotted against the excitation energy of the ^{8}Be nucleus. Groups are visible at excitation energies of 0, 2·1, 2·9, 4·05 and 5·25 mev. There is already reliable evidence for the existence of levels in ^{8}Be at about 2·9, 4·1 and 5·3 mev

(Titterton 1955), and some evidence for one at about 2·2 MeV (Trumpy 1952, Erdos 1953, Catala 1953). The width of the ground state group is 0·3 MeV, all of which must be due to the imperfect resolution of the experimental method as it is known that the true width of this state is less than 100 ev (Wheeler 1941). Subtracting this experimental width from the width of the group at 2·9 MeV, we obtain a true width for this level of 0·8 MeV which compares favourably with the results of other workers (Azjenberg and Lauritsen 1955). It should be noted that if the existence of a level at 2·1 MeV is denied, the width and position of the 2·9 MeV level are incorrect.

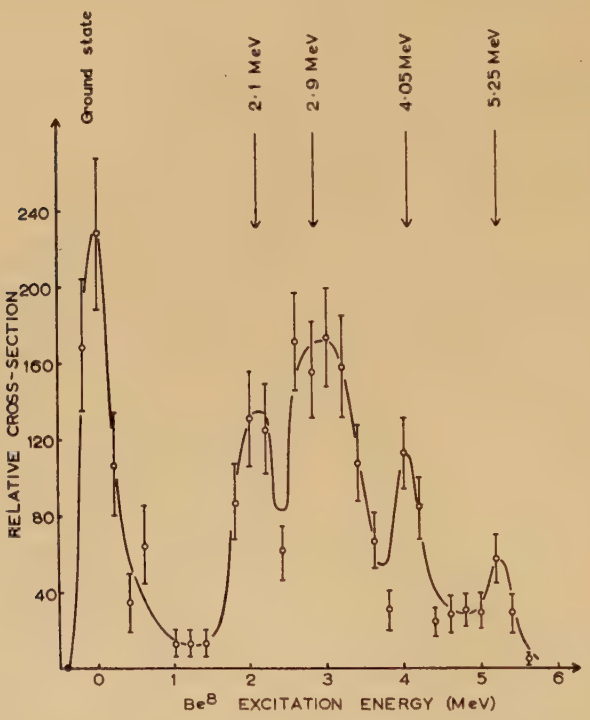

Our results differ from those of Trail and Johnson (1954), who examined the same reaction at the same angle, 120°, but at a higher bombarding energy (2·0 MeV) ; they obtained only the wide group at 3·0 MeV, although if the other groups had been present with an intensity of less than 10% of the 3·0 MeV intensity, they would not have been observed. It therefore seems that as the bombarding energy increases, the intensity of the 3·0 MeV group relative to the other groups also increases.

It would seem that the existence of the 4·1 and 5·3 MeV levels is now definitely established, and that these results tend to confirm the level first discovered at 2·2 MeV by Trumpy, Grotdal and Graue (1952).

Further work in this field is proceeding at Belfast.

We are indebted to Professor C. F. Powell for his interest and encouragement and to Mrs. B. M. Herman for most of the microscope work.

References

Azjenberg, F., and Lauritsen, T., 1955, *Rev. Mod. Phys.*, **27**, 77.
Erdos, P., Sherrer, P., and Stoll, P., 1953, *Helv. Phys. Acta*, **26**, 207.
Catala, J., Aguilar, J., and Busquets, F., 1953, *An. Real. Soc. Espan.*, **49**, 131.
Gibson, W. M., and Livesey, D. L., 1948, *Proc. Phys. Soc.*, **60**, 523.
Malm, R., and Inglis, D. R., 1953, *Phys. Rev.*, **92**, 1326.
Powell, C. F., 1940, *Nature, Lond.*, **145**, 155.
Titterton, E. W., 1954, *Phys. Rev.*, **94**, 206; 1955, *Proc. Glasgow Conference on Nuclear Physics* (London: Pergamon Press).
Trail, C. C., and Johnson, C. H., 1954, *Bull. Amer. Phys. Soc.*, **29**, No. 7, 34.
Treacy, P. B., 1953, *Phil. Mag.*, **44**, 325.
Trumpy, B., Grotdal, T., and Graue, A., 1952, *Nature, Lond.*, **170**, 1118; 1953, *University of Bergen Yearbook*, No. 8.
Sleator, W., 1947, *Phys. Rev.*, **72**, 207.
Wheeler, J. A., 1941, *Phys. Rev.*, **59**, 27.

---

*The Strength of Single Crystal and Polycrystalline Corundum**

By Elizabeth A. Jackman and J. P. Roberts
Royal Aircraft Establishment, Farnborough, Hants.

[Received April 1, 1955]

The strength in bend of corundum single crystals and of a dense sintered corundum material have been compared up to 1300°C. (We define the strength as the maximum tensile fibre stress at fracture.)

Specimens of length 58 mm and with square cross-section of side 2 mm were bent by equal and opposite couples, so that 28 mm of the length were subjected to the constant maximum bending moment. The single crystal specimens were ground from $\frac{1}{8}$ in. diameter rod made by the Verneuil method, whilst the polycrystalline specimens were ground from a single good-quality commercial tube (95% of crystal density; $>99{\cdot}3\%$ Al_2O_3).

As shown in fig. 1, the strength of the polycrystalline material remained nearly constant up to 700°C and then decreased slowly with increasing temperature. Previous measurements (Roberts and Watt 1949) on a variety of sintered corundum materials are consistent with the present result.

In contrast, the strength–temperature characteristic of the single crystals showed a pronounced minimum and, furthermore, differed among the various rods from which sets of the specimens had been

machined. The heavy curves in fig. 1 show typically the behaviour of sets of specimens from different parent rods.

No connection between the strength–temperature characteristic and the crystallographic orientation of the single crystals was found. All specimens were prepared by the same machining procedure, so that the surface condition could not vary markedly. However, the severe internal stresses which usually occur in Verneuil crystals could account readily for the observed influence of the parent rods, since it is unreasonable to expect that the conditions of growth of the different rods could have been identical. On this basis, the increased strength at higher temperatures would be associated wtih relief of the stresses and also probably with a rounding off (by surface diffusion) of the ends of surface cracks, upon which the internal stresses must act with the greatest effect.

Fig. 1

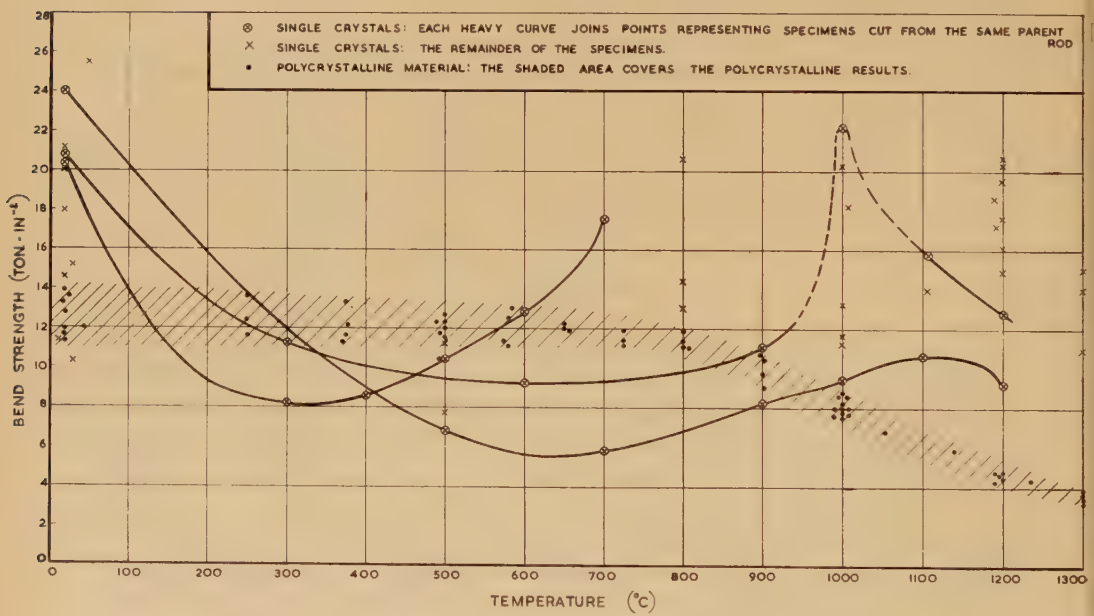

Strength of single crystal and polycrystalline corundum.

The following conclusions may be drawn from comparison of the measured strength of the single crystals and of the polystalline material.

(*a*) Around room temperature, the fracture of polycrystalline material is mainly, but not all, intercrystalline (since the majority of the single crystals were stronger than the polycrystalline specimens). This deduction is consistent with the results of a microscopical study of room temperature fractures in polycrystalline corundum (Roberts 1949), when both trans- and intercrystalline failures were found.

(*b*) Between 300° and 600°c, the crystals in polycrystalline material are stronger than the large single crystals.

(*c*) Above 1000°C, intercrystalline fracture is again common. An improvement of the high-temperature strength of sintered corundum might therefore be realised by addition of substances which modify the properties of the crystal boundaries.

The authors are indebted to the Chief Scientist, Ministry of Supply, for permission to publish this letter.

REFERENCES

ROBERTS, J. P., 1949, *Proc. Phys. Soc.* B, **62**, 248.
ROBERTS, J. P., and WATT, W., 1949, *Trans. Brit. Ceram. Soc.*, **48**, 343.

The Thermal and Electrical Conductivity of Palladium at Low Temperatures

By W. R. G. KEMP, P. G. KLEMENS, A. K. SREEDHAR* and G. K. WHITE
Division of Physics, National Standards Laboratory,
Commonwealth Scientific and Industrial Research Organization, Sydney

[Received May 24, 1955]

RECENT work in this Laboratory on the thermal conductivity of silver–palladium alloys (Kemp, Klemens, Sreedhar and White 1954) made it desirable to have information on the ideal thermal resistivity W_i of pure palladium, which is defined by

$$1/\kappa = W = W_0 + W_i \quad . \quad . \quad . \quad . \quad . \quad . \quad . \quad (1)$$

where

$$W_0 = \rho_0/L_0T = AT \quad . \quad . \quad . \quad . \quad . \quad . \quad . \quad (2)$$

is the residual thermal resistivity, κ is the thermal conductivity, ρ_0 the residual electrical resistivity and L_0 the Lorenz number. Theoretically

$$W_i = BT^2 \quad . \quad . \quad . \quad . \quad . \quad . \quad . \quad . \quad (3)$$

where B should depend only weakly on ρ_0. (See review by Olsen and Rosenberg 1953.)

Mendelssohn and Rosenberg (1952) have measured κ in the range 2 to 30°K for a palladium rod of 99·99$_5$% purity and found

$$A \simeq 11 \text{ w}^{-1} \text{ cm deg}^2, \qquad B = 6{\cdot}4 \times 10^{-4} \text{ w}^{-1} \text{ cm deg}^{-1}.$$

Rosenberg (1954) has found $B = 4{\cdot}1 \times 10^{-4}$ for a similar specimen.

The lack of agreement between the above values and those of Grueneisen and Reddemann (1934) made it desirable to obtain values over a wider range of temperature and residual resistivity.

The thermal conductivity was measured in a cryostat described previously (White 1953) using a 3 mm diameter rod of high purity (>99·99$_5$%) palladium (J M2928), for which spectroscopic analysis indicated strong silver lines and faintly visible lines of Ca, Cu, Si and Mg. Measurements were made with the rod in various physical conditions.

---

* Australian Commonwealth Government Fellow under the Colombo Plan.

All annealing was carried out *in vacuo* for about 4 hours. The results are given in fig. 1 and in the table. Electrical resistance measurements were made on Pd 6 with a galvanometer amplifier (MacDonald 1947).

Fig. 1

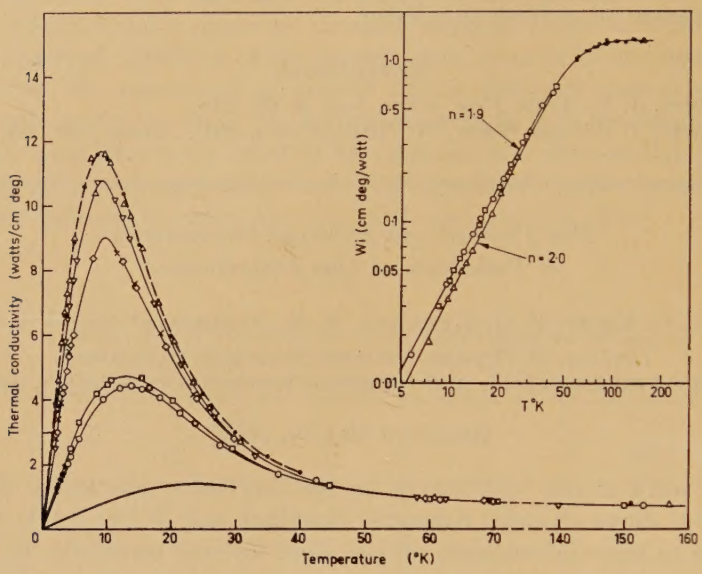

Thermal conductivity of pure palladium at low temperatures.
Inset shows the variation of the ideal thermal resistivity W_i with temperature.

⊙ Pd 1 (strained). ▽ Pd 4 (annealed 650°C).
□ Pd 2 (annealed 250°C). ◊ Pd 5 (annealed 1000°C).
△ Pd 3 (annealed 450°C). × Pd 6 (restrained and annealed 450°C).
– · – · – · $\kappa=(0{\cdot}516/T+3{\cdot}5\times10^4T^2)^{-1}$.
——— Mendelssohn and Rosenberg (1952).

Physical State and Thermal Conductivity Data for Pure Palladium Specimens

Specimen	Physical condition	A W^{-1} cm deg^2	B W^{-1} cm deg^{-1}
Pd 1	Strained 3 mm rod (as received)	1·97	$4{\cdot}00\times10^{-4}$
Pd 2	Pd 1 after annealing at 250°C	1·80	$3{\cdot}95\times10^{-4}$
Pd 3	Pd 2 after annealing at 450°C	$0{\cdot}51_6$	$3{\cdot}50\times10^{-4}$
Pd 4	Pd 3 after annealing at 650°C	0·57	$3{\cdot}60\times10^{-4}$
Pd 5	Pd 4 after annealing at 1000°C	0·76	$3{\cdot}70\times10^{-4}$
Pd 6	Pd 5 drawn to 2 mm, annealed at 450°C	0·75	$3{\cdot}70\times10^{-4}$

The residual resistance coefficient A increased with increasing annealing temperature for Pd 4 and Pd 5 but remained unchanged for Pd 6. This suggests that the high temperature anneal merely caused additional impurities to be taken into solid solution rather than the freezing in of vacancies.

The table and the inset of fig. 1 indicate deviations from the thermal analogue of Matthiessen's rule to be in the sense predicted by Sondheimer (1950).

The electrical resistivity of Pd 6 at temperatures below $\theta/5$ is well represented by

$$\rho=\rho_0+\rho_i=1{\cdot}82\times10^{-8}+2{\cdot}12\times T^{3{\cdot}2} \text{ ohm cm.}$$

The residual resistance ratio ρ_0/ρ_{293} was $1{\cdot}7\times10^{-3}$. Figure 2 shows the variation of the ratios $L=\rho/WT$ and $L_i=\rho_i/W_iT$ with temperature. At lowest temperatures L tends to L_0, indicating that (2) is satisfied for the residual resistivities. It is interesting to note that L_i does not tend to zero as T^2, as required by the Bloch theory and as is observed for monovalent metals. This may be explained as follows.

Fig. 2

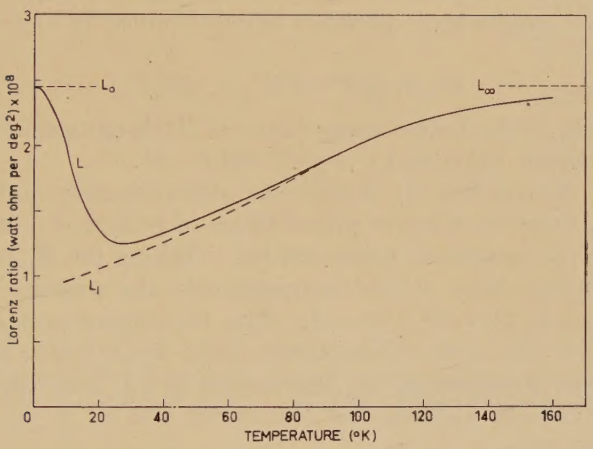

Variation of the experimental Lorenz ratio $L=(\rho/WT)$ and the ideal Lorenz ratio $L_i=(\rho_i/W_iT)$ with temperature.

In palladium there is an s-band of electrons and an overlapping d-band of holes ; the latter have a large effective mass and do not contribute appreciably to the conduction processes. The ideal resistivities arise from (s–s) and (s–d) transitions induced by phonons, so that

$$\rho_i=\rho(\text{s, s})+\rho(\text{s, d}), \quad \ldots\ldots \quad (4)$$

$$W_i=W(\text{s, s})+W(\text{s, d}). \quad \ldots\ldots \quad (5)$$

Now ρ(s, s) and W(s, s) are given by the Bloch theory, so that $\rho(\text{s, s})\propto T^5$ and $W(\text{s, s})\propto T^2$. The (s–d) transitions have been treated by Wilson (1953) ; the holes in the d-band can be regarded as undisturbed by any fields, so that a relaxation time can be defined for (s–d) transitions which is the same for electrical and thermal conduction. Therefore ρ(s, d) and W(s, d) are related by the Lorenz law

$$TW(\text{s, d})=\rho(\text{s, d})/L_0. \quad \ldots\ldots \quad (6)$$

Also, since the numbers of electrons and holes are equal, the Fermi surfaces of the two bands overlap extensively in reduced k-space, there is no lower limit on the wave-number of the phonons inducing an (s–d) transition, and $\rho(\mathrm{s,\,d}) \propto T^3$, $W(\mathrm{s,\,d}) \propto T^2$. At lowest temperatures $\rho(\mathrm{s,\,s})$ is negligible, so that ρ_i should be proportional to T^3, in rough agreement with observations; both $W(\mathrm{s,\,s})$ and $W(\mathrm{s,\,d})$ vary as T^2, and are comparable at lowest temperatures. The value of B observed here can be expressed in terms of the high temperature thermal resistance by

$$B = CW_\infty/\theta^2. \qquad (7)$$

According to the Bloch theory $C = 64{\cdot}0N^{2/3}$ (Klemens 1954), where N is the number of free electrons per atom. With $\theta = \theta_D = 275°\mathrm{K}$, the present results yield $C \simeq 20$.

Since the s-band of palladium contains only 0·6 electrons per atom, one would expect the basic postulates of the Bloch theory to be satisfied for (s–s) transitions in palladium to a better degree than for monovalent metals. Only longitudinal phonons should induce (s–s) transitions, so that

$$W_T(\mathrm{s,\,s})/T^2 = CW_\infty(\mathrm{s,\,s})/\theta_L^2, \qquad (8)$$

where $\theta_L \simeq 1{\cdot}5\theta_D$ is the Debye temperature of the longitudinal polarization branch (Blackman 1951) and $C = (0{\cdot}6)^{2/3}64{\cdot}0 = 45$.

The ratio $W(\mathrm{s,\,s})/W(\mathrm{s,\,d})$ should be approximately independent of temperature, since the relative probabilities of (s–s) and (s–d) transitions are not sensitive to phonon wave-number. Taking for $W_\infty(\mathrm{s,\,s})/W_\infty(\mathrm{s,\,d})$ the corresponding ratio at low temperatures, the present observations give the value $C \simeq (1{\cdot}5)^2 \times 20 = 45$. The theoretical and experimental values of C for the monovalent metals differ by a factor of order 4 so that, while the closeness of the agreement in the case of palladium is fortuitous, it would appear that the Bloch theory is, in fact, better obeyed in this case.

References

Blackman, M., 1951, *Proc. Phys. Soc.* A, **64**, 681.

Grueneisen, E., and Reddemann, H., 1934, *Ann. Phys., Lpz.* (5), **20**, 843.

Kemp, W. R. G., Klemens, P. G., Sreedhar, A. K., and White, G. K., 1954, *Proc. Phys. Soc.* A, **67**, 728.

Klemens, P. G., 1954, *Aust. J. Phys.*, **7**, 64.

MacDonald, D. K. C., 1947, *J. Sci. Instrum.*, **24**, 232.

Mendelssohn, K. M., and Rosenberg, H. M., 1952, *Proc. Phys. Soc.* A, **65**, 388.

Olsen, J. L., and Rosenberg, H. M., 1953, *Advances in Physics*, **2**, 28.

Rosenberg, H. M., 1954, *Phil. Trans. Roy. Soc.* A, **247**, in the press.

Sondheimer, E. H., 1950, *Proc. Roy. Soc.* A, **203**, 75.

White, G. K., 1953, *Proc. Phys. Soc.* A, **66**, 559.

Wilson, A. H., 1953, *Theory of Metals* 2nd ed. (Cambridge: University Press), p. 272.
